Alma Mater Studiorum – Università di Bologna

in cotutela con Katholieke Universiteit Leuven

DOTTORATO DI RICERCA

Scienze Biomediche e Neuromotorie

Ciclo XXXI

Settore Concorsuale: 05/D1

Settore Scientifico Disciplinare: BIO/09

Functional heterogeneity of medial posterior parietal cortex of macaque monkey
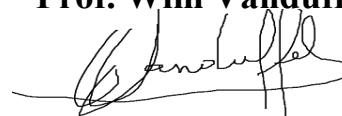
Presentata da: **Marina De Vitis**

Coordinatore Dottorato
Prof. Pietro Cortelli

Supervisore
Prof.ssa Patrizia Fattori

Supervisore
Prof. Wim Vanduffel

Co-Supervisore
Dr. Annalisa Bosco

Esame finale anno 2020

Abstract

The importance of the posterior parietal cortex (PPC) in multiple cognitive processes of the brain has been recognized since the latter half of the 20th century. PPC of primates represents a remarkable platform that has evolved over time to solve some of the difficult computational challenges that we face in the everyday life, such as sensorimotor integration, spatial attention and navigation, and early motor planning. Parietal lesions result in severe impairments in the control of eye movements towards visual targets, in the guidance of reaching actions and of the grasping of nearby objects, and in the ability to direct attention to visual stimuli.

With the aim of further investigating the multifaceted functional characteristics of macaque medial PPC, we conducted three studies to explore the visuomotor, somatic, visual, and attention-related properties of two cortical areas belonging to this brain region: V6A, a visuomotor area part of the dorsomedial visual stream, and PE, an area strongly dominated by somatomotor input, residing mainly on the exposed surface of the superior parietal lobule. In the first study, we tested the impact of visual feedback on V6A grasp-related activity during arm movements towards objects of different shapes. We observed that separate sub-populations of V6A cells are engaged during the different task conditions: Visual cells were activated only during grasping performed in the light, thus receiving a visual feedback of the moving arm and the object to be grasped. Motor neurons were equally activated during grasping in the dark and in the light. Visuomotor cells were differently activated while grasping in the dark and in the light. Our results demonstrate that V6A is modulated by both grip type and visual information during grasping preparation, execution, and object holding, with a predominance of cells influenced by grip type. In the second study, we explored the influence of depth and direction information on reach-related activity of neurons in the medial part of area PE and characterized their temporal evolution over the course of a reaching task in darkness towards targets in the 3D space. We showed that tuning of activity by direction was stronger at the beginning of the task, whereas depth tuning mainly occurred during movement

execution. When comparing our results with those found in the nearby areas V6A and PEc, a rostro-caudal trend of increased convergence of depth and direction signals on single cells emerged. The sensory signals affecting V6A, PEc and PE may explain the presence of this trend, as visual sensitivity increases along an antero-posterior axis towards area V6A, and somatosensory sensitivity increases in the opposite direction, towards area PE. In the third study, we used a combined fMRI-electrophysiology experiment to investigate the neuronal mechanisms underlying covert shift of attention processes in area V6A. Guided by fMRI maps, that showed the engagement of area V6A during covert shifts of spatial attention, we targeted electrophysiological recordings to the ventral V6A of one monkey. Our preliminary results reveal that more than half of the total recorded cells showed shift-selective activity when the monkey was covertly shifting its allocation of attention towards the location of the visual receptive field. We also demonstrated that V6A shift-related activity did not depend on eye movements directed towards the stimuli cuing the attention shifts, as the monkey did not perform any significant eye deviation from the central fixation point.

All together these findings highlight the important role played by the medial PPC in integrating information coming from different sources (vision, somatosensory and motor) and emphasize the involvement of action-related regions of the dorsomedial visual stream in higher level cognitive functions.

Table of Contents

Chapter 1

General Introduction

1.   General Introduction

Here I am, sitting at my desk, in an attempt to focus on writing my PhD thesis. I am thirsty -I didn't have anything to drink in a while now- so I decide to leave my comfortable seat to take a sip of fresh water. As I approach the fridge, I find myself spontaneously hyperextending and guiding the arm in the direction of my target. Next, I shape my hand to form the correct grip necessary to grasp the handle of the refrigerator. When I finally manage to grab the much-desired water, I can't help but move my focus of attention on the leftover piece of cake from my sister's birthday.

Reaching a target in the three-dimensional space, shaping the hand with the aim of grasping an object, shifting the allocation of attention towards an interesting item in the visual environment. By performing all these actions, I am pretty sure that the medial sector of my posterior parietal cortex (PPC) has been highly engaged.

The medial PPC is part of a neuronal network involved in the association of information coming from frontal and visual cortices (Goodale and Milner, 1992; Rizzolatti and Matelli, 2003; Galletti and Fattori, 2017). Medial PPC areas are implicated in a vast array of tasks and operate on a multiplicity of signals, such as attentional, visual, somatosensory, vestibular, and auditory signals, to cite only a few of them. The present thesis will examine in particular: i) the visual, somatosensory and motor-related properties used in the arm movement control; ii) the attention-related signals necessary for spatial information processing. To this purpose, we performed three studies on non-human primates: the first study (2nd chapter of this thesis) explored the relative contribution of visual information and of hand shaping for grasping to the neuronal activity of area V6A, a visuo-motor area, also identified as part of the cortical grasping circuit in monkey. The second study (3rd chapter of this thesis) focused on the

largely unexplored medial part of area PE, and was primarily aimed at evaluating the relative influence of reach depth and direction signals in 3D space on the activity of medial PE cells. In the last study (4th chapter of this thesis), we aimed to investigate the neural correlates of covert shifts of spatial attention across visual hemifields in the ventral part of area V6A.

1.1 The Posterior Parietal Cortex

1.1.1 Anatomical organization

The PPC of primates holds a collection of association areas involved in somatosensory and visual processing. It is located in the caudal part of the parietal lobule in both human and non-human primates, immediately posteriorly to the postcentral gyrus, which is the seat of the primary somatosensory cortex (Fig. 1.1). The PPC is composed of two lobules: the inferior parietal lobule (IPL) on the lateral surface of the brain, and the superior parietal lobule (SPL) on the medial part of the lateral surface and on the mesial surface of the cerebral hemisphere. IPL and SPL are separated by the intraparietal sulcus, whose walls are part of the PPC. The IPL in humans extends to the angular and supramarginal gyrus, the regions classified as Brodmann area 39 and 40, respectively. The parieto-occipital sulcus represents the caudal border of the SPL, dividing the PPC from the occipital cortex, that contains the cortical visual areas. Functional and anatomical studies showed that within the SPL there are two heavily interconnected flows of information, a visual one moving from the posterior areas to the anterior ones, and a somatosensory one moving in the opposite direction. The more central areas within SPL, where the two sensory streams overlapped, are typically sensori-motor areas.
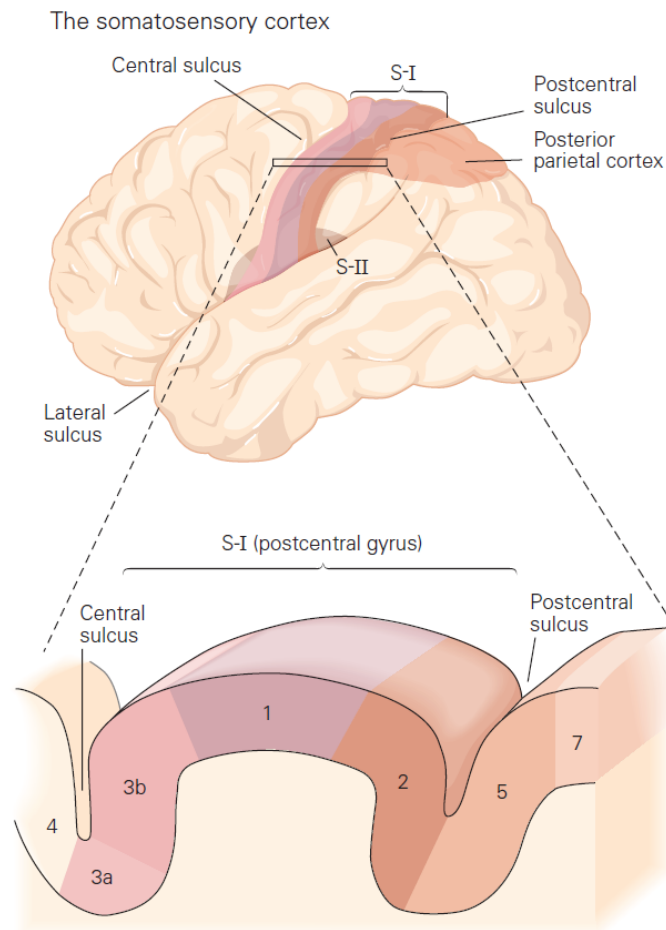
Figure 1.1 Lateral view of a left hemisphere of a human brain showing the location the primary (S-I) and secondary (S-II) somatosensory cortices and the posterior parietal cortex. A sagittal section shows the distinct cytoarchitectonic regions of S-I (Brodmann's areas 3a, 3b, 1, and 2) and the adjacent posterior parietal cortex (areas 5 and 7) and motor cortex (area 4). From Kandel et al. 2013.

The SPL, that covers the medial part of PPC, encompasses a group of areas (Fig. 1.2) which are particularly important for visuomotor integration and direction of attention to specific parts of extrapersonal space: area PGm, on the mesial surface of the hemisphere, the medial intraparietal area (MIP), hidden in the medial bank of intraparietal sulcus, areas PE and PEc, located nearby on the exposed surface of SPL, and area V6A hidden in the parieto-occipital sulcus, in the caudalmost part of the SPL (Pandya and Seltzer, 1982; Cavada and Goldman-Rakic, 1989a, 1989b; Colby and Duhamel, 1991; Galletti et al., 1999; Bakola et al., 2010,

2013). These brain areas have been identified based on their functional repertoire and cortico-cortical connections in non-human primates and in human brain, thanks to the development of different neurophysiological methodologies.
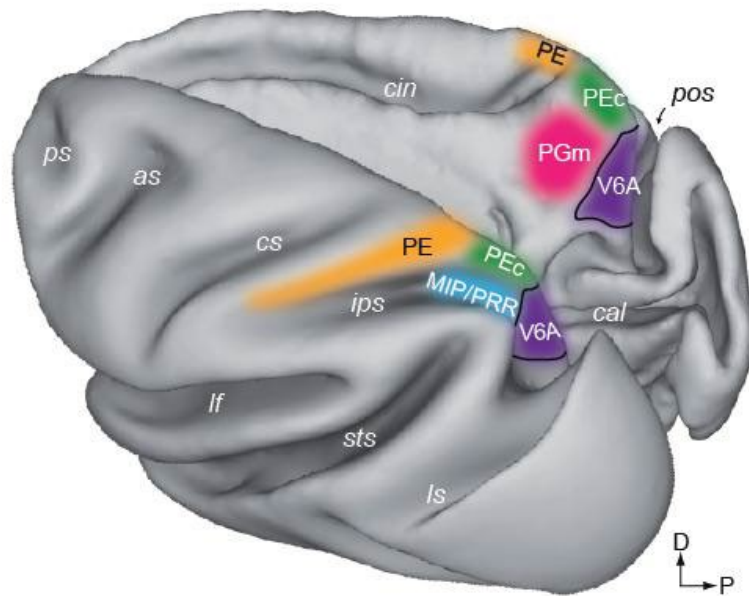
Figure 1.2 Dorsal view of left hemisphere (left) and medial view of right hemisphere (right) of a *Macaca fascicularis* brain reconstructed in three dimensions using Caret software (http://brainvis.wustl.edu/wiki/index.php/Caret:Download) showing the location and extent of SPL areas: purple V6A (Galletti et al., 1991); green: PEc (Pandya and Seltzer, 1982); orange: PE (Pandya and Seltzer, 1982); blue: MIP/PRR, medial intraparietal area/parietal reach region (Colby and Duhamel, 1991; Snyder et al., 1997); magenta: PGm (Pandya and Seltzer, 1982). Sulci are also shown: as, arcuate sulcus; cal, calcarine sulcus; cin, cingulate sulcus; cs, central sulcus; ips, intraparietal sulcus; lf, lateral fissure; ls, lunate sulcus; pos, parieto-occipital sulcus; ps, principal sulcus; sts, superior temporal sulcus. D, dorsal; P, posterior. Adapted from Fattori et al. 2017.

1.1.2   Medial PPC as an integrative hub for multiple functions

Medial PPC, situated at the junction of multiple sensory regions, projects to several cortical and subcortical areas and serves a crucial role in transforming sensory input into motor output. To achieve this goal, an array of cognitive computations engages medial PCC, including processing related to representing space, in addition to attention, transformation of coordinate systems, and motor planning. Medial PPC lesions produce complex defects in (peri)personal spatial perception, visuomotor integration, and selective attention (see section 1.2). The functional characteristics of the SPL areas V6A and PE, specific target regions of the present thesis, will be described here below.

1.1.2.1 Area V6A

Visual information leaves the primary visual cortex following two main pathways: a ventral one, directed to the inferotemporal cortex, dedicated to the identification of the objects features (also known as "what" pathway), and a dorsal one, that reaches the PPC, involved in the guidance of actions (also known as "where/how" pathway) (Ungerleider and Mishkin, 1982; Goodale and Milner, 1992; Milner and Goodale, 2006). In the classical view, the dorsal stream has been further divided in at least two separate branches, which mediate different aspects of visual behavior (Galletti et al., 2003; Rizzolatti and Matelli, 2003): a dorsal one, traditionally proposed to control reaching actions, and a lateral circuit, proposed to control grasping actions (Fig. 1.3).
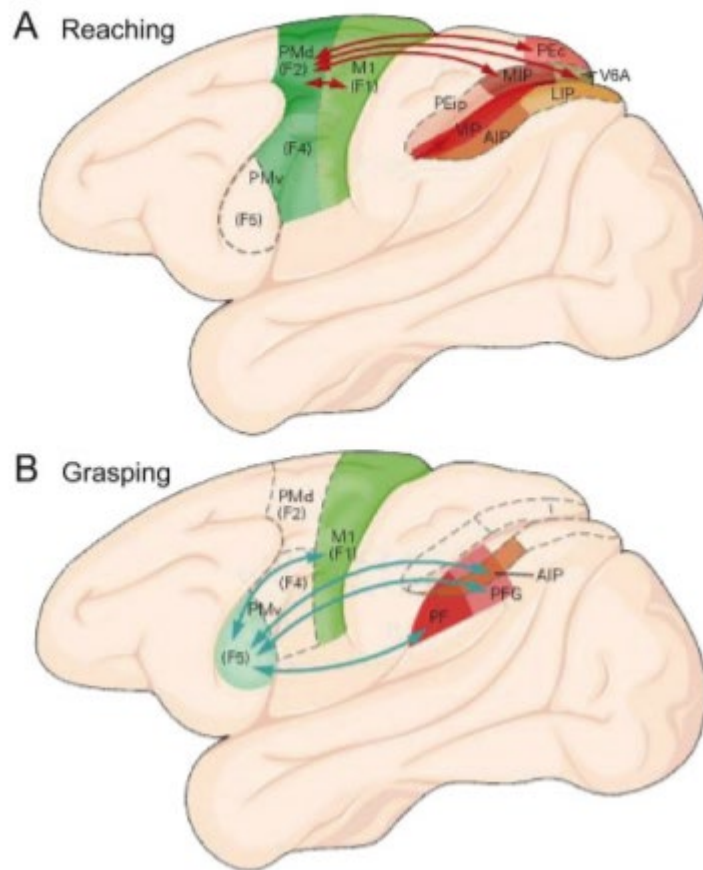
Figure 1.3 Widely accepted view of the division of the dorsal stream in two sub-circuits. **A**. Dorsomedial pathway, linking the SPL (areas V6A, PEc, MIP) with the dorsal premotor cortex (PMd, area F2), traditionally proposed to control reaching actions. **B**. Dorsolateral pathway, linking the IPL (areas AIP, PFG, PF) with the ventral premotor cortex (PMv, area F5), traditionally associated with grasping movements. From Galletti and Fattori (2017).

Recent discoveries seem to challenge this view of two independent pathways, supporting a more integrated view based on the reciprocal interplay between these two streams (Nelissen and Vanduffel, 2011; Galletti and Fattori, 2017).

Area V6A belongs to the to the dorsomedial stream (Galletti et al., 2003; Rizzolatti and Matelli, 2003) and is a functionally multifaceted area. It contains cells that encode the spatial location of visual targets (Galletti et al., 1993, 1995), as well as neurons with reaching, grasping, and oculomotor-related activity (Kutz et al., 2003; Gamberini et al., 2011; Fattori et al., 2017). Recently, V6A has been cytoarchitectonically subdivided into a ventral (V6Av) and a dorsal (V6Ad) portion (Luppino et al., 2005). These two portions have also shown functional differences, mainly in the sensory domain. V6Av contains a majority of visual cells with receptive fields that are mostly in the lower periphery; V6Ad, in contrast, shows a higher number of cells sensitive to somatic stimulation, and the visual cells mostly represent the central part of the visual field (Galletti et al., 1999; Gamberini et al., 2011). It has been demonstrated that V6A grasp-related activity is modulated by different wrist orientations (Fattori et al., 2009) and different grip types (Fattori et al., 2010, 2012) in darkness. More recently, the modulation of V6A grasping activity by wrist orientation has been linked to the visual feedback from the moving arm (Breveglieri et al., 2016). However, the interplay between visual feedback and grip-related information has never been tested in V6A. In the 2nd chapter of the present thesis we investigated the relative influence of grip type and visual condition of the grasping action on the discharge of V6A neurons. We also compared grasp-related properties of V6A cells with those of AIP, a grasping area belonging to the dorsolateral pathway.

Aside its implication in the control of reaching and grasping actions, the dorsal stream is also responsible for the spatial localization of the objects, directing the gaze towards the objects of interest in the visual environment, hence the deployment of attentional control. Thus, V6A activity is not merely involved in visuomotor processing. This area has been recently identified to belong to a network of cortical areas clearly activated during attention shifting events (Caspari et al., 2015). The researchers adopted an event-related fMRI paradigm,

closely resembling a human experiment (Molenberghs et al., 2007), that basically consisted of two main events: i) SHIFT event, where a change in location of a relevant stimulus cued the monkey to make a covert shift of spatial attention towards it; ii) STAY event, where the monkey was supposed to maintain its covert attention to the same spatial location. They characterized a network of areas activated during spatial shifting events including parietal areas V6/V6A, medial intraparietal area, caudo-dorsal visual areas, the most posterior portion of the superior temporal sulcus, and several frontal areas.

Previously, there was an attempt of investigating the attention-related properties of area V6A at a neural level. In (2010), Galletti and coworkers tested whether covert attention shifts modulate ongoing V6A neuronal activity, using a task where the monkey was required to shift its attention outward to a peripheral cue and inward again to a central fixation point. They showed that V6A cells are activated during covert shifts of attention, but they could not disengage this activity from the monkey's behavior. The poor knowledge about the neuronal mechanisms underlying covert shift of attention processes prompted us to perform an electrophysiology experiment in which we aimed at further investigating attention-related properties of V6A at a neural level. Preliminary results from one subject are reported in the 4th chapter of this thesis.

1.1.2.2 Area PE

Area PE lies anterior to area PEc, on the exposed surface of the SPL (Fig. 1.2; Pandya and Seltzer 1982). PE neurons are mainly activated by proprioceptive stimulation, although some of them respond to tactile stimulation (Duffy and Burchfiel, 1971; Sakata et al., 1973; Mountcastle et al., 1975) and receive robust somatic input information and projections from motor and premotor cortex (Sakata et al., 1973; Jones et al., 1978; Pandya and Seltzer, 1982; Johnson et al., 1996; Bakola et al., 2013). PE represents one of the key nodes of the reaching

circuit of the medial PPC. Reaching movements in the real world have typically a direction component, where the subject has to perform conjugated eye movements to foveate the target of interest, and a depth component, where the subject makes disconjugated eye movements to foveate the target to reach. Over the past decades, many studies have investigated the direction influence on PE neural activity, using center-out reaching tasks (Kalaska et al., 1983, 1990; Mackay et al., 1994; Scott et al., 1997; Menzer et al., 2014). A few studies have found tuning by reach depth in PE, however without simultaneously addressing direction processing (Ferraina et al., 2009; Brunamonti et al., 2016). Only, Lacquaniti and collaborators (1995) made a further step by investigating the effect of the three spatial coordinates (azimuth, distance and elevation) on PE neural responses during reaching movements. In that experiment, the animals performed goal-directed movements towards targets located at similar directions within three different workspaces starting from three initial hand positions. Each of these initial hand positions was located in the middle of an imaginary cube where at each corner a reach target was placed. The researchers found that different neuronal populations processed the three parameters independently. However, eye position was not monitored, and targets were distributed only between two depth planes.

In the 3rd chapter of this thesis, we aimed at: i) evaluating the relative influence of depth and direction signals on the activity of medial PE cells during a Fixation-to-Reach task in 3D; ii) characterizing the sensory properties, by qualitatively examining the visual and somatosensory responses of PE neurons; iii) comparing the obtained results with those found in the nearby areas V6A and PEc (Hadjidimitrakis et al., 2014a, 2015) to provide a picture of the spatial information processing for reaching in the whole SPL.

1.1.2.3 Putative human homologous of areas V6A and PE

Establishing homologies between cortical areas in animal models and humans is a key aspect in translational neuroscience, as it expands understanding of brain structure, function and disease, and turns this knowledge into clinical applications and novel therapies of nervous system disorders. Recent functional MRI studies have proposed a putative human homologue of area V6A (Pitzalis et al., 2013; Tosoni et al., 2015), which is likely located in the medial part of the posterior parietal cortex (mPPC, Pitzalis et al., 2015), and closely resembles the retinotopic organization and functional properties described for macaque V6Av and V6Ad (Galletti et al., 1999; Gamberini et al., 2011). Human V6A shows a clear over-representation of the contralateral lower visual field and responded only to visual stimulation of the far periphery (starting from 30°, Pitzalis et al., 2013). This region responds to pointing (Simon et al., 2002; Astafiev et al., 2003; Connolly et al., 2003; Tosoni et al., 2008, 2015; Pitzalis et al., 2013) as well as to reaching and grasping movements (Beurze et al., 2007, 2009; Filimon et al., 2007, 2009; Cavina-Pratesi et al., 2010; Vesia et al., 2010; Galati et al., 2011; Gallivan et al., 2011; Konen et al., 2013). The human mPPC also plays a critical role in transient shifts of spatial attention, producing signals independent of the direction of the attention shift (Vandenberghe et al., 2001; Yantis et al., 2002; Molenberghs et al., 2007; Kelley et al., 2008; Caspari et al., 2018). This evidence is supported by the fact that people suffering from Balint's syndrome, a rare manifestation of visual and spatial difficulties due to bilateral SPL lesions, show an impairment in detecting the displacement of a visual stimulus (Phan et al., 2000) (see section 1.2). Recently, Caspari et al. (2018) showed correspondences between the shift SPL-network in humans and the superior parietal network processing attention shifts in monkeys, suggesting medial intraparietal area and V6/V6A as functional counterparts of human medial superior parietal lobule (mSPL).

Area PE of the monkey is often referred to as Brodmann's area 5 (Brodmann, 1909). According to Brodmann's representation, area 5 is placed posteriorly to areas 3, 1, 2 in both monkey and human brains. So far, only two groups have explored the functional properties of a potential putative human homologous of area PE. First, Sereno and coworkers have identified a second somatosensory homunculus in a region of the human SPL located in the postcentral gyrus, right posterior to the primary somatosensory cortex, in a location that matches the one of Brodmann's area 5 (Parietal Body Area, PBA) (Huang et al., 2012; Huang and Sereno, 2018). The PBA contains a rough topographical map of the body resembling the one observed in macaque area PE (Seelke et al., 2012). The parietal cortex posterior to PBA was activated by goal-directed reaching movements, but it didn't show any topographical organization (Huang and Sereno, 2018). In a very recent neuroimaging study, Pitzalis et al. (2019) defined as human PE (hPE) a region within human mSPL exhibiting significant responses during active leg movements, consisting of leg rotation and flexion, and foot pointing towards a memorized target. These functional characteristics parallel the one described in macaque PE (Seelke et al., 2012, see also section 3.3.4 of the present thesis). However, the definition of a human homologous of monkey PE is still a controversial subject, and further studies are needed to better relate the functional organization of monkey PE with its possible human counterpart.

1.2   Effect of damage of posterior parietal cortex

The study of brain activity, either through fMRI, electrophysiology, or other methods, tests whether cognitive processes are associated with activity in neurons, brain regions, or networks. These techniques represent a formidable set of research tools yet cannot differentiate between regions that are engaged during a cognitive process from those that are

essential for that process (Vaidya et al., 2019). Lesion of a specific brain area is one of the techniques used by researchers in order to correlate specific dysfunctions to the brain region involved in the lesion. Complex sensorimotor abnormalities can be observed subsequent to a PPC lesion, including the inability to accurately process stimuli in the contralateral visual field or contralateral half of the body. Poor motor coordination and poor eye-hand coordination during reaching, grasping, and hand orientation lead to neglect in usage of the hand (Bisiach and Luzzatti, 1978; Marshall and Halligan, 1995).

Lesions of the parietal lobe or parieto-temporo-occipital lobe (posterior association areas) of either the right or left hemisphere produce a particular form of agnosia (astereognosis), which is the inability to identify an object by active touch of the hands without other sensory input, such as visual or sensory information (Gerstmann, 2001; O'Sullivan and Schmitz, 2007). With the absence of vision (i.e. eyes closed), an astereognosic patient is unable to identify what is placed in his hand based on cues such as texture, size, spatial properties, and temperature (O'Sullivan and Schmitz, 2007). Another neurological disorder associated with PPC damage is the contralateral neglect syndrome, characterized by a difficulty in exploring the space and perceive or pay attention to objects, people, representations placed in the visual hemifield contralateral to the lesion, and to act in that side of the space. The disturbance can involve outer space, but also the peripersonal one, reachable with the gesture of a hand: it is not rare to see patients who shave, make up or comb only the right side of their face. Frequently, the lesion is located in the right hemisphere and the deficit manifests itself as an inability to direct attention to the hemifield opposite to the lesion, thus to the left. In the acute phase, patients have head and eyes deviated to the right and do not pay attention to what happens to their left. For example, they do not respond to an interlocutor, do not collect food on the left side of the plate, neglect the left side of their body, have difficulty in dressing, and do not use the left limbs. In some patients the ability to copy the left side of a drawing is

severely compromised (Bloom et al., 1985). When asked to draw a clock, the patient may ignore the numbers on the left: their drawing might show only the numbers from 1 to 7 (Fig. 1.4), or all 12 numbers might be on the right half of the clock with the other half distorted or blank.
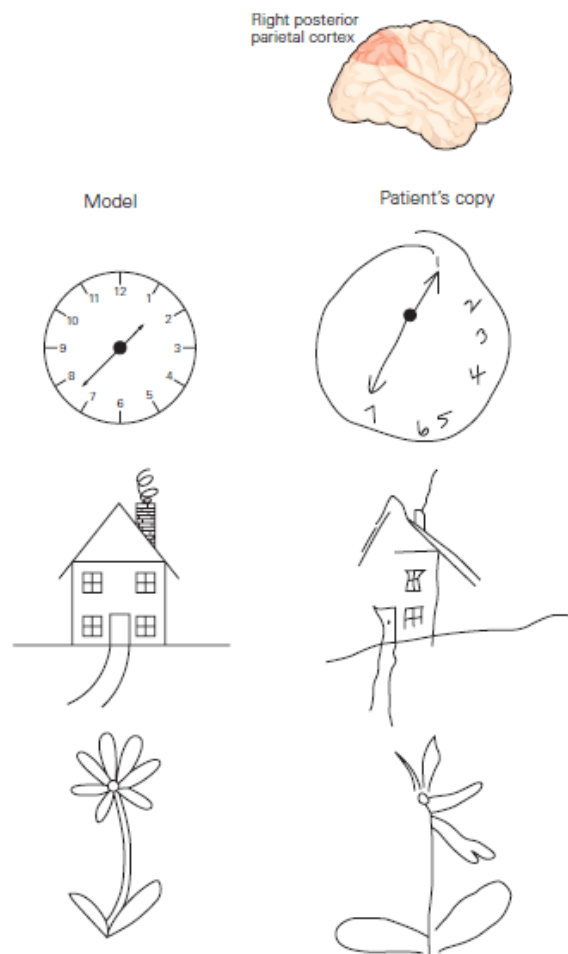
Figure 1.4 Drawings made by a patient suffering from contralateral neglect syndrome. The patient was asked to draw a clock/house/flower by copying the figure on the left; the subject 's imitation is on the right. From Kandel et al. 2013.

In 1909, the Austro-Hungarian neurologist Balint first described another group of behavioral impairments specifically associated with damage to the SPL and the parieto-occipital

junction. Since patients with such type of lesions did not show any sensory or motor deficits, it was suggested that the impairment was at a more integrative, sensorimotor level. Balint's syndrome includes difficulty in executing eye movements to engage visual targets (ocular apraxia), inability to perceive multiple objects simultaneously (simultanagnosia), and inability in reaching for visual targets (optic ataxia). All these symptoms heavily impact visuospatial skills, visual scanning and attentional mechanisms (Zgaljardic et al., 2011).

Patients with simultanagnosia are unable to perceive multiple items in a visual display, while preserving the ability to recognize single objects. Dalrymple and colleagues (2010) suggested that simultanagnosia may result from an extreme form of competition between objects which makes it difficult for attention to be disengaged from an object once it has been selected. Patients have a restricted spatial window of visual attention and cannot see more than one object at a time (Jackson et al., 2006). They see their world in a sparse manner. For instance, if presented with an image of a table containing both various objects and food, a patient will report seeing only one item, such as a spoon. If the patient's attention is redirected to another object in the scene, such as a glass, the patient will report that they see the glass but no longer see the spoon (Coslett and Lie, 2008). As a result of this impairment, patients with simultanagnosia often fail to comprehend the overall meaning of a scene. Garcin et al. (1967) were the first to report that optic ataxia can also appear as a distinct disorder in isolation. It can occur with unilateral (Perenin and Vighetto, 1988; Karnath and Perenin, 2005) or bilateral SPL lesion (Pisella et al., 2000, 2004; Karnath and Perenin, 2005; Khan et al., 2005). Patients suffering from optic ataxia show a peculiar characteristic, that is the contrast between the occurrence of spatial errors while executing reaching movements in the visual periphery and unimpaired movements to targets in the center of the visual field (Borchers et al., 2013). After lesions of the SPL, the parieto-occipital junction, or the intraparietal sulcus (Karnath and Perenin, 2005; Martin et al., 2015), ataxic patients experience difficulty in

making visually guided arm movements towards an object in the visual environment. The impairment is severe when the target is located peripherally in the visual field, less when the target lies in the parafoveal region, and negligible when the patient fixates the target. Figure 1.5 shows a typical behavior between ataxic patients, who misreach the non-foveated target when guiding the limb in peripheral space (Perenin and Vighetto, 1988; Karnath and Perenin, 2005). Performance is generally worse with the hand contralateral to the lesion and in the visual field contralateral to the lesion (Khan et al., 2005, 2007; Blangero et al., 2008).

Figure 1.5 Reaching for a target in an exemplary patient with optic ataxia. Left: the patient showed misreaching for a target in peripheral vision (when he had to fixate the camera lens in front of him). Right: the patient showed normal reaching under foveal vision (when he had to orient eyes and head towards the object while reaching for it). Typically, such ataxic reaches were performed most frequently with the contralesional hand in contralesional space. From Karnath and Perenin 2005.

Besides misreaching, optic ataxia patients also exhibit deficits in adjusting hand orienting (Perenin and Vighetto, 1988) and shaping (Jeannerod, 1986; Jakobson et al., 1991) during prehension of objects under visual guidance. It has been hypothesized that optic ataxia reflects a failure to transform retinal information into appropriate spatial coordinates for

22

action (Buxbaum and Coslett, 1997), and that this failure is due to the fact that the brain damage involves the human cortical territory of area V6A (Galletti et al., 1999, 2003; Pitzalis et al., 2013; Fattori et al., 2017). In agreement with this hypothesis, brain lesions restricted to area V6A in monkey produce misreaching and misgrasping during visually guided movements (Fig 1.6; Battaglini et al., 2002). In particular, V6A lesions produced underestimation of the position of reach/grasp targets, increase of reaching and grasping times, abnormality in conforming and orienting the hand towards to the targets. The overall result was an inability of correctly reaching and grasping a visual target (Fig. 1.6 C-D), especially with the arm contralateral to the lesion.
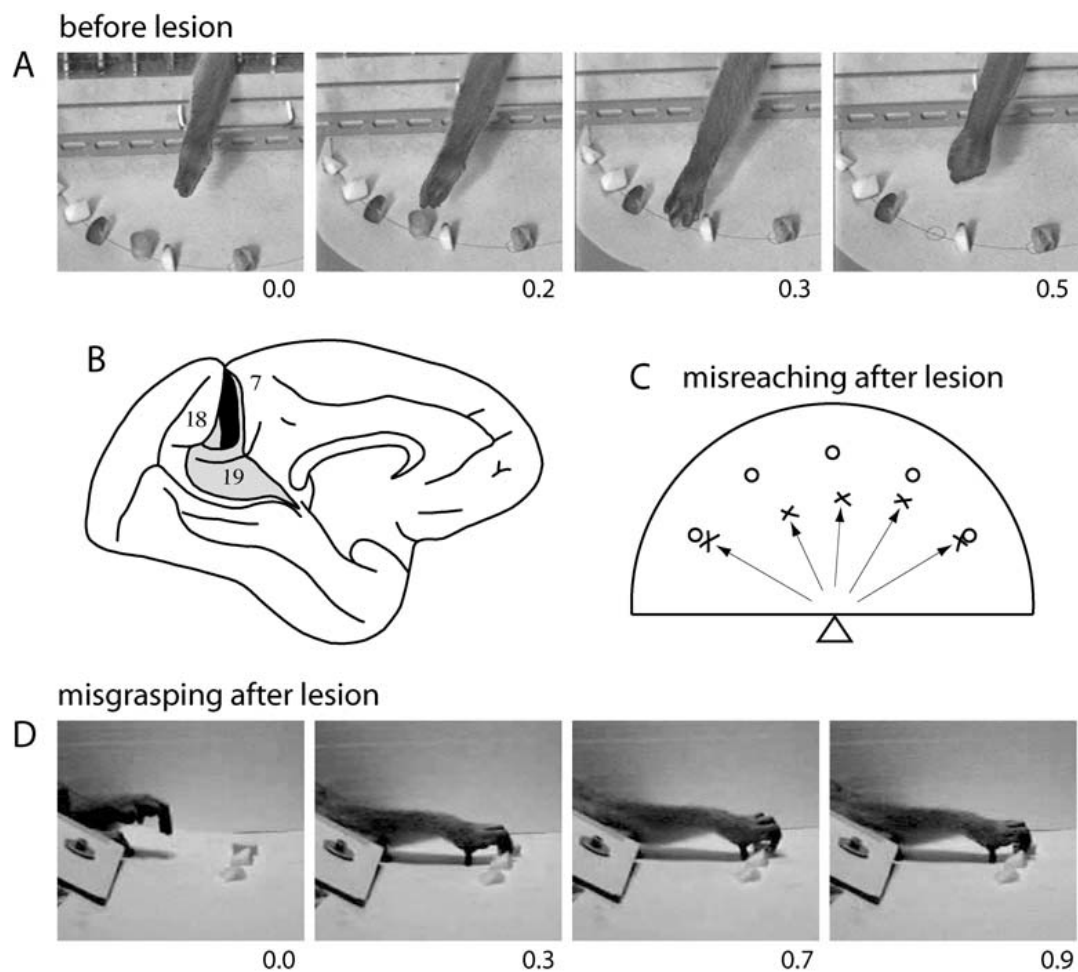
Figure 1.6 Misreaching and misgrasping after lesion of monkey area V6A. **A** Frames from a digital TV camera illustrating the behaviour of a normal animal in reaching and grasping food. Time below frames is in seconds. **B** Reconstruction of location and extent of the brain damage in case V6M2 of Battaglini et al. (2002). The lesion is indicated on the silhouette of monkey brain reported by Brodmann (1909), adapted in size to match the brain of the monkey reported by Battaglini et al. (2002). The lesion was bilateral, but here is reported (in black) only the lesion in the left hemisphere; that in the right hemisphere was very similar in location and extent (see Battaglini et al. 2002). Dorsal area 19 is shown in grey; its location and extent, as well as locations of areas 18 and 7, are according to Brodmann (1909). **C** Misreaching after bilateral V6A lesion. Food (raisins) was distributed on a semicircular plate placed horizontally in front of the animal, as shown in the frames at the top of the figure. The plate is seen here from above, and the position of the monkey is indicated by the triangle. Open circles indicate food locations. Crosses indicate the locations where the hand landed in the first attempt to reach the food. **D** Frames from a video camera the anomalous rotation of the wrist that led the fingers to close laterally rather than downward. Time below frames is in seconds. Modified from Galletti et al. 2003.

The functional characteristics of single V6A cells are congruent with the misreaching and misgrasping observed after V6A lesion. In fact, V6A neurons are influenced by the direction of arm movement (Fattori et al., 2005) as well as the depth of reaching movement (Hadjidimitrakis et al., 2014a). V6A also contains cells modulated by wrist rotation (Fattori et al., 2009; Breveglieri et al., 2016), cells active only during grasping movements and cells with a somatosensory receptive field located on the distal part of the arm, particularly on the hand (Galletti et al., 2003).

In 2013, Battaglia-Mayer and collaborators reversibly inactivated the superior parietal area 5 (PE/PEc) while monkeys executed reaches and saccades to visual targets, when the target position changed unexpectedly. After bilateral muscimol injection, researchers observed an increase of both reaction- and movement-times necessary to adjust the trajectory towards the

target. They interpreted these findings as a deficit in the online control similar to that observed in optic ataxia patients.

These evidences highlight the crucial role played by the medial PPC in spatial attention and in encoding of target location for the online control of arm movements.

1.3 Experimental techniques

1.3.1 Magnetic and Functional Magnetic Resonance Imaging

Most of the atoms that constitute the human body (including the brain) have nuclear magnetic resonance (NMR) properties: they behave like small magnets (magnetic dipoles) that spin around their axis and thus have a magnetic momentum. Normally protons contained in the atoms are aligned in a random fashion (Fig. 1.7 A). When they are exposed to a strong external magnetic field (B_0) they tend to align along the axis of the static magnetic field either in a parallel (low energy state), or in an anti-parallel configuration (high energy state) (Fig. 1.7 B). As the strength of the magnetic field increases (i.e. more Tesla), more and more atoms are in the parallel state. This increase is crucial for the quality of the magnetic resonance imaging (MRI) signal (signal-to-noise ratio). The difference of the numbers of atoms in parallel and anti-parallel state is the net magnetic moment (M), that represents the sum of the magnetic momenta of all atoms. The precessing frequency of the atoms (called the *Larmor frequency*) depends linearly on the magnetic field strength. When a radiofrequency (RF) pulse, B_1, is applied transversely to B_0, which oscillates at the *Larmor frequency*, the magnetized atoms enter in the excitation phase, and this results in a perturbation of the spins (Fig. 1.7 C).
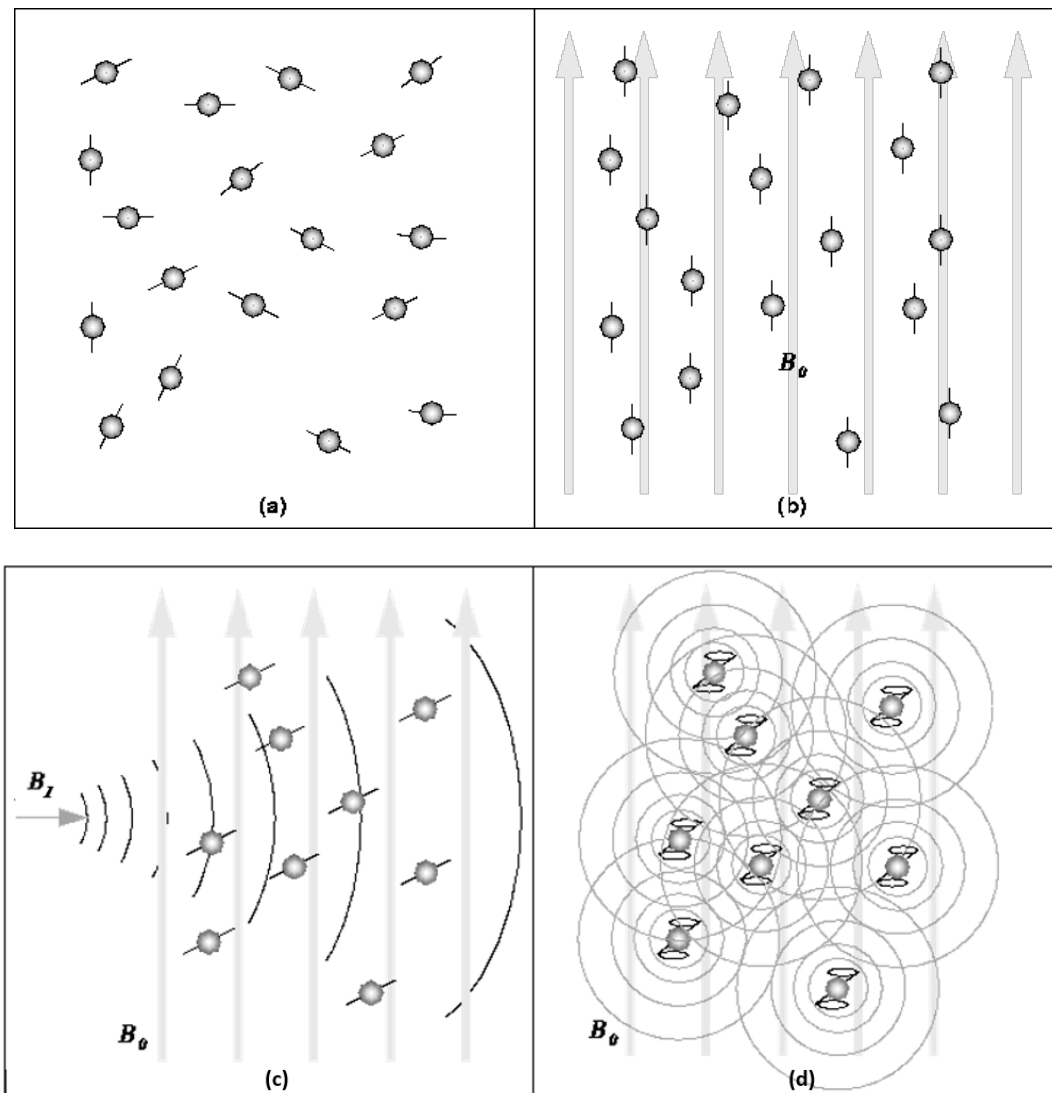
Figure 1.7 In the absence of a strong magnetic field (M=0), hydrogen nuclei are randomly aligned as in (**a**). When a strong magnetic field (**B$_0$**) is applied, the hydrogen nuclei precess about the direction of the field as in (**b**). (**c**) The RF pulse, **B$_1$**, causes the net magnetic moment of the nuclei to tilt away from **B$_0$**. (**d**) When the RF pulse stops, the nuclei return to equilibrium such that M is again parallel to **B$_0$**. During realignment, the nuclei lose energy and a measurable RF signal is emitted.

The signal can be detected by a receiver coil, as the nuclei realign themselves such that their M is again parallel with B$_0$ (relaxation), delivering back the absorbed energy (Fig. 1.7 D). The amount of released energy corresponds to the MR signal, which is composed by two

main elements: T1 (recovery), or longitudinal relaxation time, is the time constant which determines the rate at which excited protons return to equilibrium (i.e. realign itself with B_0); T2 (decay), or transverse relaxation time, is a measure of the time taken for spinning protons to lose phase coherence among the nuclei spinning perpendicular to the main field. T1 and T2 are two independent properties of each type of tissue and allow us to distinguish between them in an MR image. Local magnetic field inhomogeneities are usually observed in physiological tissues, and this adds a supplementary effect that modifies the decay phase. In this case the time constant T2 is called T2*. This latter is similar to T2, but also depends on local inhomogeneities in the magnetic field caused, for example, by changes in blood flow and oxygenation. These inhomogeneities cause the nuclei to de-phase quicker than normally. In the brain, the magnitude of these inhomogeneities depends on the physiological state, the composition of the local blood supply (Logothetis and Wandell, 2004), and the neural activity itself.

Functional Magnetic Resonance Imaging (fMRI) scans use the same basic principles of atomic physics as MRI, but MRI scans image anatomical structure whereas fMRI image metabolic function. Also, for fMRI the energy emitted from the relaxation of protons is measured, but the calculations are instead aimed at determining how the amount of oxygenated blood flow changes (hemodynamic response). Blood Oxygen Level Dependent (BOLD) fMRI depicts changes in deoxyhemoglobin concentration consequent to task-induced or spontaneous modulation of neural metabolism (Ogawa et al., 1990). This can be explained by the fact that an increase of blood flow in a specific brain region alters the local ratio of (paramagnetic) deoxyhemoglobin to (diamagnetic) oxyhemoglobin (Fig. 1.8), thus affecting T2 and T2*.
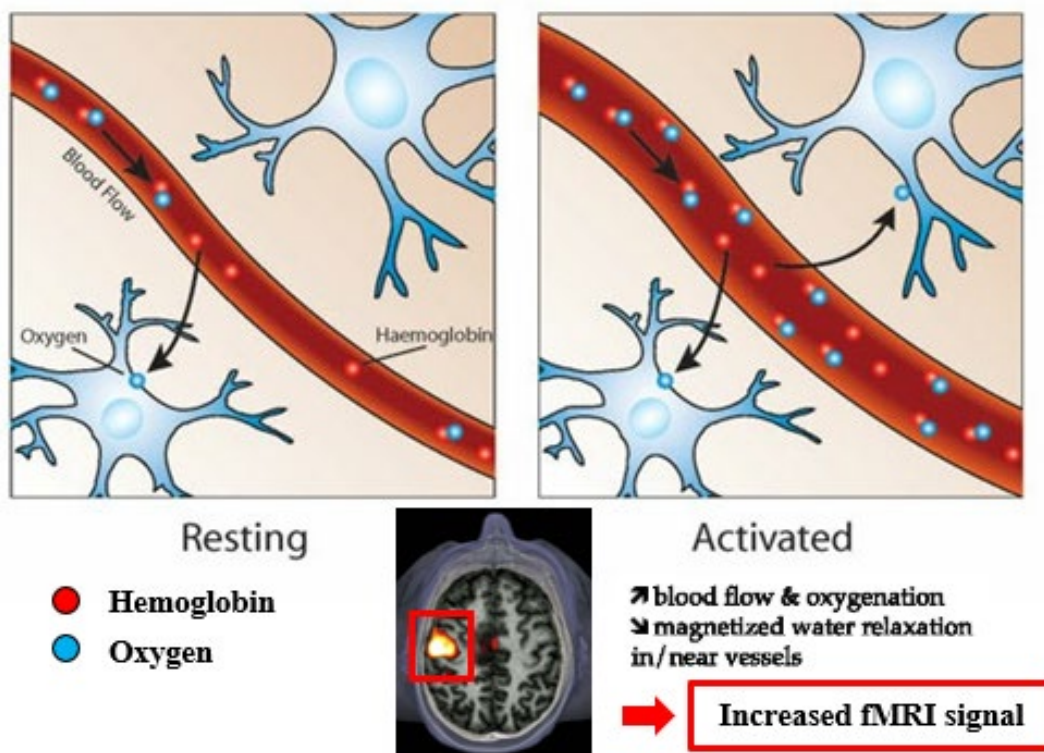
Figure 1.8 Brain activation mapping with BOLD fMRI. Water magnetization in and around small vessels is modulated by the flow of red blood cells containing paramagnetic deoxyhemoglobin. During fMRI, T2* weighted images of the activated condition (right) are compared with the same images during the rest condition (left). Adapted from Raichle (1994).

In response to brain activation, more oxygenated blood than required is supplied through the cerebral blood flow to compensate for the decrease in oxygen. This reduces the concentration of paramagnetic deoxyhemoglobin, which results in a decrease of local field inhomogeneities, an increase of the T2* and, thus an increase in the signal intensity associated with neural activity (Fig 1.8). The BOLD response generated from an event occurring at a certain time is known as Hemodynamic Response Function (HRF) (see Fig. 1.9).

Later, an alternative method, sensitive to cerebral blood volume (CBV) changes, was developed (Mandeville et al., 1998; Chen et al., 2001) to improve the sensitivity of fMRI.

This technique, known as Increased Relaxation for Optimized Neuroimaging (IRON) fMRI, is now standard use in monkey fMRI (Vanduffel et al., 2001; Leite et al., 2002; Leite and Mandeville, 2006; Zhao et al., 2006) and uses Monocrystalline Oxide Nanoparticle (MION) as exogenous contrast agent. This approach has been shown to yield a better spatial localization of the active brain regions (Mandeville and Marota, 1999; Vanduffel et al., 2001), and has been demonstrated to yield a higher contrast-to-noise ratio compared with experimental BOLD studies (Vanduffel et al., 2001; Leite et al., 2002). In comparison to BOLD signals, MION contrast is negative, due to the strong paramagnetic properties of MION, that produces a substantial increase of field inhomogeneities in the activated brain regions. This results in a drop of signal in these areas proportional to the local increase of the CBV. However, IRON contrast is usually reported as an inverted positive signal, as it is an indicator of activation (blue, Fig. 1.9).

When comparing the BOLD HRF (in red) with the HRFs used in monkey (blue, inverted to simplify comparison with the human HRF), the MION HRF peaks well earlier and decreases with a slower rate than the BOLD one.
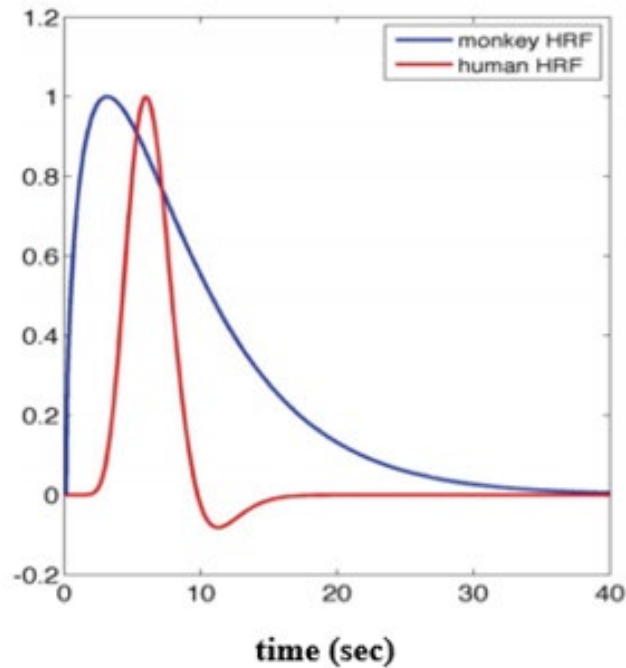
Figure 1.9 Hemodynamic response functions used in humans (red) and monkeys (blue) fMRI data analysis. Adapted from Mantini et al. 2012.

1.2.2 fMRI guided electrophysiology

fMRI is an MRI technique little more than twenty-five years old which has revolutionized the study of the human brain functions in vivo. This technique has achieved a scientific impact comparable to other important biomedical discoveries (Rosen and Savoy, 2012). Undoubtedly, it is a very useful research tool, but it has limitations. First, fMRI is an indirect measure of the activity of a large population of neurons, and this casts some doubts on the reliability of the fMRI activity maps. Moreover, each area of the brain is made up of thousands of individual neurons, each of which might have a unique story to tell. fMRI lacks sufficient spatial and temporal resolution to measure the responses of individual neurons (Logothetis, 2008; Sirotin and Das, 2009). Finally, the interpretation of fMRI data can be highly challenging and not only depends on scientific frameworks, but also on the cultural and social context (Illes and Racine, 2005).

For all these reasons, electrophysiological characterization of neural activity in fMRI-identified brain regions is critically needed. Once a region of interest is localized with fMRI, an electrode can be positioned there to record the action potentials of single or multi units and to measure the Local Field Potential (LFP) signals. Unlike unguided electrophysiological strategies (Bosman et al., 2012), fMRI-defined targets for electrophysiology experiments could restrict random recordings precisely to the regions of interest (Vanduffel et al., 2014). Because of the invasive nature of electrophysiological recordings, they cannot be performed in healthy humans. The only exception is represented by patients that have to undergo specific neurosurgical interventions. Therefore, non-human primates -most commonly macaque monkeys- are often subjects of electrophysiology experiments.

Technologies to record the spikes of individual neurons in vivo have shown an accelerating improvement over the last decades. Since their refinement in the early 1950s (Woldring and Dirken, 1950; Dowben and Rose, 1953; Green, 1958), extracellular, single-unit recording methods have been used to obtain a wealth of data about the properties of central nervous system structures. When a neuron generates an action potential, the electric current propagates through the cell, flowing in and out of the soma and axons at excitable membrane regions. If a microelectrode is inserted into the brain (Fig. 1.10), it can record the rate of change in voltage with respect to time. The most common types of microelectrodes used for recording from single neurons in behaving animals are: glass micro-pipettes, that have to be filled with an electrolyte in order to be conductive, or etched tungsten, stainless steel, or platinum–iridium wires, insulated with glass or polymers along their whole body except for the last 20-30 μm from the tip (Humphrey and Schmidt, 1990). These types of electrodes typically record from one neuron at a time.
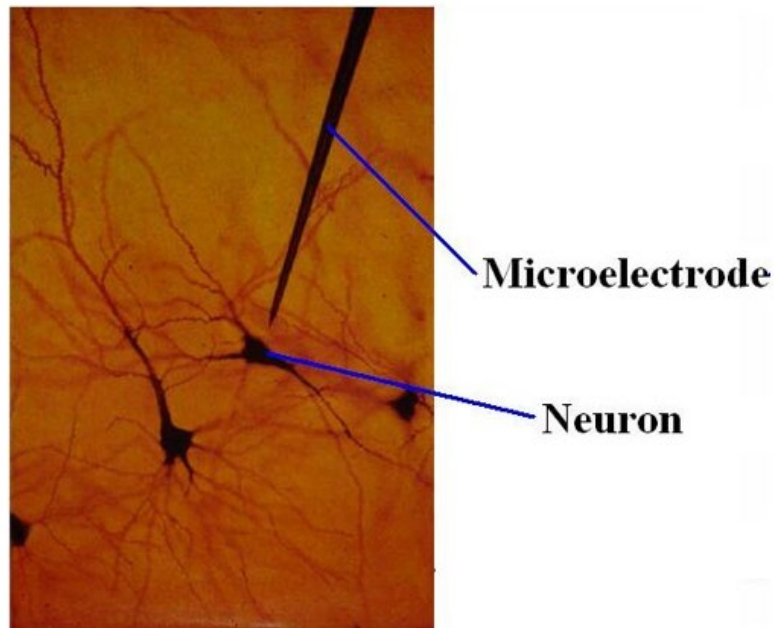
Figure 1.10 Single channel microelectrode positioned in the extracellular space.

Recent technological innovations have developed devices (i.e. multielectrode arrays) containing multiple (tens to thousands) microelectrodes through which neural signals can be recorded. Such arrays allow the simultaneous extracellular recording of multiple neurons (Fig. 1.11) in several cortical and subcortical regions of the brain of awake, behaviorally trained non-human primates (Hatsopoulos and Donoghue, 2009; Fraser and Schwartz, 2012; Schwarz et al., 2014; Dotson et al., 2015). The advantages of these tools are multiple: the possibility to place several electrodes at once, rather than individually; the ability to simultaneously receive information from numerous sites, and to select different recording sites within the array; the possibility to arrange multiple recording sites over distance of millimeters, allowing to record simultaneously across different cortical columns or across multiple layers in a single cortical column. Importantly, geometrically precise distribution of recording sites also allows to investigate spatial relation between neuronal populations.
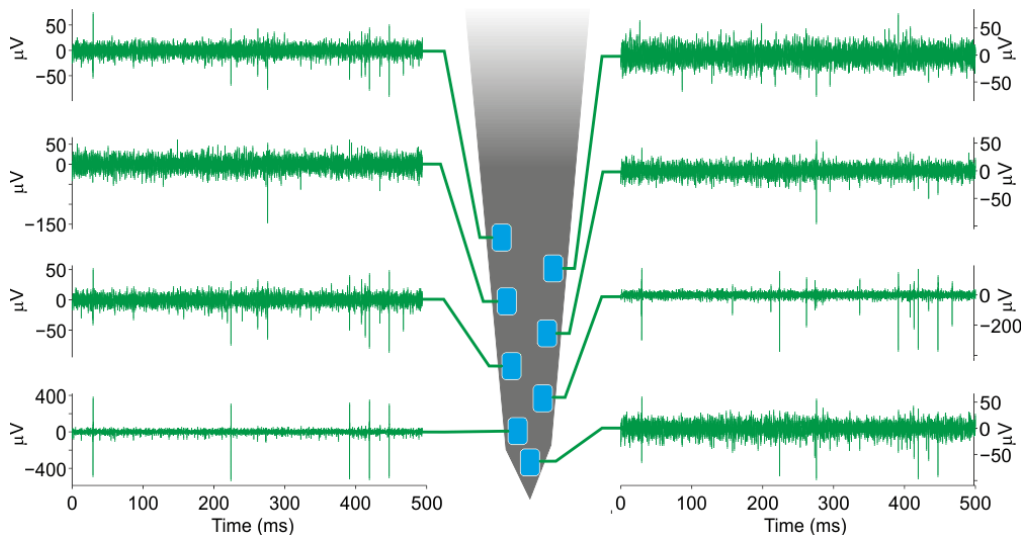
Figure 1.11 Example 8-channel probe from Cambridge Neurotech, recording activity from different thalamic neurons.

When recording in awake monkeys, the animal's head is usually fixed in place by a headpost that is cemented to the skull and anchoring screws, so that movement artifacts are minimized. This technique also allows precise measurement of the direction of gaze by monitoring eye position, an especially valuable aspect in studies where monitoring and controlling attention is important. Once having penetrated the dura mater, the (single or multiple channel) electrode is slowly lowered in the brain by means of a microdrive. Once the target region is reached, the neural signal is amplified, filtered (bandpass filter 300 Hz – 5000 Hz) and digitized.

Thanks to high spatial and temporal resolution, extracellular recordings in awake behaving animals have become a very powerful method to investigate the properties of individual neurons and to characterize the functional selectivity of a brain region.

In chapters 2 and 3 of the present thesis, we based the definition of our single-cell recording targets on the analysis of published monkey brain atlases (Paxinos et al., 2000) and *post-mortem* histology of monkeys' brains performed at University of Bologna. In the 4th chapter,

we defined our electrophysiology targets based upon the task-related activation of an fMRI experiment performed at the KU Leuven.

1.4   Objectives of research

The overall goal of this thesis was to investigate the heterogeneous functional nature of monkey medial PPC. To do this, we performed three experiments involving two cortical areas positioned at the border between visual and somatosensory systems: area V6A, a visuomotor area located in the anterior bank of the parieto-occipital sulcus, and area PE, residing mainly on the exposed postcentral gyrus, directly caudal to the somatosensory cortex. The specific aims of our studies were:

1. Investigate the relative contribution of visual information and hand shape to the neuronal activity of area V6A during a Reach-to-Grasp task performed, both in darkness and under light conditions. This required the subjects to grasp objects of different shapes (See chapter 2: "Interplay between grip and vision in the monkey medial parietal lobe" – published).

2. Investigate depth and direction coding of arm reaching movements and their time course during a Fixation-to-Reach task performed in the darkness. This required the subjects to reach targets in the 3D space. We used the same task configuration as in our previous studies of more caudal PPC sectors (areas V6A and PEc, Hadjidimitrakis et al., 2014a, 2015), thus allowing a direct comparison between these three PPC areas (See chapter 3: "The neglected medial part of macaque area PE: segregated processing of reach depth and direction" – published).

3. Examine the neural correlates of covert shifts of spatial attention in the ventral part of area V6A, using a covert selective spatial attention paradigm highly resembling the one used in human (Molenberghs et al., 2007) and monkey (Caspari et al., 2015) fMRI experiments (See chapter 4: "fMRI guided electrophysiology of spatial attention shifts in the macaque superior parietal lobule" – in preparation).

Chapter 2

Interplay between Grip and Vision in the Monkey Medial Parietal Lobe.

2. Interplay between grip and vision in the monkey medial parietal lobe

2.1 Abstract

We aimed at understanding the relative contribution of visual information and hand shaping to the neuronal activity of medial posterior parietal area V6A, a newly added area in the monkey cortical grasping circuit. Two *Macaca fascicularis* performed a Reach-to-Grasp task in the dark and in the light, grasping objects of different shapes. We found that V6A contains Visual cells, activated only during grasping in the light; Motor neurons, equally activated during grasping in the dark and in the light; Visuomotor cells, differently activated while grasping in the dark and in the light. Visual, Motor, and Visuomotor neurons were moderately or highly selective during grasping, whereas they reduced their selectivity during object observation without performing grasping. The use of the same experimental design employed in the dorsolateral grasping area AIP by other authors allowed us to compare the grasp-related properties of V6A and AIP. From these data and from the literature a frame emerges with many similarities between medial grasping area V6A and lateral grasping area AIP: both areas update and control prehension, with V6A less sensitive than AIP to fine visual details of the objects to be grasped, but more involved in coordinating reaching and grasping.

2.2   Introduction

Information about the physical characteristics of objects to be grasped (such as size, shape and orientation) and their spatial location is fundamental for the correct execution of a grasping movement. The ability to grasp objects relies on a network of areas in the parietal and frontal cortex (Jeannerod et al., 1995; Rizzolatti, 1997; Janssen and Scherberger, 2015; Fattori et al., 2017). Among areas involved in the grasping circuit, area V6A has been recently added; this area is located in the posterior parietal cortex (PPC), in the caudalmost part of the superior parietal lobule. V6A belongs to the dorsomedial visual stream (Galletti et al., 2003; Rizzolatti and Matelli, 2003), but is directly connected with the dorsolateral grasping parietal area (anterior intraparietal area, AIP) (Borra et al., 2008; Gamberini et al., 2009). Thanks to the seminal works by Sakata and collaborators (Taira et al., 1990; Sakata et al., 1995; Murata et al., 1996, 2000), who tested AIP neurons when grasping of different objects occurred in the light and in the dark, area AIP was proved to be involved in grasping actions. Moreover, it was shown that some AIP neurons received both visual and grip information ('Visual and Motor' neurons), some others received only visual input ('Visual dominant' neurons) and others only motor-related information ('Motor dominant' neurons) (Taira et al., 1990; Sakata et al., 1995; Murata et al., 2000). More recent works shed new light on other grasp-related properties of AIP, demonstrating that its neurons are modulated by the context of the grasping action (Baumann et al., 2009) and by directional signals of arm movements (Lehmann and Scherberger, 2013) and that signals from AIP can be used to decode grasping actions (Schaffelhofer et al., 2015; Schaffelhofer and Scherberger, 2016). Even more recently, it was demonstrated that AIP cells respond to the vision of one's own hand in action (Maeda et al., 2015) and that they are specialized in shape processing and

processing of object features important for grasping (Gardner et al., 2007b; Chen et al., 2009; Schaffelhofer and Scherberger, 2016).

Thanks to the functional properties of its neurons (Fattori et al., 2017), and to its connections with area AIP and premotor area F2 (Matelli et al., 1998; Shipp et al., 1998; Borra et al., 2008; Gamberini et al., 2009), both containing grasping cells (Taira et al., 1990; Raos et al., 2004), V6A has the necessary functional properties and anatomical connectivity to support, in principle, the integration of visual and motor signals needed for visual guidance of prehension. In other words, V6A can be assigned the role of 'dorsomedial grasping area'. Up to now, V6A grasp-related neurons were studied for natural grasping (Fattori et al., 2004), and in controlled tasks testing different hand orientations (Fattori et al., 2009) and different grip types (Fattori et al., 2010, 2012) in darkness. More recently, it has been demonstrated that the modulation of V6A grasping activity by wrist orientation is deeply influenced by visual feed-back (Breveglieri et al., 2016) however, the effect of visual feed-back on modulation of V6A grasping activity by grip type has never been tested .

The main purpose of the present work was to analyze the interplay between grip type and visual information in V6A cells, using a paradigm with several objects of different shapes (requiring different grip types) and different visual backgrounds. Moreover, we compared V6A grasping responses with grasping responses of area AIP studied in similar experimental conditions (Murata et al., 2000). We also studied the grasp-related properties of V6A cells using the same paradigm designed for AIP by Baumann and coworkers (2009) and Schaffelhofer and Scherberger (2016) in order to compare the grip preference and temporal evolution of neural discharges from object vision to grasp performance between V6A and AIP.

2.3   Materials and Methods

2.3.1   Experimental procedures

The study was performed in accordance with the guidelines of EU Directives (EU 116-92; EU 63-2010) and Italian national law (D.L. 116-92, D.L. 26-2014) on the use of animals in scientific research. During training and recording sessions, particular attention was paid to any behavioral and clinical sign of pain or distress.

Two male *Macaca fascicularis*, weighing 2.5-4.0 kg, were trained to perform a Reach-to-Grasp task and an Observation task under controlled conditions.

2.3.2   Behavioral tasks

The monkey was seated in a primate chair (Crist Instrument) with the head fixed, in front of a box containing a PC-controlled rotating carousel subdivided into five sectors, each containing a different object presented one at a time, in a random order.

A variety of objects of different shapes were used (Fig. 2.1A). The types of grip evoked by the various objects changed according to their physical characteristics. The two monkeys used identical hand postures for grasping the same objects and the overall similarity of the grips performed by the two monkeys was confirmed by comparing the video images of their hand postures during grasping. The objects and the grip types used for grasping them (Fig. 2.1A) are as follows: "ball" (diameter: 30 mm) grasped with *whole-hand prehension*, with all the fingers wrapped around the object and with the palm in contact with it; "handle" (thickness, 2 mm; width, 34 mm; depth, 13 mm; gap dimensions, 2x28x11 mm) grasped with *finger prehension*, all fingers except the thumb inserted into the gap; "ring" (external diameter, 17 mm; internal diameter, 12 mm) grasped with the *hook grip*, the index finger was

inserted into the hole of the object; "plate" (thickness, 4 mm; width, 30 mm; length, 14 mm) grasped with the *primitive precision grip,* using the thumb and the distal phalanges of the other fingers; "cylinder-in-groove" (cylinder with base diameter of 10 mm and length of 11 mm, in a slot 12 mm wide, 15 mm deep, and 30 mm long) grasped with the *advanced precision grip*, with the pulpar surface of the last phalanx of the index finger opposed to the pulpar surface of the last phalanx of the thumb.

The object selected for each trial was set up by a PC-controlled rotation of the carousel during the intertrial period. Only the selected object was visible in each trial; the view of the other objects was occluded. The objects were always presented in the same spatial position (22.5 cm away from the animal, in the midsagittal plane).

Animals performed two tasks: 1) Reach-to-Grasp in the light ("visually-guided", Fig. 2.1B) and in darkness ("memory-guided", Fig. 2.1B), and 2) Observation task, where no reach-to-grasp movement was required or performed (Fig. 2.1C). All tasks began when the monkey pressed a "home" button (2.5 cm in diameter, placed outside the animal's field of view, 5 cm in front of the chest, on the animal's midsagittal line), in complete darkness (Fig. 2.1B, C). After button pressing, the animal awaited instructions in darkness (*Free*). It was free to look around, though remaining in darkness. After 0.5-1 s, the fixation LED (masked by a 1.5 mm aperture: fixation point) lit up and the monkey had to fixate on it. After a fixation period of 0.5–1 s *(Fixation)*, two white lateral LEDs were turned on and the object was illuminated (circular area of 8 cm diameter with the object in the center) for a period of 0.5 s (*View*). These events were common to all tasks; the object presentation was the cue for all subsequent events as it instructed the animal which object should be grasped.

The two tasks diverged after these events. In the *Reach-to-Grasp* task in the light, the lights on the objects stayed on and the animal could perform visually-guided reach, grasp and hold actions. In the Reach-to-Grasp task in darkness, the light on the object turned off and the

monkey had to remember the required action properly. In the dark condition, the brightness of the fixation point was reduced so that it was barely visible during the task: standing by the monkey, the experimenter could not see the object or the monkey's hand moving in the peripersonal space, even after an adaptation period. Thus, in this condition we have to exclude the possibility that the cell's modulation during grasp preparation, execution, and object holding could be the consequence of visual stimulation evoked by the vision of the arm moving in the visual field. Despite these differences, the timeline of the two conditions of the Reach-to-Grasp task was the same: after a delay period of 1-1.5 s, during which the monkey was required to maintain fixation on the fixation point without releasing the home button (*Delay*), the color of the fixation point changed. This was the go-signal for the monkey to release the button and perform a Reach-to-Grasp movement (*Mov*) to reach and grasp the object, pull it and keep holding it (*Hold*) till the fixation point switched off (after 0.8-1.2 s). The fixation point switch-off cued the monkey to release the object (*Return*) and to press the home-button again. Home-button pressing ended the trial, allowed the monkey to receive its reward, and started another trial (*Free*) in which another object, randomly chosen, was presented.

A

OBJECTS

ball   handle   ring   plate   cylinder in-groove

GRIPS

whole-hand prehension   finger prehension   hook grip   primitive precision grip   advanced precision grip

B

REACH-TO-GRASP TASK

LIGHT: visually-guided grasping

Delay   Go   Mov   Hold

Free   Fixation   View   Return

DARK: memory-guided grasping

0.5-1s   0.5-1s   0.5s   1-1.5s   0.8-1.2s

Home Button   push / release

Fixation LED   red / green / off

Illumination (dark)   on / off

Illumination (light)   on / off

Target object   pull / off

Eye   x / y

FREE   FIX   VISG   DELAY   MOV   HOLD

C

OBSERVATION TASK: no grasping

Free   Fixation   View   Go

0.5-1s   0.5-1s   1 s

Home Button   push / release

Fixation LED   red / green / off

Illumination   on / off

Eye   x / y

FREE   VIS

LONGVIS

43

Figure 2.1 Tested objects and tasks. A) Representation of the 5 objects tested and of the grip types used by the monkey: from left to right, ball (grasped with the whole hand), handle (grasped with finger prehension), ring (grasped with the index finger), plate (grasped with a primitive precision grip), cylinder-in-groove (grasped with an advanced precision grip). B) Time course and time epochs in the Reach-to-Grasp task in the light and in the dark. The sequence of status of the Home Button, color of the fixation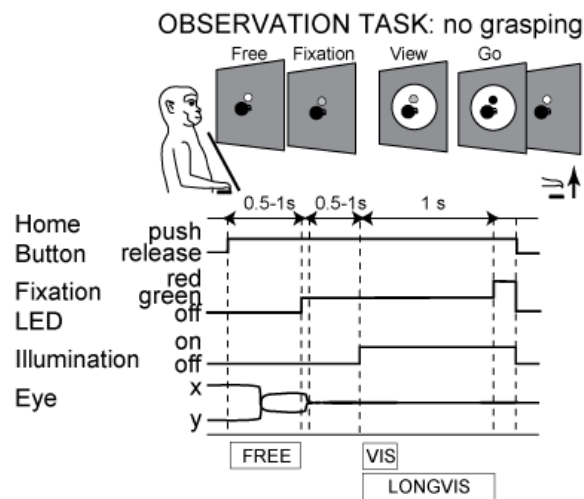 point (Fixation LED), status of the light illuminating the object (Illumination) in dark and in light condition, and status of the Target object are shown. Below the diagram, typical examples of eye traces during a single trial and time epochs are shown. Dashed lines indicate task and behavioral markers: trial start (Home Button push), fixation target appearance (Fixation LED green), eye traces entering the fixation window, object illumination onset (illumination on, both for light and dark conditions), object illumination offset (illumination off, only in dark condition), go signal for reach-to-grasp movement (Fixation LED red), movement onset (Home Button release), movement offset (Target object holding), fixation target switching off (Fixation LED off), Target object release (off, coincident with object illumination off in light condition). Rectangles below time course indicate functional time epochs. Above the time course, cartoons of the trial sequence are shown. C) Time course and time epochs in the Observation task. The sequence of status of Home Button, Fixation LED, Illumination of the object (illumination), and eye traces are shown. Markers are, from left to right: trial start (Home Button push), fixation target appearance (Fixation LED green), eye traces entering the fixation window, object illumination on (Illumination on), go signal for home button release (Fixation LED red), Home Button release, coincident with illumination off. All other details as in B).

In the *Observation* task (Fig. 2.1C), after 1s of object illumination, a color change of the fixation point (from green to red, *Go*) instructed the monkey to release the home button. The lights illuminating the object were then turned off and monkey could break fixation, receiving its reward. Reach and grasp actions were not required in this task, and a door at the front of the chair blocked hand access to the object.

All tasks (Reach-to-grasp tasks in the light and in the dark, and Observation task) were performed in separate blocks. In each task, five objects were presented 10 times each in random order in a block of 50 correct trials. The animal learned that the presence of the blocking door at the beginning of the block meant that arm movement was not required. After some training sessions in which the animal tried to perform the arm movement anyway, and was not rewarded, it learned not to move the arm during the Observation task. The purpose of this 'no reach/no grasp condition' was to change the context of the visual cue from one of motor behavior (preparation of an appropriate hand posture for grasping) to one of passive object viewing.

During all task conditions, the monkey was required to fixate on the fixation point. If fixation was broken (5°×5° electronic window), trials were interrupted on-line and discarded. The correct performance of movements was monitored by pulses from microswitches (monopolar microswitches, RS Components, UK) mounted under the home button and the objects. Button/object presses/releases were recorded with 1 ms resolution. For a detailed description of the trial execution control system see Kutz et al. (2011). Monkeys' arm movements were continuously video-monitored by means of miniature, infrared-illumination-sensitive videocameras.

2.3.3 *Surgical and recording procedures*

After training completion, a head-restraint system and a recording chamber were surgically implanted in asepsis and under general anesthesia (sodium thiopental, 8 mg/kg/h, *i.v.*) following the procedures reported in Galletti et al. (1995). Adequate measures were taken to minimize pain or discomfort. A full program of postoperative analgesia (ketorolac trometazyn, 1mg/kg, *i.m.,* immediately after surgery, and 1.6 mg/kg, *i.m.*, on the following

days) and antibiotic care [Ritardomicina® (benzathine benzylpenicillin + dihydrostreptomycin + streptomycin) 1-1.5 ml/10kg every 5-6 days] followed the surgery.

Single neurons were extracellularly recorded from area V6A of the anterior bank of the parieto-occipital sulcus. We performed single microelectrode penetrations using homemade glass-coated metal microelectrodes, and multiple electrode penetrations using a five-channel multielectrode recording minimatrix (Thomas Recording, GMbH, Giessen, Germany). The recording procedures we used are described in detail in Fattori et al. (2012). Spikes were sampled at 100 KHz and eye position was simultaneously recorded at 500 Hz using an infrared oculometer (Dr. Bouis, Karlsruhe, Germany). Behavioral events were recorded with a resolution of 1 ms.

Histological reconstruction of electrode penetrations was performed as described in detail in other works (Galletti et al., 1999; Gamberini et al., 2011). Briefly, electrode tracks and the approximate location of each recording site were reconstructed on histological sections of the brain on the basis of marking lesions and several other cues, such as the coordinates of penetrations within the recording chamber, the kind of cortical areas passed through before reaching the anterior bank of the parieto-occipital sulcus and the distance of the recording site from the surface of the hemisphere.

2.3.4   Data analysis

The analyses were performed using custom scripts in Matlab (Mathworks, Natick, MA, US) and SPSS software.

Analysis of the neuronal activity during the Reach-to-Grasp task either in the dark or in the light was made by quantifying the discharge recorded during each trial in the following time epochs (Fig. 2.1B):

• *FREE*: from home button pressing to the illumination of the fixation LED. This 0.5-1s period of darkness, when gaze was unrestricted, was used to calculate baseline firing when categorizing V6A neurons as Visuomotor, Visual, or Motor, as performed by Murata in AIP (Murata et al., 1996).

• *FIX*: the first 500 ms of gaze fixation on the fixation LED. Firing rates during this interval were used as the reference value for statistical comparison to subsequent task epochs to determine the task-related population.

• *VISG:* response to object presentation, from 40 ms after object illumination to 300 ms after it (total duration: 260 ms).

• *DELAY*: the last 500 ms before the go-signal. It contains the cell discharge during arm movement preparation.

• *MOV*: from 200 ms before movement onset (home-button release) to movement end (object pulling). It contains the discharge of the cell during grasping execution.

• *HOLD*: from object pulling to 200 ms before the onset of return movement (object release). It contains the discharge of the cell during object holding.

For the Observation task (Fig. 2.1C):

• *FREE*: from home button pressing to the illumination of the fixation LED.

• *VIS*: transient response to object presentation, from 40 ms after object illumination to 300 ms after it (total duration: 260 ms).

• *LONGVIS*: sustained response to object presentation, from 40 ms after object illumination to 1000 ms after it (total duration: 960 ms).

The epochs quantifying visual responses to object illumination (VISG, VIS and LONGVIS) start at 40 ms because visual responses in V6A have a delay of this order (Kutz et al., 2003).

We analyzed only those units tested in at least 7 trials for each object/grip. The reasons for these conservative criteria are dictated by the intrinsic high variability of biological responses (Kutz et al., 2003).

We performed a 3-way ANOVA (factor1: epoch - FIX, DELAY, MOV, HOLD; factor2: objects - 5 levels, one for each objects tested; factor3: visual condition - dark, light) on all the recorded cells. Task-related cells were defined as cells with a significant epoch effect followed by a significant difference between FIX and at least one of the epochs DELAY, MOV, HOLD (post-hoc comparisons, $p<0.05$, Bonferroni corrected for multiple comparisons). FIX was chosen as a reference because in this epoch no visual stimuli were present, the animal's gaze was still, and the monkey was not executing or preparing any arm movement. Task-related cells were further analyzed.

Significant modulation of neural activity by the grip type or visual task conditions was studied by a two-way ANOVA (factor 1: object (5 levels, one for each objects tested); factor 2: visual condition (2 levels, light, dark); $p<0.01$) in each task epoch (Fig. 2.2A).

In addition, tuning significance for grip type and visual condition was tested at multiple time points t using a two-way ANOVA on the spike count in a 200 ms window centered around t. This test was repeated in time steps of 50 ms (sliding window ANOVA, Fig. 2.2B). Criteria for significant tuning were the same as for the ANOVA analysis of the fixed time epochs. For the purpose of comparison of V6A data with AIP in the same analytical conditions, we also repeated the sliding ANOVA in time steps of 1ms (Fig. 2.8A).

Population responses of tested neurons were computed as average spike density functions (SDFs). An SDF was calculated (Gaussian kernel, half-width 40 ms) for each neuron included in the analysis. SDF was averaged across all trials for each tested grip, separately for light and dark conditions. We found the peak discharge rate of the neuron during the epoch of interest, and used it to normalize SDF. The normalized SDFs were then averaged to

derive population responses (see Marzocchi et al. 2008). We statistically compared the population SDFs in dark and light conditions with a permutation test (10,000 iterations) comparing the sum of squared errors of the actual and randomly permuted data. We ran the permutation test in the epochs VISG, DELAY, MOV and HOLD, as already defined. In the permutation test, post-hoc comparisons were performed, thus correcting for multiple comparisons.

We also performed demixed principal component analysis (dPCA, for details see Kobak et al. 2016), by the free code available at: http://github.com/machenslab/dPCA. In contrast to PCA, dPCA reduces the dimensionality of the data, taking task parameters (i.e., sensory and motor variables controlled or monitored by the experimenter) into account. Consequently, this technique avoids mixed selectivity from remaining in the data even after the dimensionality reduction step, impeding interpretation of the results. Thus, the most important advantage of dPCA, compared to standard PCA, is that each component does not show mixed selectivity, but they result 'demixed'. This demixing simplifies exploration and interpretation of neural data, as shown by Kobak and collaborators (2016). The time courses of dPCA signals were compared by a permutation test (see Fattori et al. 2010).

2.4   Results

To study the contribution of visual feedback and hand shaping on the activity of V6A neurons during grasping of three-dimensional, graspable objects, we employed a Reach-to-Grasp task in which the monkeys reached to and grasped objects of different shapes in the dark and in the light (Fig. 2.1B). In both visual conditions, the Reach-to-Grasp task required the monkey to move its hand from a position near the body to a fixed position in the peripersonal space where the object was presented. In the task performed in the dark, the

object had to be grasped in darkness after a brief visual presentation. In the task performed in the light, the object and the working space were illuminated during grasping preparation, execution, and object holding. Each trial randomly presented one of 5 objects shown in Fig. 2.1A. Each object was grasped with a distinct hand posture (Fig. 2.1A), allowing us to equate object shape to hand grip.

Single-unit activity was recorded from 317 neurons of area V6A in two monkeys (case 1, N=134; case 2, N=183). Results were consistent between animals (Chi-squared test, p>0.05), and are thus presented jointly. A three-way ANOVA was used to assess whether a cell was task-related (see Materials and Methods). Epochs of interest were: 1) movement preparation (epoch DELAY, the last 500 ms before the instruction signal to Reach-to-Grasp the object), 2) grasping execution (epoch MOV, from 200 ms before the movement onset to movement end) and 3) object holding (epoch HOLD, from the onset of object holding to 200 ms before the return movement onset). 276 of the 317 recorded cells (87%) showed task-related activity.

Furthermore, two-way ANOVA analysis (p<0.01) revealed that both visual condition (dark vs light) and grip type (specific object shape) significantly influenced the firing rates of the majority of task-related neurons in each of the three epochs (Fig. 2.2A, VISUAL CONDITION&GRIP). 41% of the task-related cells were modulated during grasping preparation (DELAY), 59-60% during movement execution (MOV) and object holding (HOLD). The individual factors (VISUAL CONDITION or GRIP) influenced only a minority of V6A cells (about 10-20% depending on the epoch).

To investigate the tuning for grip type and visual condition over time, without constraining the analysis to fixed epochs, we extended the 2-way ANOVA on a sliding window approach (width: 200 ms, step: 50 ms). As shown in Fig. 2.2B, this analysis revealed that, right after object illumination and after movement onset, the percentage of cells modulated by grip was

higher than the percentage of cells modulated by visual condition. During DELAY, before

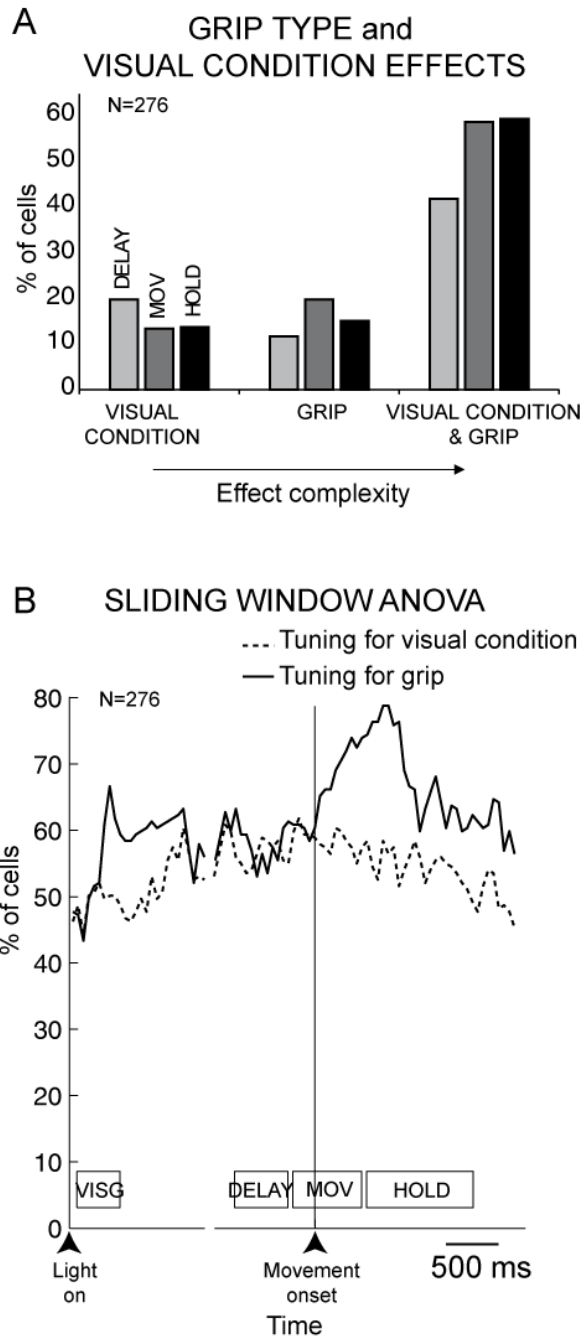movement execution, the influence of the two factors was similar.

Figure 2.2 Population data. A) Distribution of the incidence of significant effects modulating V6A

cells during the time-course of the task. Histograms show the results of two-way ANOVA as

incidence of modulated cells during the grasping preparation (epoch DELAY), execution (epoch

MOV) and object holding (epoch HOLD). The results are shown with respect to effect complexity, that is, from left to right, the main effects and the effect of both factors. Numbers of modulated cells: effect of visual condition: N= 57 (DELAY), N= 36 (MOV), N= 39 (HOLD); effect of grip type: N= 34 (DELAY), N= 52 (MOV), N= 42 (HOLD); effect of both visual condition and grip type: N= 113 (DELAY), N= 163 (MOV), N= 165 (HOLD); no effect (not shown in the figure): N= 71 (DELAY), N= 25 (MOV), N= 30 (HOLD). B) Percentage of tuned cells by grip type (continuous line) and visual condition (dashed line) in a sliding window ANOVA (width: 200 ms, centered on each data point). Trials are aligned on the 2 arrowheads: illumination of the object (light onset) and movement onset. Rectangles below each plot indicate the functional time epochs (VISG, DELAY, MOV, HOLD).

2.4.1 *Visual, Motor and Visuomotor cells*

We divided V6A neurons modulated in MOV (N=238) into three categories (Visuomotor, Visual, and Motor) based on firing rates during the MOV epoch during visually and memory guided trials in the light and dark, respectively. Murata and collaborators used the same classification scheme to study AIP (Murata et al., 2000), thus enabling a direct comparison of V6A with AIP neurons. Visuomotor neurons had different grasp-related firing rates in the light and the dark, and both rates were significantly higher than the responses in the baseline interval (FREE). Visual neurons showed grasp-related firing in the light but not in the dark. Motor neurons fired at similar rates in the light and the dark during grasping. A total of 39% were Visuomotor cells (N= 92/238), 31% were Visual cells (N= 74/238), and 30% were Motor cells (N=72/238).

Those Visual and Visuomotor neurons that were also tested with the Observation task (N=125) were further subdivided into two classes similarly to what was reported for AIP neurons (Taira et al., 1990; Sakata et al., 1995; Murata et al., 2000): 'Object-type' neurons, if the neurons also responded to the passive vision of the object in the Observation task

(Student's t-test between FREE and VIS, p<0.05) without any possibility to grasp it; 'Nonobject-type' neurons, if they did not respond to the passive vision of the object (p>0.05). We found that the majority of Visual and Visuomotor neurons were *Object-type* (N= 76/125, 61%). The remaining 59 cells were Motor cells and were not further subdivided, as done in AIP (Murata et al., 2000).

A neuron was classified as 'Visual' if its discharge during MOV was significantly higher than the discharge during FREE in the light but not in the dark (Student's t-test, p<0.05). The cell shown in Figure 2.3A is an example of Visual neuron. The activity was on average higher in light than in dark conditions. The neuron discharged strongly during the vision of the object (V in the figure) and during the execution of Reach-to-Grasp actions (M) in the light, with a preference for advanced precision grip and whole-hand prehension (1st and 3rd panels). This cell discharged weakly (or not at all) for the other three grasps. No activations were present, even in the light, during DELAY. The stronger responses during grasping observed only in the light and in MOV were likely caused by the vision of the hand approaching and grasping the objects. The fact that this response in the light occurred after the hand has left the home button (second alignment) corroborates a visually driven explanation of this discharge. This view is also supported by the fact that the 2 preferred actions did not share anything from the point of view of motor control, the advanced precision grip and the whole hand prehension being at the 2 extremes of grasping difficulty. Interestingly, the cell response during object observation is different in the dark and in the light, as reported for the population discharge (Fig. 2.5A left, see below).

A neuron was classified as 'Motor' if its discharge during MOV: i) was significantly different with respect to the discharge during FREE in both the dark and the light (Student's t-test, p<0.05) and ii) was similar in the dark and in the light (Student's t-test, p>0.05). In these cells, adding the visual information did not consistently modify the discharge during

grasping execution. The cell in Figure 2.3B is a Motor neuron. This cell fired strongly for grasping all the objects tested, with a preference for grasping the handle and the plate (2nd and 4th panels), that share a flat shape. The lack of effect of the light upon the grasp-related discharge led us to suggest that a tactile or proprioceptive input from the arm (known to affect V6A discharges, (Breveglieri et al., 2002; Gamberini et al., 2011; Fattori et al., 2017) or an efference copy of the motor command (justified by the demonstrated anatomical input of the dorsal premotor cortex to V6A; (Matelli et al., 1998; Shipp et al., 1998; Gamberini et al., 2009) may be responsible for this discharge during grasping.

A neuron was classified as 'Visuomotor' if its discharge during MOV: i) was significantly different with respect to the discharge during FREE in the dark, or in both the dark and the light (Student's t-test, $p < 0.05$) and ii) was different between the dark and the light (Student's t-test, $p < 0.05$). Fig. 2.4 shows two examples of Visuomotor cells, the most represented class of grasping cells in V6A. Figure 2.4A and B reports an example of Visuomotor 'Object-type' neuron. This cell was strongly activated during preparation and execution of grasping both in light and in dark conditions, although it discharged more in the light (Student's t-test, $p < 0.05$, Fig. 2.4A). The cell showed a clear grip sensitivity, discharging more strongly for the preparation and execution of finger prehension, whole-hand prehension and primitive precision grips (2nd, 3rd and 4th panels). It is worth noting that also the DELAY activity (D in the figure) of this cell was modulated consistently with grasping activity.
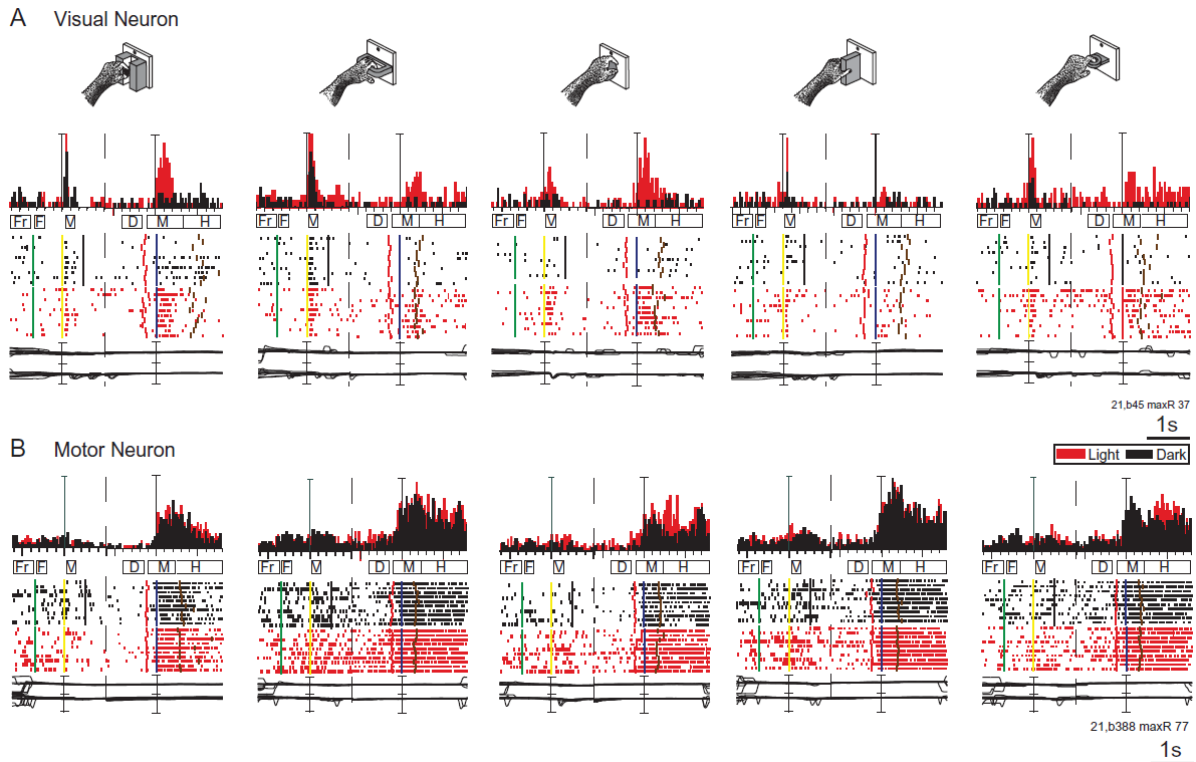
Figure 2.3 Example of the discharge of a V6A *Visual* neuron (A) and of a *Motor* neuron (B) to five different grips and to two visual backgrounds. A) Top: type of handgrips. Middle: peristimulus time histograms. Horizontal scale: 200 ms/div. Vertical scale bar on histogram: 37 spikes/s; eye traces: 60°/division. Rectangles below histograms indicate the duration of the epochs FREE (Fr), FIX (F), VISG (V), DELAY (D), MOV (M), HOLD (H). Data collected in the dark are depicted in black, those collected in the light are in red. Below histogram: raster displays of impulse activity. Behavioral markers are depicted in different colors: green: fixation point onset; yellow: illumination onset; black: illumination offset, in the dark condition; red: go signal; blue: movement onset: brown: movement end. Bottom: record of horizontal (upper trace) and vertical components (lower trace) of eye movements, shown with the same alignment as the neural activity. The activity of cells in each plot was aligned twice, on fixation onset and on arm movement onset (two continuous vertical lines), with a dashed vertical line indicating the interruption of the trials to obtain the double alignment. (B) All conventions are as in A, vertical scale on histogram: 77 spikes/s.

During the Observation task (Fig. 2.4B), the response to the object presentation ('V' in the figure) was consistent with the visual response shown by the cell in the grasping task: strongest response for observation of the handle, weakest for the cylinder in the groove. This cell also showed a sustained visual response (LV) coherent with the transient visual response (V). This sustained visual response that follows the brisk response to object presentation may reflect object affordance (Fattori et al., 2012; Breveglieri et al., 2015). In other words, we suggest that V6A Visuomotor cells encode visuomotor parameters even when an explicit motor activation is not required. The fact that the activity in the DELAY is tuned according to the grasping sensitivity but is different in the light and in the dark suggests that the cell receives somatosensory/motor-related and visual information. In summary, this Visuomotor cell was modulated by grasping in the dark, by hand-object vision, and by object observation outside the grasping context.

Figure 2.4C, D shows an example of Visuomotor Nonobject-type neuron. In the Reach-to-Grasp task (Fig. 2.4C) the activity of this cell was not tuned for objects during grasping preparation (D). It was tuned during grasping execution (M), showing very low grip sensitivity and higher activity in light conditions no matter what type the grasping was. In the Observation task (Fig. 2.4D), this cell was not activated during viewing of any object, showing neither a transient (V) nor a sustained (LV) visual response. In summary, this neuron was sensitive to information related to the arm movement and to visual information related to the occurrence of the grasping, but it was not sensitive to the visual features or affordance of the object to be grasped.
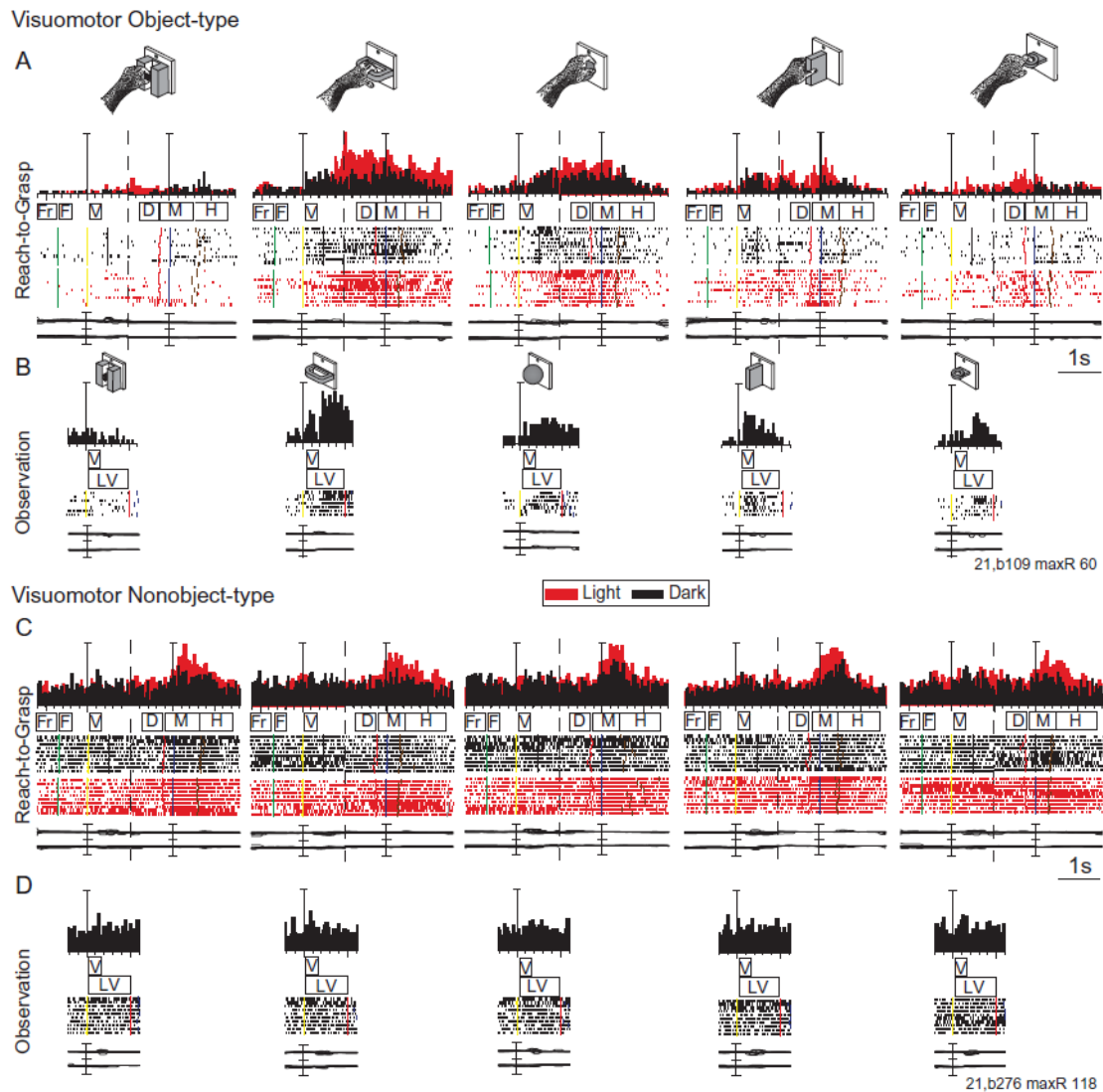
Figure 2.4 Neuronal examples of *Visuomotor* neurons. A-B) Example of a V6A *Visuomotor Object-type* neuron. Neural discharge in the Reach-to-Grasp task (A) and in the Observation task (B). Vertical scale bar on histogram: 60 spikes/s. C-D) Example of a V6A *Visuomotor Nonobject-type* neuron. Discharge in the Reach-to-Grasp task (C) and in the Observation task (D). Vertical scale bar on histogram: 118 spikes/s. In the Observation task, rectangles below histograms indicate the duration of the epochs VIS (V) and LONGVIS (LV) that capture the transient and the sustained visual response to object presentation. Rasters, histograms and recordings of x and y components of eye position are aligned (vertical bar) on the onset of the Reach-to-Grasp movement (A, C) and on the object illumination (A, B, C, D). Other conventions as in Fig. 2.3.

To examine whether and to what extent visual feed-back affected the activity of Visual, Motor, and Visuomotor neurons, we calculated the average normalized SDFs for each visual condition, separately for the different classes. They are illustrated in Figure 2.5. As expected, Visuomotor neurons (Fig. 2.5A, left panel) discharged significantly more in the light than in the dark for all the epochs of interest (permutation test, $p<0.05$),including object presentation (VISG). Visual cells (Fig. 2.5B, left panel) showed stronger activity in the light than in the dark in all the epochs considered (permutation test for DELAY, MOV and HOLD, $p<0.05$). It is worth noting that in the light these cells had a stronger discharge also at object presentation (permutation test, $p<0.05$), though the visual stimulation was the same as in dark condition (see Fig. 2.1B).

The Motor neurons (Fig. 2.5C) showed activities that were not significantly different in light and dark conditions in all epochs considered (permutation test, n.s., $p>0.05$). The small peak of activity recorded at object presentation before grasping (VISG) in light and in dark conditions (significantly different from the baseline activity, permutation test $p<0.05$) prompted us to check how many Motor neurons showed this 'visual' response. We found a complex frame. Some Motor neurons were responsive to object illumination (VISG) in the Reach-to-grasp task in the dark (44%), and 28% in the Reach-to-grasp task in the light. The remaining 56% of Motor cells were not responsive during VISG in the dark, and 72% in the light.

To better define these unexpected 'visual' responses of Motor neurons to object presentation, we compared the response to object presentation before the grasp (VISG) with the response to object presentation in the observation task (VIS): 39% of Motor cells did not respond to object presentation either in the Reach-to-grasp task (VISG) or in the Observation task (VIS), thus confirming their complete motor/somatosensory nature. Another portion of Motor cells (28%) showed a significant response to object illumination both in the Reach-to-grasp task

(VISG, t-test, p<0.05) and in the Observation task (VIS, t-test, p<0.05), suggesting that they received visual information on the observed object. Finally, 33% of Motor neurons showed a response to object illumination only in the Observation task (VIS), indicating a possible context-dependent discharge, as discussed below.
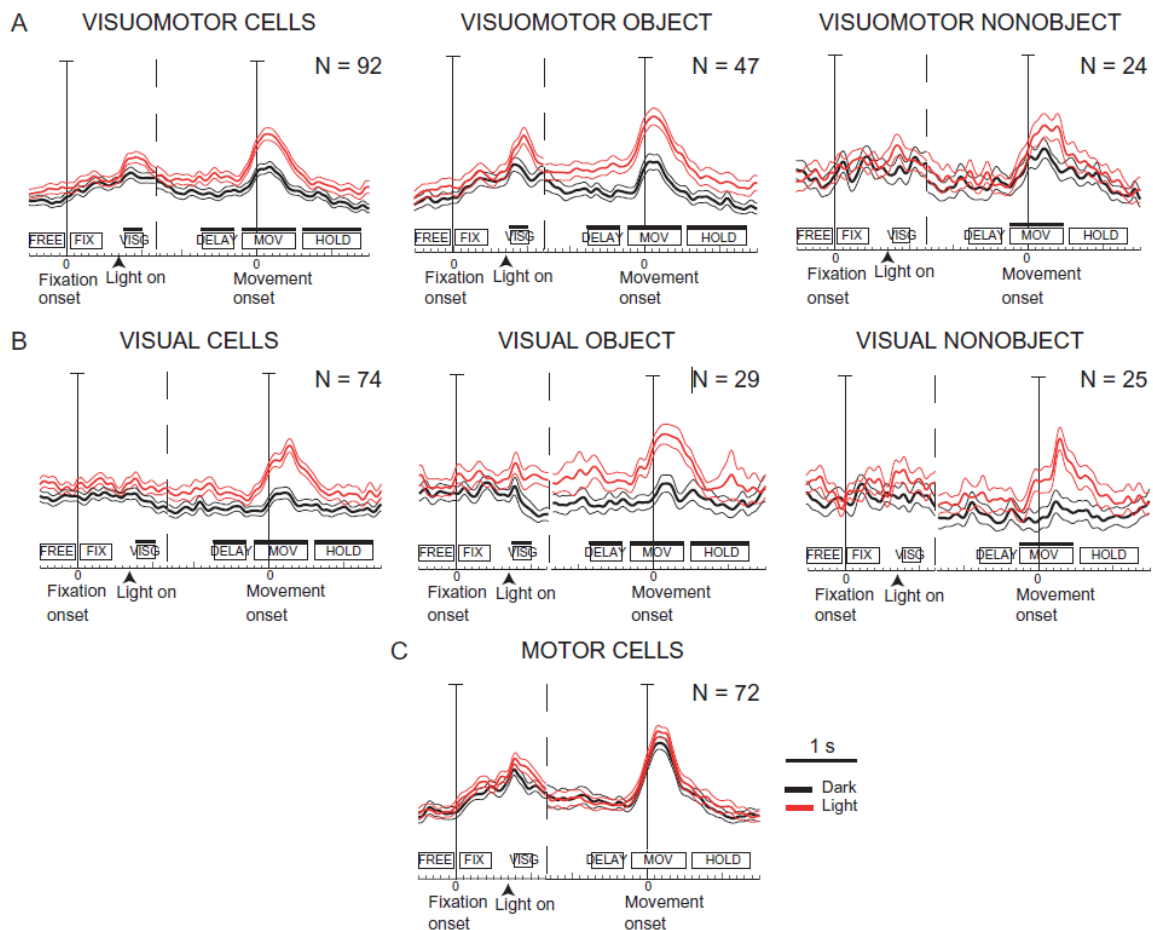
Figure 2.5 Population activity of different categories of V6A cells. Visuomotor (A, N= 92, 39%) and Visual (B, N= 74, 31%), population discharges, divided into Object and Nonobject-type, and Motor (C, N= 72, 30%), expressed as averaged spike density functions (SDFs), where red lines indicate neural activity recorded in the light; black lines indicate activity in the dark. The thin lines indicate the variability band (SEM). Lines above epoch rectangles indicate epochs where the permutation test (p<0.05) was significant. All other conventions are as in Fig. 2.3.

2.4.2 *Relative weight of visual information and grip type on neuronal modulation*

Area V6A is known to encode multiple factors related to the control of prehension (see for a review Fattori et al. 2015). In the current study, we employed a task where multiple objects and two visual conditions were used, increasing potential confounds in the interpretation of the data. To represent the main factors influencing the neural population, we used the demixed principal component analysis (dPCA, see Kobak et al. 2016), a dimensionality reduction method for extracting low-dimensional linear combinations of a population that represents specific task features. Figure 2.6 shows the results of dPCA of task-related units. As shown in Figure 2.6A, the amount of variance explained by dPCA was very similar to that extracted by classical PCA, suggesting that the dPCA method can properly extract the most relevant task features from our population of cells. The principal dPCA component explaining the most variance overall was a condition-independent signal (Figure 2.6B) that begins right before the movement onset, as shown by the analysis of its time course (Fig. 2.6C). This component may reflect signals present in V6A and common to all the conditions tested in this task design. An example of a condition-independent signal may be related to the transport phase of the arm movements performed in the current task, as it is well known that reaching signals do influence V6A cells (Fattori et al., 2005; Hadjidimitrakis et al., 2014a). In any case, the variance captured by the condition-independent variable is present in other neurophysiological data (see Kobak et al. 2016); indeed in our case the influence of the condition-independent signal was lower.
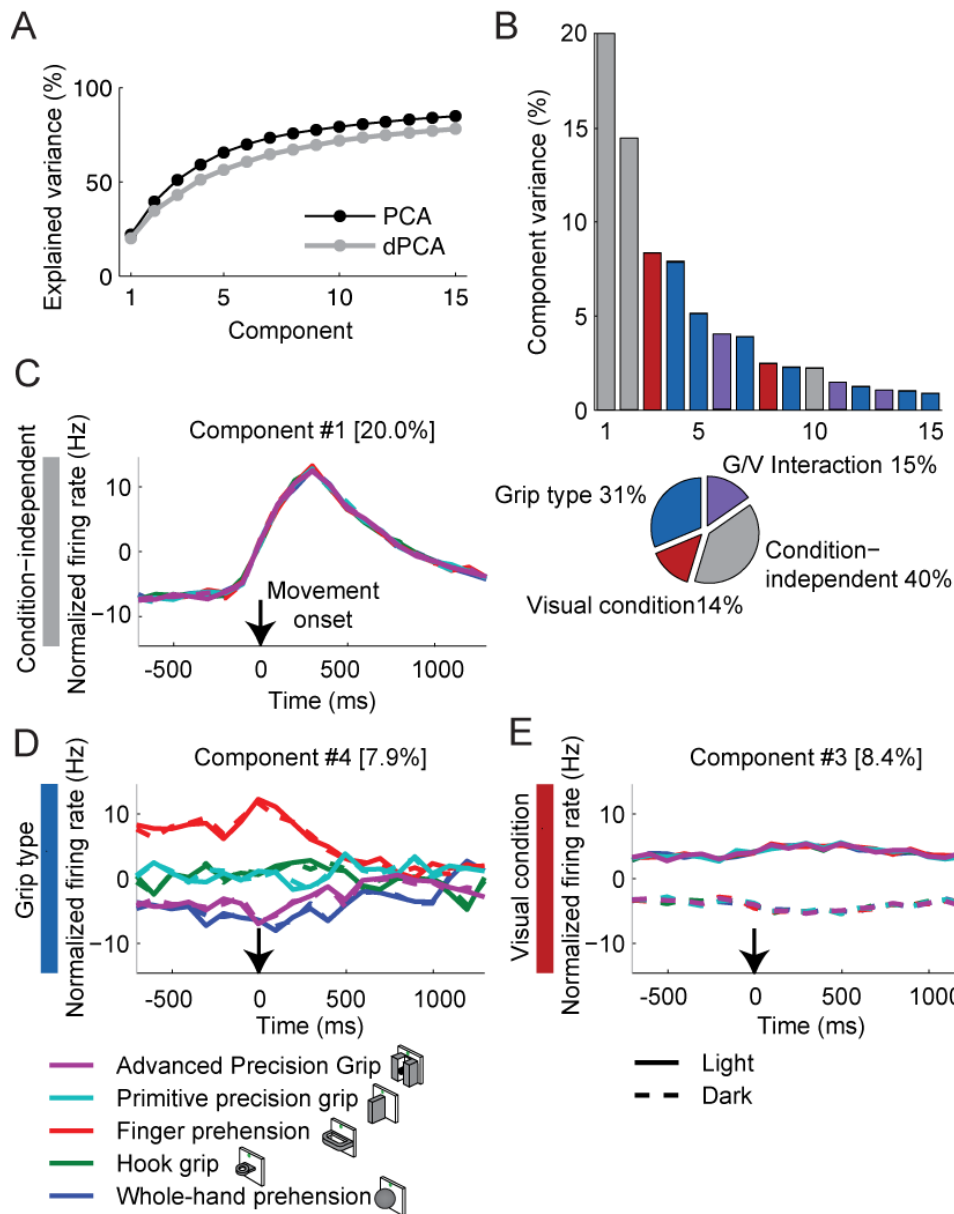
Figure 2.6 Results from demixed principal components (dPCA). A) Cumulative signal variance explained by PCA (black) and dPCA (grey). Demixed PCA explains almost the same amount of variance as standard PCA. B) Variance of the individual demixed principal components. Each bar shows the proportion of total variance. Pie chart shows how the total signal variance is split between parameters (visual condition, and grip). C, D, E) Time course of the signal of single components: C) Condition-independent; D) Grip type; E) Visual condition. For the grip component, the separation of the different grips starts well before the grasp onset (arrow) and continues till grasp completion.

Interestingly, grip type represented an important component (31%, Fig. 2.6B). The timing of the first component of grip type (Component #4, Fig. 2.6D) revealed that the components of grip types were well separated from movement planning up to grasping execution, with the highest separation at the end of delay and onset of grasping execution. In addition, the signal related to the handle grasping was separated from the other signals during grasping preparation and execution (permutation test, $p < 0.05$), but not during object holding where all the curves converge. The dPCA also shows the low influence of visual information (14%, Fig. 2.6B). The timing of this signal shows that light and dark signals were well separated for the entire task, since the beginning of the delay (Fig. 2.6E).

2.4.3   Comparison with AIP

To better identify whether V6A plays similar or different functional roles with respect to the classic PPC grasping area AIP, we compared our results with those obtained by other labs on AIP (Murata et al., 2000; Baumann et al., 2009; Schaffelhofer and Scherberger, 2016), using the same experimental design and analyses.

The results of the comparison (Fig. 2.7A) showed that the incidence of Visual, Motor, and Visuomotor cells (Object- and Nonobject-type) was statistically not different in areas V6A and AIP (Chi-squared test, $p > 0.05$). To examine whether Visual, Motor, and Visuomotor neurons exhibit a grip selectivity similar to that reported by Murata and collaborators in AIP (Murata et al., 2000), thus enabling a direct comparison of V6A with AIP, we analyzed the activity of neurons during MOV when grasping the five objects in the light. In agreement with the analysis performed by Murata et al. (2000) in AIP, we excluded those neurons that were not studied with the Observation task and those neurons that were not tuned by grip type (1-way ANOVA, $p > 0.05$). The remaining 140 Visual, Motor, and Visuomotor neurons were further subdivided according to their degree of selectivity for the objects (the Student-

Bonferroni procedure, 2-tail; p<0.01). We classified them as *highly selective*, when the activity of the neurons for one object was significantly higher than that for all the other objects, or *moderately selective*, when, despite the cells being tuned for objects according to ANOVA, not all the posthoc comparisons were significant (Student-Bonferroni procedure, n.s.). The remaining neurons that did not show any significant difference in the activity level for the five objects were classified as *nonselective* (Student-Bonferroni procedure, n.s.). To evaluate the selectivity for the passive observation of the object, we performed the same analysis considering the discharge during the epochs VIS and LONGVIS in the Observation task (the Student-Bonferroni procedure, 2-tail; p<0.01). The selectivity for 'active' object observation (observation in the Reach-to-Grasp task) was evaluated using epoch VISG.

As shown in Figure 2.7B, C, the distribution of V6A and AIP cells based on their selectivity was similar in the two areas (Chi-squared test, p>0.05). Considering all neuronal categories together (Fig. 2.7 B and C), the incidence of highly selective cells (38%) was slightly smaller than that of moderately selective cells (44%) in V6A, a result similar to AIP.

The most interesting result regarding the cell categories is related to the selectivity of these cells for objects observed in the Observation task (Table 2.1). The discharge for passive object observation was nonselective in the overwhelming majority of Object-type cells (about 80% VIS, see Table 2.1), whereas in the Reach-to-Grasp task the active vision of the object (VISG) gave rise to a higher incidence of selective (highly or moderately) neurons. In other words, most of the cells significantly tuned for object presentation during grasping in the light lost their object selectivity when simply observing the object without any grasping preparation.
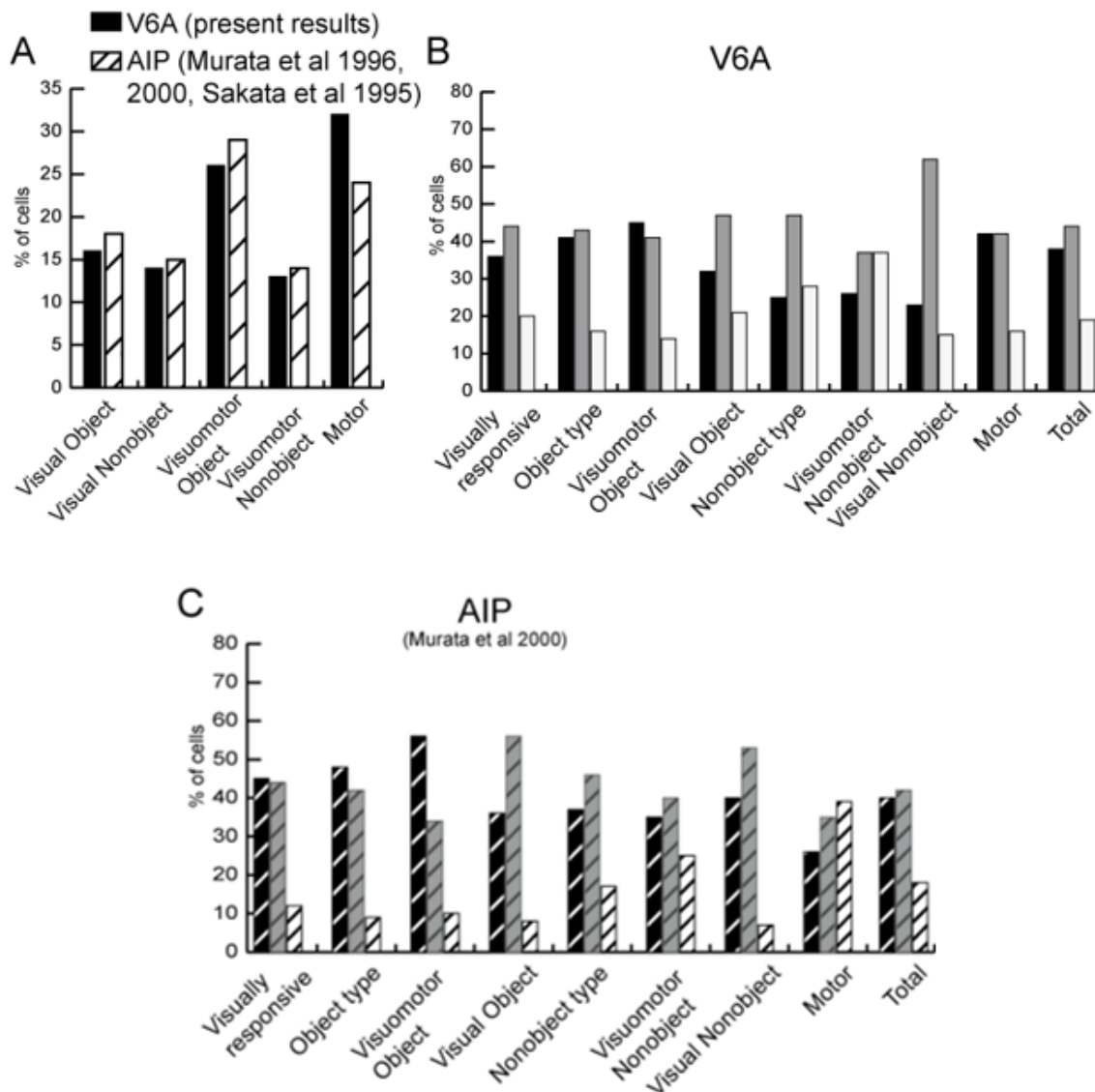
Figure 2.7 Comparison of cell categories between V6A and AIP. A) Incidence of different categories of cells. Distribution of Visual (Object-type, Nonobject-type), Visuomotor (Object-type, Nonobject-type) and Motor cells in V6A (black bars) and in AIP (white hatched bars) (Chi-Squared test: n.s.). Data of area AIP were derived by averaging the data reported in studies of AIP from Sakata's lab (Sakata et al., 1995; Murata et al., 1996, 2000). B-C) Distribution of different categories of cells on the basis of their selectivity in V6A (B) and AIP (C) (Chi-Squared test: n.s.). Data of area AIP were taken from Murata et al., (2000).

To make a direct comparison with AIP, we have to take into account the late, sustained part of the visual response to object observation (LONGVIS), as done by Murata (Murata et al., 2000). Doing this (Table 2.1), the selectivity in V6A Visual Object neurons increases to 53%, similarly to AIP (at least 57%, (Murata et al., 2000); in contrast, the percentage of selective neurons among V6A Visuomotor category is 43%, much less than those in AIP (at least 81%; Murata et al., 2000).

Differently from AIP (Murata et al., 2000), not only were there very few neurons in V6A selective for objects in the Reach-to-Grasp and Observation tasks , but also in just a minority of them (3/11 in VIS and 12/29 in LONGVIS) there was the same object preference between object observation and grasping. Consistency was, instead, a rule for AIP (Murata et al., 2000).

Type of cell	Highly selective	Moderately selective	Nonselective	Total
VIS (Observation task)				
Visuomotor Object	4 (9%)	4 (9%)	36 (82%)	44 (100%)
Visual Object	1 (5%)	2 (11%)	16 (84%)	19 (100%)
LONGVIS (Observation task)				
Visuomotor Object	9 (20%)	10 (23%)	25 (57%)	44 (100%)
Visual Object	3 (16%)	7 (37%)	8 (47%)	19 (100%)
VISG (Reach-to-grasp task)				
Visuomotor Object	7 (22%)	9 (28%)	16 (50%)	32 (100%)
Visual Object	2 (11%)	3 (17%)	13 (72%)	18 (100%)

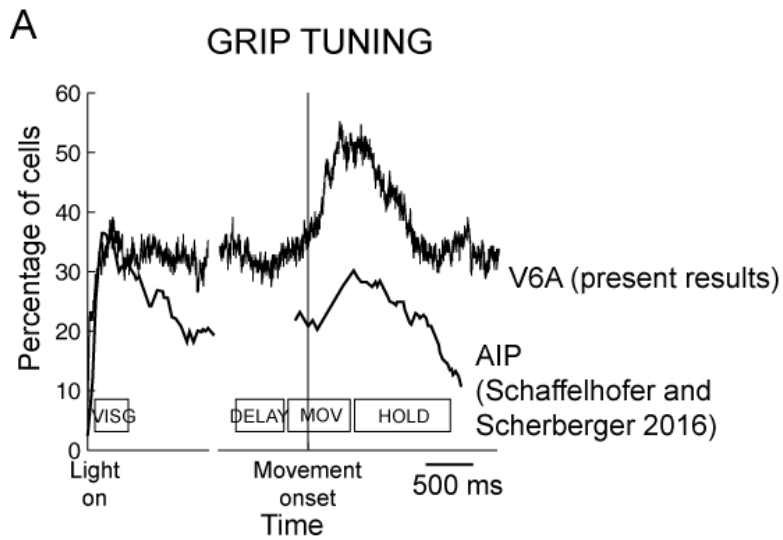**Table 2.1.** Selectivity for objects of visually responsive grasp-related neurons during object viewing with (Reach-to-grasp task) and without grasping (Observation task). For each type, the number and incidence (in brackets) is indicated.

To further compare the contribution of AIP and V6A to grasp encoding, we evaluated the incidence of grip tuned cells in the two areas. For the sake of comparison, we used only V6A data recorded in the dark and AIP data recorded with the set of objects (called "mixed objects") of Schaffelhofer and Scherberger (2016) more similar to ours, so as to better match the two studies. In addition, we performed the sliding window ANOVA in time steps of 1ms and set the significance level at 0.01, to use the same conditions applied by Schaffelhofer and Scherberger (2016) in AIP. The comparison is shown in Figure 2.8A: during object illumination, the incidence of grip tuned cells in AIP and V6A was similar (about 40%); during grasping preparation, the incidence of tuned cells decreased in AIP while in V6A it remained more or less constant; during grasping execution, the incidence of grip tuned cells rose to about 60% in V6A while the increase in AIP was much less pronounced. These data show a similar involvement of neural populations in the two areas at the beginning of the trial, when object shape is encoded to drive the subsequent grasping, but later in the trial V6A remains higher when action needs to be launched and monitored inflight.

To perform another direct comparison between the functional properties of V6A and AIP, we analyzed task-related cells of V6A tested in the dark with the same grips (finger prehension and advanced precision grip) used in another study of AIP (Baumann et al., 2009). The results are shown in Fig. 2.8B, C. Fig. 2.8B shows the ratio of cells preferring precision vs power grip in V6A (top) and AIP (bottom). The ratio was similar (half of the cells preferred precision and half power grip) in VIS, quite similar in DELAY, and clearly different in MOV, where power grip was preferred in V6A and precision grip in AIP.

Fig. 2.8C shows the changes of preference of individual V6A and AIP cells along the time-course of the task. In V6A, about 40% of the cells changed their preference, passing from VISG to DELAY, whereas about 70% of cells maintained the same preference, passing from DELAY to MOV. In AIP, instead, the tuning preference remained more constant, passing

from about 60% between VIS and DELAY to about 70% between DELAY and MOV. Overall, the distributions of these AIP and V6A data are statistically different (Chi-squared test, p<0.05).

A GRIP TUNING

V6A (present results)

AIP (Schaffelhofer and Scherberger 2016)

B PREFERRED GRIP TYPE

V6A

| Visg | Delay | Mov |

Precision 50% / Power 50%
Precision 46% / Power 54%
Precision 35% / Power 65%

Precision | Power

AIP (Baumann et al 2009)

| Cue | Planning | Movement |

50% / 50%
54% / 46%
61% / 39%

C GRIP TUNING CONSISTENCY

V6A (present results)

AIP (Baumann et al 2009)

Same tuning
Different tuning
No longer tuned
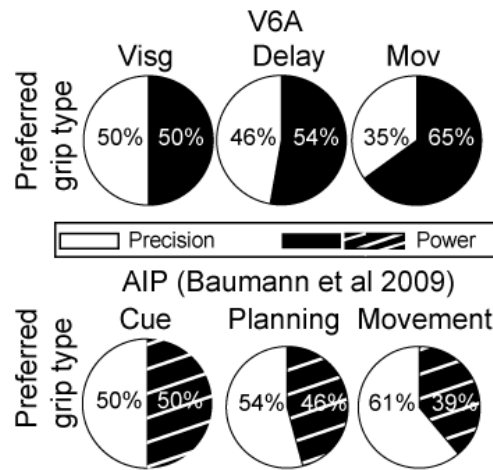
Figure 2.8 Comparison between grasp-related properties of V6A and AIP. A) Percentage of tuned cells in a sliding window one-way ANOVA in time steps of 1ms in V6A (thick black; N= 276) and AIP (thin black). The plot of AIP was redrawn from Fig. 2.3B of Schaffelhofer and Scherberger (2016). Plots are aligned on object illumination onset and on movement onset (vertical lines). B) Preferred grip types in V6A (top) and AIP (bottom). Pie charts show the distribution of preferred grip type in various task epochs. The percentage of cells preferring precision grip is represente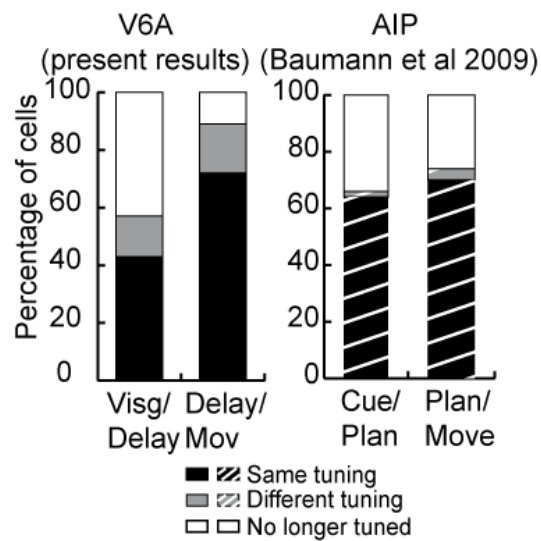d in white, the power grip in black/hatched black. C) Grip type tuning consistency across task epochs in V6A (left) and AIP (right), data from Fig. 2.7A in Baumann et al. (2009). Histogram bars indicate the percentage of cells that stay tuned for the same grip (black-hatched black), change preference to the opposite grip (grey-hatched gray) or lose their tuning (white) when transitioning between consecutive task epochs (Visg/Delay and Delay/Mov). Significance level was chosen as 0.01, as performed by Baumann et al. (2009). AIP data were taken from Fig. 2.8 of Baumann et al. (2009). The terms CUE-PLAN-MOVE used for AIP are those of Baumann et al. (2009), but are qualitatively similar to VISG-DELAY-MOV used for V6A.

2.5 Discussion

In this work, we investigated the relative influence of grip type and visual condition of the grasping action on the discharge of neurons in area V6A, a visuomotor area located in the medial PPC. We also compared the functional properties of grasp-related cells of V6A with those of AIP, the grasping area of the lateral PPC. The present study demonstrates that the majority of V6A neurons are modulated by both grip type and visual information, from grasping preparation up to execution and object holding. As shown by the dPCA and sliding window analyses, grip type influences the discharge of V6A cells more than visual information available when grasping is prepared and accomplished. The higher grip-related than visual-related selectivity found in V6A may suggest that, despite its name starting with

the letter "V", V6A should not be counted among the extrastriate visual areas, but among the posterior parietal grasping areas.

In our Reach-to-Grasp task, each tested object was grasped with a distinct grip. Thus, grip type is not dissociated from object feature/affordance, and we cannot distinguish which of the two is encoded by the cells. In a previous work, we demonstrated that the response of V6A neurons to the presentation of objects to be grasped does reflect the object affordance (Breveglieri et al., 2015). The present findings suggest that the response to object presentation may include, together with an encoding of the visual attributes of the object and of its affordance, context-dependent factors too. As context-dependent responses have been found in ventrolateral prefrontal cortex and pre-SMA (Bruni et al., 2015; Simone et al., 2015; Lanzilotto et al., 2016), which are directly connected to V6A (Gamberini et al., 2009; Lanzilotto et al., 2016), we speculate that context-dependent information could impinge upon V6A cells and be responsible for at least some of the behavior we observed in the present paper, like the response to object illumination of Motor neurons only in the Observation task. This complex visual encoding performed by V6A, together with the influx of attentional shifts on V6A discharges (Galletti et al., 2010; Ciavarro et al., 2013), suggest that V6A provides critical visual and cognitive information to motor structures controlling hand action (see Fattori et al. 2017).

The present data, as well as previous reports from our laboratory (Fattori et al., 2010, 2012), have shown that V6A cells were deeply influenced by grip type during movement execution and object holding. In a recent study measuring hand kinematics during grasping, Schaffelhofer and Scherberger (2016) reported that the first principal component of hand movements could be attributed to wrist orientation and the second principal component to grip aperture. Although there are no doubts that V6A cells encode wrist orientation used for grasping (Fattori et al., 2009; Breveglieri et al., 2016), as all the objects were grasped with a

constant wrist orientation in the present task (see Figure 2.1A), one would expect more convergence of firing rates for the different grasps than is reported here if the cells were *only* modulated by wrist orientation. Actually, the high percentage of cells modulated by grip type (around 70-80%) during grasping execution and object holding suggests that V6A cells are not only modulated by wrist orientation, but also by hand shaping.

This study demonstrates that several V6A neurons are strongly modulated by grip type during DELAY, i.e. during the period in which the monkey withholds the grasping action. This activity could be related to grasping preparation, or, especially in darkness, to the memory of the object to be subsequently grasped. This feature makes V6A similar to premotor area F2 (Raos et al., 2004), and to parietal area AIP, where limited set-related activity and extensive memory-related activity was found (Murata et al. 1996; Schaffelhofer et al. 2015; Schaffelhofer and Scherberger 2016). However, our task does not make it possible to ascertain what is encoded by V6A in the delay between object observation and action execution, because there is a one-to-one correspondence between object shape and grip type. Our previous work with the grasping performed only in the dark showed that in the delay before grasping, V6A cells started encoding object features and then switched to encoding grip type (see Fig. 8 of Fattori et al., 2012). Further work is needed to disentangle what is encoded in the delay epoch by V6A neurons.

The use of objects with different shapes, that require different grips, allowed us to investigate the presence of Motor, Visual, and Visuomotor neurons, similarly to what has been previously done in AIP (Sakata et al., 1995; Murata et al., 2000). The present data show that V6A contains 30% of Motor cells, 31% of Visual cells, and 39% of Visuomotor neurons. We suggest that, while Visual neurons receive only visual signals, the Visuomotor neurons incorporate both visual and somatosensory/motor efferent copy signals and integrate them in guiding prehension. The Motor neurons do not receive visual information about hand/object

interaction, because they show the same response in MOV in the dark and in the light. Some of them, however, may receive visual information about the observed object.

About 40% of the V6A cells were the 'Object-type' because they discharged also on passive observation of the object. The Object-type neurons likely represent visual physical characteristics of the objects. However, since in V6A the object selectivity of this type of neuron found when the monkey observed the objects at the beginning of the grasping trials was reduced during passive object observation (i.e., observation outside the grasping context), we believe that these neurons did not encode the visual features of the objects, useful for object recognition. We suggest, instead, that they encoded the visual information useful for the subsequent grasping action (the visual affordance; Breveglieri et al., 2015). The 'Nonobject-type' neurons are influenced by visual information only during movement execution – not before - (see Fig. 2.5) and this could be useful for the online control of reach-to-grasp movements, including the adjustment of grip around the object.

The discharge stronger in the light than in the dark conditions in Visual and Visuomotor cells deserves some considerations. As pointed out above, it is worth noting that before and at object presentation the visual stimulation was the same in the two visual conditions (View, see Fig. 2.1B). Thus, what is the reason for a stronger discharge in the light? The fact that the phenomenon is present in Object-type but not in Nonobject-type cells (fig 5A and B, center and right panels) excludes the possibility that it is caused by the block design. Interestingly, while Nonobject-type neurons show a significant difference only during the execution of grasping action, Object-type neurons start differentiating the discharge between light and dark conditions at object vision, and continue through the delay up to grasping execution. Since in the dark, monkeys had to memorize the object to be grasped and likely had to pay more attention because they knew that the information about the object would not be available for the rest of the trial, it could be that the difference in discharge in the two

conditions is due to the attentional level, with an inhibitory effect tied to the attentional enhancement. This view is supported by the report that many V6A neurons are inhibited when the animal starts to work in a fixation task (see Fig. 16 in Galletti, 1996).

As an alternative explanation, it could be that a higher likelihood of shifts of attention in the light compared to the dark may be responsible for the higher activity we observed in the light. In support of this attentional shift hypothesis is the report that V6A activity is strongly modulated by the shifts of attention (Galletti et al., 2010; Ciavarro et al., 2013), a finding recently confirmed by Caspari et al (2015).

The dPCA analysis of the present data allowed us to measure the relative influence of visual information and of grip type. We found that the influence of visual information in V6A is quite weak (14%), and lower than the influence of grip type (31%, see Fig. 2.6B). This result is surprising, given that the majority of V6A cells are visual neurons (Galletti et al., 1999; Fattori et al., 2017). However, this might have some functional explanations. For example, in humans it has been demonstrated that the impact of a specific source of sensory information (visual, haptic) on the sensorimotor transformation is regulated to satisfy task requirements (Säfström and Edin, 2004). Since in our experiments the animals were overtrained to perform Reach-to-Grasp tasks in light and in dark conditions, the visual information available during grasping in light was not necessary to allow task completion. Hence, the neural modulations we observed in V6A during grasping could be strictly tied to the strong somatosensory/motor activities because they are behaviorally relevant in our conditions. Further, specific experiments are needed to confirm this suggestion.

2.5.1 Medial versus lateral parietal grasping areas

The use of the same experimental protocol used in AIP studies allowed us to compare the grasping properties of the lateral parietal area AIP with those of the medial parietal area V6A. In a comparison with Sakata's work, V6A shows a similar incidence of grasp-related cells with respect to AIP (78% vs. 67%, Taira et al. 1990). In a direct comparison of the current results with those of Scherberger and coworkers, it emerges that at the object presentation V6A and AIP recruit a similar amount of cells (see Fig. 2.8A), whereas during the subsequent grasping preparation and execution V6A seems to recruit more cells than AIP. Of course, this comparison is only suggestive, as the data come from different laboratories and from different recording apparatuses (chronic arrays for AIP, vs single electrodes for V6A). However, a possible explanation for the higher incidence of grasp-related cells in V6A could be the presence of somatosensory cells in this area, but not in AIP (Murata et al., 2000; Breveglieri et al., 2002). Somatosensory cells related to the arm (as they are in V6A; Breveglieri et al. 2002) fire immediately before arm movement, when the muscles start contracting, and during reach-to-grasp execution and hand-object interaction.

The incidence of Visual, Motor, and Visuomotor neurons, as well as that of Object and Nonobject-type neurons is similar in V6A and AIP (see Fig. 2.7A) (Sakata et al., 1995; Murata et al., 1996, 2000). However, the discharge of the subset of V6A Motor neurons at object presentation is different from that of AIP motor neurons, that '..were not activated during the fixation period of the manipulation task in the light…' (Murata et al., 2000). For all the other aspects, the three classes of neurons were similar between V6A and AIP. Moreover, the grip selectivity in the two parietal grasping areas turned out to be remarkably similar. The distribution of highly selective, moderately selective, and nonselective cells was similar in the two areas (see Fig. 2.7B, C). However, most of the AIP neurons (at least 81% of the Visuomotor Object-type cells and at least 57% of the Visual Object-type cells) were

selective for grips during manipulation task and for objects during passive object observation (Murata et al., 2000). On the contrary, only a minority of V6A neurons did so. Thus, it seems that while both visual and motor components do influence the selectivity of Visual and Visuomotor cells in AIP, in V6A it is the motor component that particularly drives a cell's selectivity, a view strongly supported by the results of dPCA analysis, as recalled above (see Fig. 2.6).

At individual cell level, AIP showed high consistency of object preference between visual presentation of the object and its grasping, whereas in V6A this consistency was poor. This lack of consistency in V6A may reflect contextual information and/or attentional signals, summing up with the visual and motor-related ones that largely impinge on V6A. At population level, the number of V6A cells modulated in the delay before action and in grasping execution is higher than in AIP (see Fig. 2.8A). This, together with the rich direct connections between V6A and MIP and dorsal premotor cortex (Gamberini et al., 2009), and the high incidence in V6A of neurons processing spatial signals for reaching (Fattori et al., 2005, 2017; Hadjidimitrakis et al., 2014a), suggests a deeper involvement of V6A in linking object information to the orchestration of reaching and grasping actions.

Previous experiments demonstrated that about 90% of AIP neurons were sensitive to simple visual stimuli, like fragments of shapes (Romero et al., 2014), whereas only about 30% of V6A neurons were sensitive to simple visual stimuli (Galletti et al., 1999; Gamberini et al., 2011). This difference in visual sensitivity between the two grasping areas has been recently confirmed by reporting a stronger influence of object shape in AIP than in V6A (35% in AIP, Schaffelhofer and Scherberger 2016, versus 25% in V6A, Fattori et al. 2012). Both areas are sensitive to wrist orientation in a similar manner (around 50%, Baumann et al. 2009; Fattori et al. 2009), while, a marked difference between them is evident in the somatosensory domain: somatosensory cells were not found in AIP (Murata et al., 2000), whereas V6A

contains about 30% of somatosensory cells (Breveglieri et al., 2002). Thus, AIP seems to be more visually driven than V6A, which instead is more influenced by somatosensory/motor inputs such as the hand posture used for grasping. This different balance of sensory sensitivity in the two areas is in agreement with their different pattern of cortical inputs, with AIP receiving inputs from the ventral visual stream and the dorso-lateral fronto-parietal network (Borra et al., 2008), and V6A from the extrastriate cortex, the superior parietal lobule and the mesial parietal cortex, but not receiving a direct input from the ventral stream (Gamberini et al., 2009; Passarelli et al., 2011).

A further difference between the two grasping areas concerns the population preference for grips during grasping performance. When precision grip and power grip are compared, AIP showed an over-preference for precision grip (Baumann et al., 2009), V6A for power grip (Fig. 2.8B). This difference likely reflects a different functional role of the two grasping areas, with AIP more involved in manipulation and V6A in secure grasping of objects also in dynamic conditions (Galletti and Fattori, 2017). However, this proposed difference between the two grasping parietal areas should not be considered as a dichotomy but as a concurrent involvement in controlling grasping, because V6A and AIP are also reciprocally connected (Borra et al., 2008; Gamberini et al., 2009) and share many grasp-related properties, as shown here. This proposed interplay between the medial and lateral grasping areas is in line with recent brain imaging work in humans (Di Bono et al., 2015; Fabbri et al., 2016). Together, the dorsomedial parieto-frontal stream involving V6A and dorsal premotor cortex and the dorsolateral stream involving AIP and ventral premotor cortex can cooperate in orchestrating how to approach an object to be grasped in the most appropriate way, according to the type of object and also to the context in which the grasping needs to be accomplished (see also Galletti and Fattori, 2017 for a discussion on this topic).

2.6   Conclusions

The present results demonstrate that parietal area V6A is modulated by visual information available during the execution of prehension and grip type, with this latter representing the most influencing factor. The activity modulation changes during the trial, from object presentation up to action preparation and execution, with an evolution indicating that V6A processes vision for action, taking into account also attentional signals and contextual information (Fattori et al., 2017). This functional role well suits the characteristics of the dorsal visual stream of which V6A is an important node (Galletti et al., 2003; Galletti and Fattori, 2017).

These results also reveal that area V6A shares many features with the other grasp-related parietal area AIP, that allow both areas to integrate visual and motor information to orchestrate grasping actions. AIP seems to be more involved in fine control of precision grip and manipulation, V6A in fast, coarser control of object grasping and in directing the hand to the correct spatial position of the object (Fattori et al., 2017; Galletti and Fattori, 2017). A possible role for V6A may be to orchestrate the coordination between reaching and grasping so as to contribute to the control of the entire prehension.

Chapter 3

The neglected medial part of macaque area PE: segregated processing of reach depth and direction.

3. The neglected medial part of macaque area PE: segregated processing of reach depth and direction

3.1 Abstract

Area PE (Brodmann's area 5), located in the posterior parietal cortex (PPC), is involved in the control of arm movements. Many monkey studies showed PE's involvement in reach directions, while only a few revealed signals coding the depth of reaches. Notably, all these studies focused on the lateral part of PE, leaving its medial part functionally largely unexplored. We here recorded neuronal activity in the medial part of PE in three male *Macaca fascicularis* while they performed coordinated eye and arm movements in darkness towards targets located at different directions and depths. We used the same task as in our previous studies of more caudal PPC sectors (areas V6A and PEc), allowing a direct comparison between these three PPC areas. We found that in medial PE reach direction and depth were encoded mainly by distinct populations of neurons. Directional signals were more prominent before movement onset, whereas depth processing occurred mainly during and after movement execution. Visual and somatosensory mapping of medial PE revealed a lack of visual responses yet strong somatosensory sensitivity, with a representation of both upper and lower limbs, distinct from the somatotopy reported in lateral PE. This study shows that PE is strongly involved in motor processing of depth and direction information during reaching. It highlights a trend in medial PPC, going from the joint coding of depth and direction signals caudally, in area V6A, to a largely segregated processing of the two signals rostrally, in area PE.

3.2 Introduction

The posterior parietal cortex (PPC) plays a key role in sensorimotor transformations required to locate targets in 3D space and transforms this spatial information into motor commands to move the hand towards targets in goal-directed actions (Andersen and Cui, 2009; Hadjidimitrakis et al., 2012; Andersen et al., 2014). Area PE is part of Brodmann's area 5 (Brodmann 1909), located between Brodmann's areas 2 and PEc in the rostral PPC (Pandya and Seltzer, 1982) (Fig. 3.1). PE receives robust somatic inputs and projections from motor and premotor cortex (Sakata et al., 1973; Jones et al., 1978; Pandya and Seltzer, 1982; Johnson et al., 1996; Bakola et al., 2013). Most PE neurons respond to proprioceptive stimulation, with fewer cells sensitive to visual or tactile stimulation (Duffy and Burchfiel, 1971; Sakata et al., 1973; Mountcastle et al., 1975; Padberg et al., 2007). The lateral sector of PE contains a rough topographic organization (summarized in Fig. 3.1a), dominated by the representation of the hand, forelimb, and shoulder (Pons et al., 1985; Taoka et al., 1998; Hinkley et al., 2007; Padberg et al., 2007; Seelke et al., 2012), with occasional leg representations. However, the sensory organization of the medial sector of PE is still unknown.
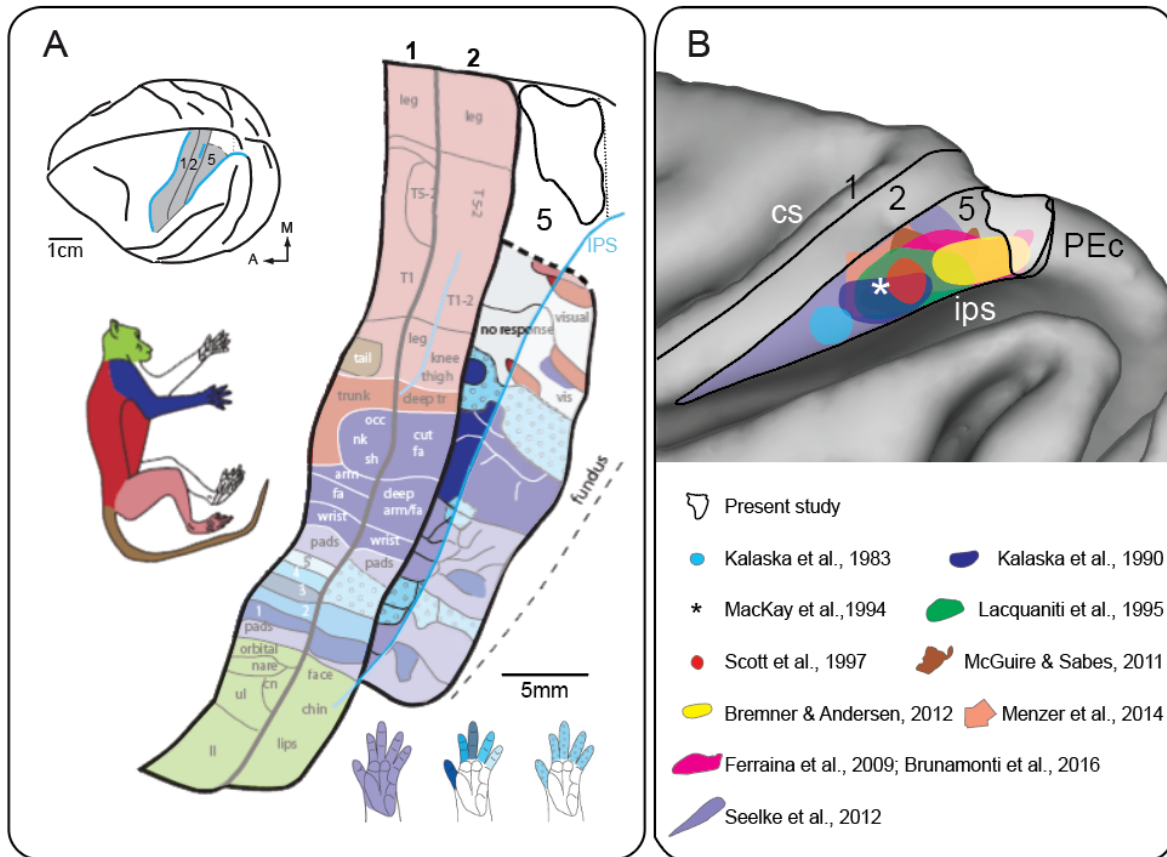
Figure 3.1 Recording sites in different PE studies. **a)** Cortical representation of somatosensory responses in area PE and indication of the presently recorded part of area PE (white spot with black outline). Top left: dorsolateral view of a macaque brain highlighting in grey the extent of Brodmann's areas 1 and 2 and the explored part of area 5. Right: somatosensory responses recorded from Brodmann's area 5 (bright colors) and from nearby areas 1 and 2 (faint colors) (modified from Seelke et al. 2012). Notice that the lateral part of area 5 is dominated by the representations of the digits, hand, and forelimb. The posteromedial part of area 5 has been barely studied. Abbreviations: IPS, intraparietal sulcus; cn, chin; fa, forearm; hl, hindlimb; tr, trunk; occ, occiput; nk, knuckle; sh, shoulder; tr, trunk; ul, upper lip; vis, visual. **b)** Enlargement of the superior parietal lobule (SPL) with the location of the parts of area PE previously studied electrophysiologically (colors according to the legend) and of the present study (white spot). Only the papers in which the authors explicitly declared the locations of the penetrations were taken into account for the purpose of reconstructing the recording sites. The tasks used in these studies were: a) center-out reaches performed with a joystick

(Kalaska et al., 1983, 1990; Scott et al., 1997; Menzer et al., 2014), b) 2D reaches on a touchscreen, either single reaches (Bremner and Andersen, 2012), or reaches in a sequence (Mackay et al., 1994) and c) 3D reaches, either both upward and downward (Lacquaniti et al., 1995), or only upward reaches (Ferraina et al., 2009; Brunamonti et al., 2016), or purely forward reaches at targets located at waist level (McGuire and Sabes, 2011). It is worth noting that until now, reaching and somatosensory studies (Fig. 3.1a) mainly focused on the lateral part of area 5 (PE). Our study is the first investigating the functional properties of the posteromedial part of the area. Abbreviations: cs, central sulcus; IPS, intraparietal sulcus; PEc, area Pec.

In addition to receiving sensory information, area PE is involved in motor preparation (Burbaud et al., 1991) and in generating body-, shoulder-, or hand-centred coordinates for reaching (Ferraina and Bianchi, 1994; Lacquaniti et al., 1995; Kalaska, 1996; Ferraina et al., 2009; Bremner and Andersen, 2012). PE also sends "command" signals (Mountcastle et al., 1975) directly to spinal cord circuits involved in finger and wrist movements (Rathelot et al., 2017), thereby supporting the earlier view that PE is involved in the coordination of reaching and grasping movements (Gardner et al., 2007a; Nelissen and Vanduffel, 2011; Gardner, 2017; Nelissen et al., 2018).

Most PE studies used center-out reaches without considering reach depth, and reported a high incidence of neurons modulated by arm movement direction (Kalaska et al., 1990, 1983, 1985; Kalaska and Crammond, 1992; Ashe and Georgopoulos, 1994; Johnson et al., 1996; Kalaska, 1996; Scott et al., 1997; Batista et al., 1999; Buneo et al., 2002; Maimon and Assad, 2006; Cui and Andersen, 2011; Bremner and Andersen, 2012; Li and Cui, 2013; Shi et al., 2013; Menzer et al., 2014). A few studies have found tuning by reach depth in PE, however without simultaneously addressing direction processing (Ferraina et al., 2009; Brunamonti et al., 2016). In lateral PE, Lacquaniti and colleagues (1995) (see Fig. 3.1b) varied the azimuth, elevation and distance of reach targets with respect to the body and found different neuronal

populations processing these parameters. However, in that study, eye position was not monitored, and targets were distributed only between two depth planes.

According to a recent neural tracer study (Padberg et al., 2019), the PE territory is not homogeneous. The medial sector receives stronger afferents from PEc and primary motor cortex (M1) than the lateral sector, and its pattern of connections suggests a more general role in movement coordination (Bakola et al., 2013). In addition, Padberg and colleagues (2018) found a somatosensory representation of the hand but not of the leg in medial PE. In the present study, we conversely found not only robust arm reach-related activity and somatosensory neurons with receptive fields encompassing the upper limbs, but also strong lower limb representation. We also studied depth and direction coding of arm reaching movements and examined their time course. Finally, we compared present results with those obtained in the nearby areas V6A and PEc (Hadjidimitrakis et al., 2014a, 2015) to provide a picture of the spatial information processing for reaching in the whole superior parietal lobule (SPL). Our results suggest a substantial degree of functional heterogeneity in the reaching network of SPL and support the view of independent processing of depth and direction information in PE.

3.3   Materials and Methods

3.3.1   General procedures

Three male macaque monkeys (*Macaca fascicularis*) with a weight ranging between 3.7 and 7.5 kg were involved in the experiments. The study was performed in accordance with the guidelines of EU Directives (86/609/EEC; 2010/63/EU) and Italian national laws (D.L. 116-92, D.L. 26-2014) on the protection of animals used for scientific purposes. Protocols were approved by the Animal-Welfare Body of the University of Bologna. During

training and recording sessions, particular attention was paid to any behavioral and clinical sign of pain or distress.

3.3.2 *Behavioral tasks*

Monkeys sat in a primate chair (Crist instruments, Hagerstown, MD, USA) and were trained to perform a Fixation-to-Reach task under controlled conditions to evaluate the effect of depth and direction on reach-related activity of PE cells. Moreover, animals were also trained to perform a Visual fixation task to keep the eyes still during visual stimulations, and to stay relaxed during somatosensory stimulations.

3.3.2.1 Fixation-to-Reach task

This task was performed in darkness with the arm contralateral to the recording hemisphere. During the task, the animals maintained steady fixation on the cued (green) reaching target with their head restrained. Before starting the arm movement, the monkeys kept their hand on a button (home button [HB], 2.5 cm in diameter) located 5 cm in front of the chest on the midsagittal plane (Fig. 3.2b). Reaches were performed to one of nine light-emitting diodes (LEDs, 6 mm in diameter). The LEDs were mounted on a horizontal panel located in front of the animals, at different distances and directions with respect to the eyes but always at eye level, so the movement performed by the monkeys to reach and press the LED was upward. Target LEDs were arranged in three rows: one central, along the sagittal midline, and two lateral, at version angles of -15° and +15°, respectively (Fig. 3.2c). Along each row, three LEDs were located at vergence angles of 17.1°, 11.4°, and 6.9°. The nearest targets were located at 10 cm from the eyes, whereas the LEDs placed at intermediate and far positions were at a distance of 15 and 25 cm, respectively. The range of vergence angles was

selected to include most of the peripersonal space in front of the animals, from very near (10 cm) to the farthest distances reachable by monkeys (25 cm).

The time sequence of the task was identical to the one used in two recent reports involving other SPL areas (Hadjidimitrakis et al. 2014a, 2015, see Fig. 3.2d). The trial began when the animals pressed the button near their chest, outside the field of view (HB press). After 1s, one of the nine LEDs was switched on to green (Green-on). The monkeys had to fixate the LED within 500 ms, while keeping the HB button pressed. Then, the monkeys had to wait 1.5–2.5 s for a change in the color of the LED (from green to red) without performing any eye or arm movement. The latter color change was the go signal (Go) for the animals to release the home button and to start an arm movement toward the foveated target (M). Then, the monkeys reached the target (H) and held their hand on the target for 0.8–1.2 s. When the target cue was switched off (Red-off), the monkeys had to release this cue and return to the HB (HB press), which ended the trial and allowed the monkeys to receive a reward. The task was performed in blocks of 90 randomized trials, 10 for each target position. The luminance of LEDs was regulated to compensate for difference in retinal size between LEDs located at different distances. To prevent dark adaptation, the background light was switched on between blocks.

The presentation of stimuli and the animals' performance were automatically controlled and monitored by LabVIEW-based software (National Instruments) as described previously (Kutz et al., 2005), enabling the interruption of the trial if the monkeys broke fixation, made an incorrect arm movement, or did not respect the temporal constraints of the task described above. The correct performance of movements was monitored by pulses from microswitches (monopolar microswitches, RS Components, UK) mounted under the home button and each LED.
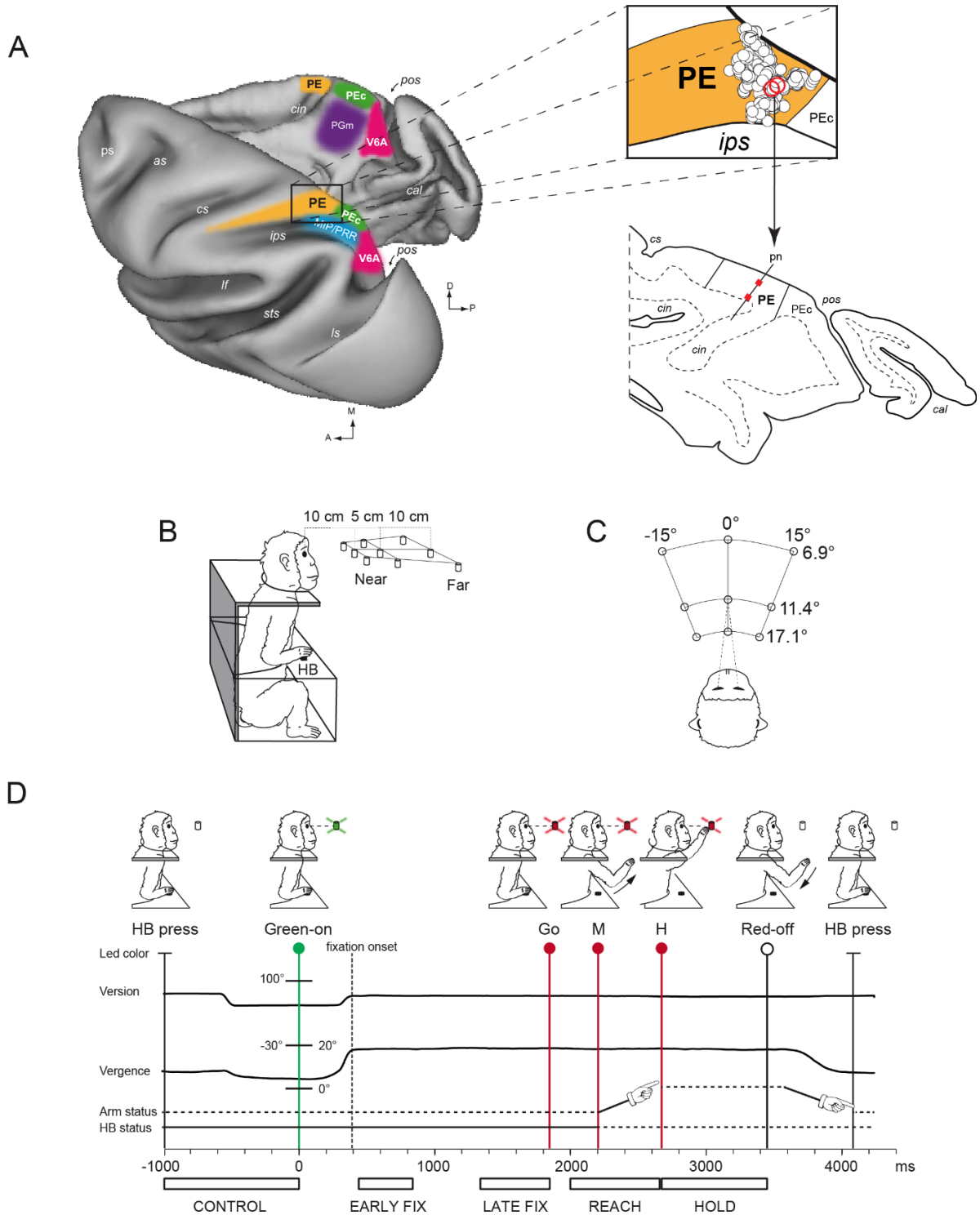
Figure 3.2 Reconstruction of our recording site within area PE, experimental set-up and task sequence. **a)** Left: Dorsal view of the left hemisphere and a medial view of the right hemisphere of a Macaca fascicularis brain reconstructed in three dimensions using Caret software (http://brainvis.wustl.edu/wiki/index.php/Caret:Download) showing the location and extent of area

PE (orange). The other medial PPC areas are also shown: V6A (pink, Galletti et al., 1999); PEc (green, Pandya and Seltzer 1982); medial intraparietal area/parietal reach region (MIP/PRR, light blue; Colby and Duhamel 1991; Snyder et al. 1997); PGm (purple, Pandya and Seltzer 1982). Abbreviations: as, arcuate sulcus; cal, calcarine sulcus; cin, cingulate sulcus; cs, central sulcus; ips, intraparietal sulcus; lf, lateral fissure; ls, lunate sulcus; pos, parieto-occipital sulcus; ps, principal sulcus; sts, superior temporal sulcus; D, dorsal; P, posterior; A, anterior; M, medial. Top right: Enlarged dorsal view of the recorded region, as reconstructed after the histological procedures. Each white dot represents one recorded cell. Bottom right: Parasagittal section of the brain with the reconstruction of a microelectrode penetration ('pn') passing through medial area PE. The red circles indicate recording sites of the cells circled in red in the upper figure. **b)** Scheme of the setup used for the Fixation-to-Reach task. Nine light-emitting diodes (LEDs) that were used as fixation and reaching targets were located at eye level. The distances of the 3 targets of the central row from mid-eye level are shown. HB, home button. **c)** Top view of the target configuration showing the values of version and vergence angles. **d)** Time sequence of task events with LED color, the eye's vergence and version traces, arm status, and HB status. From left to right, vertical lines indicate, respectively, trial start (HB press), target appearance (Green-on), fixation onset (dashed line, end of saccade movement), go signal (Go), start of the arm movement (M), holding phase of the target (H), turning off of the LED (Red-off), and trial end (HB press). The time between the Green-on and the fixation onset was not fixed, as illustrated, but it variated depending on animal's reaction time. Arm drawings indicate the forward and backward arm movement. White bars below the time axis illustrate the time intervals (epochs) used for the analysis of neural activity, from left to right: CONTROL, from home button pressing to fixation LED (green-on); EARLY FIX, from 50 ms after fixation onset till 450 ms after it; LATE FIX, the last 500 ms before the Go signal; REACH, from 200 ms before the start of the arm movement (M) to the pressing the LED; HOLD, from LED pressing till the offset of the LED (Red-off).

At the beginning of each recording session, the monkeys were required to perform a

calibration task to calibrate an eye tracker (ISCAN, see below). For the calibration, animals sequentially fixated 5 LEDs mounted on a vertically arranged panel placed at a distance of 15 cm from the eyes. For each eye, we extracted signals for calibration during fixation of five LEDs, arranged in the shape of a cross. One LED was centrally aligned with the eye's straight-ahead position and four LEDs were peripherally placed at an angle of ±15° (distance: 4 cm) both in the horizontal and vertical axes. From the two individually-calibrated eye position signals, we derived the mean of the two eyes (conjugate or version signal) and the difference between the two eyes (disconjugate or vergence signal) using the following equations:

$$\left[VERSION = \frac{(R+L)}{2} \right] \quad \& \quad [VERGENCE = R - L]$$

where R and L are the gaze direction of the right and left eye respectively, expressed in degrees of visual angle from the straight-ahead direction.

3.3.2.2 Visual stimulations

In the Visual fixation task, monkeys were trained to fixate a 0.5° diameter fixation point (FP) on a tangent screen (80° x 80°), 57 cm in front of them, ignoring any other visual stimulus still or moving across the visual field. Monkeys started each trial by pressing the HB and, after 2-6s, the FP turned green. Monkeys had to respond when the FP turned red by releasing the HB in order to receive a reward. The fixation target could appear at different positions on the screen in order to allow visual stimulations even in the far periphery of the visual field. While monkeys were performing the Visual fixation task, individual cells' visual sensitivity was first tested with a series of simple visual stimuli, like light/dark borders, light/dark spots, and bars that were rear-projected on the tangent screen. A cell was

considered sensitive to visual stimulations if the discharge, amplified and transformed in audio signals, was higher or lower during stimulations with respect to the baseline discharge, in absence of any other stimulations. If the neuron was unresponsive to these simple visual stimuli, testing was continued using more complex stimuli (light/dark gratings, shadows with irregular contours, shadows rapidly changing in size and/or shape, and corners of different orientation, direction, and speed of movement). If the cell was visually responsive, we mapped the borders of visual receptive field with the stimulus eliciting the best response. Cells responsive to either simple or complex visual stimuli were classified as visual, whereas unresponsive cells were classified as non-visual. A detailed description of the methodology used to test the visual sensitivity in SPL is reported in other papers (Gamberini et al., 2011, 2018).

3.3.2.3 Passive somatosensory stimulations

Animals got used to be manipulated and touched on the whole body by the experimenter, being rewarded with water and fruits during manipulation. Passive somatosensory stimuli, such as soft manual touching, palpation of deep tissue and joint rotation at different velocities were carried out on the entire body in darkness. Somatosensory stimulation started with superficial tactile stimulation, such as hair bending, superficial touch, or light pressure of the skin. Then we performed deep tactile stimulation (deep pressures of subcutaneous tissues) as well as proprioceptive stimulations (slow and fast rotations of the joints). When a cell responded to joint rotation, we compared neural responses obtained by superficial and deep tactile stimulation of the skin around the joint with those evoked by joint rotation performed without touching the skin around the joint. In some trials, tactile stimulations evoked neural responses that remained constant or were weakened during joint rotation; in others, tactile stimulations were ineffective while joint rotations evoked strong

89

responses. In the first case, the cell was classified as tactile sensitive; in the second, as joint sensitive. In some trials, the cell was responsive to tactile stimulation of the skin around a joint and responded more strongly to joint rotation: these cells were classified as tactile and joint sensitive. We are aware that our operational criteria do not exclude the possible participation of other somatosensory afferences, including muscle proprioception, and that neck rotation could not be tested in our experimental conditions because the experiments were performed with the monkey's head fixed. The same procedure has been used by our lab in other SPL areas (Breveglieri et al., 2002, 2006, 2008; Gamberini et al., 2018).

In both Visual fixation task and somatosensory stimulations, eye position was monitored to exclude the possibility that observed neuronal modulations were due to oculomotor activity. If the neural discharge was influenced by eye movements, visual/somatosensory stimulations were repeated until neural activity was collected under stable fixation behavior.

3.3.3   Surgical and recording procedures

A head-fixation system and a recording chamber were surgically implanted using aseptic procedures and under general anesthesia (sodium thiopenthal, 8 mg/kg/h, *i.v.*) following the procedures reported in Galletti et al. (1995). A full program of postoperative analgesia (ketorolac trometazyn, 1mg/kg, *i.m.,* immediately after surgery, and 1.6 mg/kg, *i.m.*, on the following days) and antibiotic care [Ritardomicina® (benzathine benzylpenicillin + dihydrostreptomycin + streptomycin) 1-1.5 ml/10kg every 5-6 days] followed the surgery. Extracellular recording techniques and procedures to reconstruct microelectrode penetrations were similar to those described in other studies (Galletti et al., 1996; Breveglieri et al., 2006, 2014; Gamberini et al., 2011, 2018). Single-cell activity was extracellularly recorded from area PE, located mainly on the exposed cortex of postcentral gyrus, between somatosensory cortex and PEc (Fig. 3.2a) (Pandya and Seltzer 1982). We performed single microelectrode

penetrations from the posteromedial part of PE, using multielectrode recording systems (5-channel MiniMatrix, Thomas Recording, GMbH, Giessen, Germany, for 2 animals, and 4-channels Alpha Omega Tower, Alpha Omega Engineering, Nazareth, Israel, for 1 animal). The electrode signals were amplified (at a gain of 10,000) and bandpass filtered (between 0.5 and 5 kHz). Action potentials in each channel were isolated online with a waveform discriminator (Multi Spike Detector; Alpha Omega Engineering, Nazareth, Israel, sampling rate 60 KHz). Eye position signals were sampled with 2 cameras (one for each eye) at 100 Hz and were controlled by a virtual window (4 x 4 degrees) centered on the fixation target. If monkeys fixated outside this window, the trial was aborted.

Histological reconstruction of electrode penetrations was performed following the procedures detailed in studies from our lab (Gamberini et al., 2011, 2018). Briefly, electrode tracks and the approximate location of each recording site were reconstructed on histological sections of the brain on the basis of electrolytic lesions and the coordinates of penetrations within the recording chamber. Present work includes only the neurons assigned to area PE following the cytoarchitectonic criteria according to Pandya and Seltzer (1982). The recording site involved the medial part of area PE (Fig. 3.2a).

3.3.4 Data analysis

All the analyses were performed using custom scripts in Matlab (Mathworks, Natick, MA, US, RRID: SCR_001622) and STATISTICA software (StatSoft, Tulsa, OK, US, RRID: SCR_014213). Most of these analyses have been performed also in two recent papers from our lab (Hadjidimitrakis et al., 2014a, 2015), which allows direct comparisons among the three SPL areas: PE, PEc, and V6A.

Analysis of the neuronal activity during the Fixation-to-Reach task was made by quantifying the discharge recorded during each trial in the following time epochs:

• *Control*: from HB pressing to fixation LED lighting up. It contains the neural discharge before fixation onset. This epoch has been only used to calculate the latency of the reach-related responses (see following Materials and Methods);

• *Early Fix*: from 50 ms after the end of the saccade to the green LED till 450 ms afterwards. It contains the neural discharge for LED fixation;

• *Late Fix*: the last 500 ms before the go-signal. It contains the cells' discharge during arm movement preparation;

• *Reach*: from 200 ms before arm movement onset (HB release) until the red target LED was reached. It contains the discharge of the cells during reaching execution. From trial to trial, this epoch was of different duration, depending on animal's movement times;

• *Hold*: from LED pressing till the target (red LED) offset. It contains the discharge of the cells during LED pressing.

Movement times in reaching trials were calculated as the time difference between HB release and target LED press, as detected by presses/releases of the microswitches.

The effect of target depth and direction on neural activity was analyzed only for those units with a mean firing rate higher than 3 spikes/s in at least one spatial position. In addition, we only included those neurons that were recorded during at least 7 trials per spatial position. The reasons for these conservative criteria are dictated by the intrinsic high variability of biological responses, particularly in the PPC, and are explained in detail in Kutz et al. (2003). We first used a 2-way analysis of variance (ANOVA) to quantify the proportion of neurons modulated by each variable in each epoch. Target depth was defined as the distance of the target from the animal (near, intermediate, far), and target direction as its position with respect to the recording hemisphere (ipsilateral, central, contralateral). We considered that neurons were modulated by a given factor only when the factor's main effect was significant ($p < 0.05$). Given that the target was foveated in all epochs of interest, its depth and direction

in space were determined by the vergence and version angles of the eyes, respectively. That said, when we refer to spatial tuning analysis and data in the remainder of this article, the terms depth and vergence, as well as direction and version, are interchangeable.

We applied a two-proportion z-test (Zar, 1999), as detailed in Fluet et al. (2010), to make comparisons between the proportion of cells modulated by depth, direction or both. To perform this test, the SE of the sampling distribution difference between two proportions was computed as:

$$SE = \sqrt{p(1\text{-}p)[(1\div n_1)(1\div n_2)]}$$

with $p = [(n_1 \times p_1)(n_2 \times p_2)] \div (n_1 + n_2)$ representing the pooled sample proportion and n_1/p_1 and n_2/p_2 representing the size and proportion, respectively, of each sample. Subsequently, the z score was calculated as $z = (p_1 - p_2)/SE$, and its corresponding P value was obtained from the (cumulative) normal distribution.

To investigate the population activity during the course of a trial, we tested for significant tuning at multiple time points t using a 2-way ANOVA on the spike count in a 200 ms window centered around t. This test was repeated in time steps of 50 ms (sliding window ANOVA, $p < 0.05$, Fig. 3.4b). Criteria for significant tuning were the same as for the ANOVA analysis of the fixed time epochs.

To analyze the spatial tuning of activity, a stepwise multiple linear regression model was applied in each epoch of interest.

To relate the neural activity in the epochs of interest to the different target positions, we applied the following equation for the firing rate using this regression model:

$$A(X_i, Y_i) = b_0 + b_1 X_i + b_2 Y_i$$

where *A* was the neural activity in spikes per second for the *i*th trials; X_i and Y_i the positions of the target defined as vergence and version angles, respectively, of the eyes; b_1 and b_2 were regression coefficients and b_0 the intercept. After being tested for their significance, the vergence and version coefficients were normalized with the standard deviation of vergence and version, correspondingly. The normalized coefficients allow a comparison among the independent variables and provide information about their relative influence in the regression equation. In the present study, this allowed us to compare the vergence and version coefficients and to account for differences in range of angles for vergence and version (10.2° vs. 30°, respectively). The regression coefficients were selected using a backward stepwise algorithm (Matlab function "stepwise") that determined whether the coefficients were significantly different from zero. At the end of the stepwise algorithm, only the coefficients that were statistically different from zero remained ($p<0.05$). These coefficients were then used to determine the spatial preference only in the cells with a significant main effect (ANOVA, $p<0.05$) in a certain epoch. In each neuron, the sign of the linear correlation coefficients (normalized) were used to determine the spatial preference in a certain epoch. In those cases in which the linear coefficients were not significant, but the neurons were modulated by at least one of the two factors considered in the ANOVA (i.e depth and direction), a Bonferroni post hoc test ($p<0.05$) was applied to define the preferred position.

To quantify the spatial selectivity of neurons linearly modulated by depth or direction, we calculated selectivity indices (SI) which take into account the magnitude of the neurons' response to the movement depth and direction evoking the highest discharge. We calculated the SI separately for depth and direction using the following equations:

$$\left[SI_{depth} = \frac{(best\ far\ \text{-}\ best\ near)}{(best\ far\ +\ best\ near)} \right] \quad \& \quad \left[SI_{direction} = \frac{(best\ contra\ \text{-}\ best\ ipsi)}{(best\ contra\ +\ best\ ipsi)} \right]$$

where 'best far' and 'best near' are the activities for the far and near positions, respectively, evoking the highest discharge, and 'best contra' and 'best ipsi' are the activities for the contralateral and ipsilateral positions, respectively, evoking the highest discharge. The indices range from -1 to 1. Neurons with values close to -1 indicate a high selectivity for NEAR (or IPSILATERAL) positions, whereas values close to 1 denotes neurons with a high selectivity for FAR (or CONTRALATERAL) positions in 3D space. Values close to 0 indicate a similar response for all reach depths (or directions). We used a two-sample Kolmogorov–Smirnov test to compare the cumulative distributions of SI_{depth} and $SI_{direction}$ in each epoch ($p<0.01$).

Population responses of neurons modulated by target depth/direction in the epochs of interest were computed as averaged spike density functions (SDFs). For each neuron, an SDF was calculated (Gaussian kernel, half-width at half maximum 40 ms) for each trial and averaged across all the trials of the preferred and non-preferred depths and directions as defined by the linear regression analysis. We found the peak discharge rate of the preferred condition and used it to normalize the SDF. Population SDF curves representing the activity of the preferred and non-preferred target positions were constructed by averaging the individually-normalized SDFs of the cells (Marzocchi et al., 2008), aligned at the behavioral event of interest. We statistically compared the population SDFs curves of preferred and non-preferred positions with a permutation test (10,000 iterations) comparing the sum of squared errors of the actual and randomly permuted data. The intervals of the curve that we compared were different according to the epoch considered: for cells modulated by depth/direction during EARLY FIX, the interval was from 50 to 450 ms after saccade offset; for cells modulated during REACH, the interval was from 200 ms before the movement onset until the red target LED was reached.

To find the onset of the reach-related response, a sliding window (width = 20 ms, shifted by 2 ms) was used to measure the activity starting from 200 ms before the movement onset in all of the tested conditions. This activity was compared with the firing rate observed in the 1000 ms before fixation LED onset (CONTROL epoch, Student's t-test, $p<0.05$) in agreement with what was used in another PE study (Kalaska et al., 1983). The onset of the response was determined as the time of the first of 5 consecutive bins (10 ms), where comparisons were statistically significant ($p<0.05$). The above procedure, also used in a recent V6A paper (Hadjidimitrakis et al., 2014a), was adapted from earlier work (Nakamura and Colby, 2000).

3.4   Results

In the present study, we investigated the functional properties of the medial part of PE (see Fig. 3.1), a cortical area largely neglected in previous studies. We evaluated the influence of depth and direction of reaching on the activity of PE cells during reaches in 3D space. We used a Fixation-to-Reach task whereby target elevation was kept constant at eye level (Fig. 3.2b), to avoid the possible modulating effect of gaze elevation on cell discharge, a factor effectively modulating many PPC cells (see Galletti et al., 1995; Hadjidimitrakis et al., 2011). This task required the monkeys to transport the hand from a fixed position near the body to one of nine targets in peripersonal space.

We recorded activity of 176 single PE neurons in five hemispheres of three monkeys (left hemisphere/total: M1, 24/90; M2, 51/73; M3= 13/13). No significant differences between results from different monkeys were found in all the analyses performed (Chi squared test, $p>0.05$), thus they will be presented jointly. The histological reconstruction of recording sites showed that microelectrode penetrations were performed in the medial part of area PE (see inset in Fig. 3.2a). We examined the neural responses during four epoch intervals: initial

LED fixation (EARLY FIX, see Materials and Methods), movement preparation (LATE FIX), movement execution (REACH), and LED holding (HOLD).

Figure 3.3 shows two examples of the most represented classes of PE cells: those tuned only by depth (Fig. 3.3a, 2-way ANOVA, $p<0.0001$ in EARLY FIX, $p<10^{-9}$ in LATE FIX, $p<10^{-27}$ in REACH, $p<10^{-26}$ in HOLD) and those tuned only by direction (Fig. 3.3b, 2-way ANOVA, $p<10^{-5}$ in LATE FIX, $p<0.01$ in REACH, $p<10^{-10}$ in HOLD). The neuron in Fig. 3.3a increased its discharge rate right before the movement onset (mean reach-related incremental response relative to HB release: -120 ± 83 ms, SD) and peaked in activity during the arm movement. The cell exhibited a preference for near and intermediate space (Fig. 3.3a, bottom and intermediate rows) during all the epochs considered, particularly during the execution of reaching movement and LED pressing (epochs REACH (R) and HOLD (H) in Fig. 3.3a). The neuron in Fig. 3.3b discharged strongly during the execution of reaches and LED pressing for ipsilateral and central positions with respect to the recording hemisphere (Fig. 3.3b, left and central columns). Contrary to the previous example, the discharge rate increased after the arm movement onset (reach-related incremental response: $+102 \pm 93$ ms, SD) and was maintained during the HOLD epoch.

The neuron of Fig. 3.3a showed also a weak tuning of activity and slightly increased its discharge rate during the EARLY FIX and LATE FIX epochs (Fig. 3.3a, EF and LF respectively). As in the reaching and holding epochs, the activity was higher during EARLY FIX and LATE FIX for the nearest positions. The neuron of Fig. 3.3b reduced its activity during the last part of EARLY FIX and throughout the LATE FIX part of the trial (Fig. 3.3b, EF and LF respectively). This inhibition of activity during LATE FIX was spatially tuned, with stronger effects for the ipsilateral and near space.
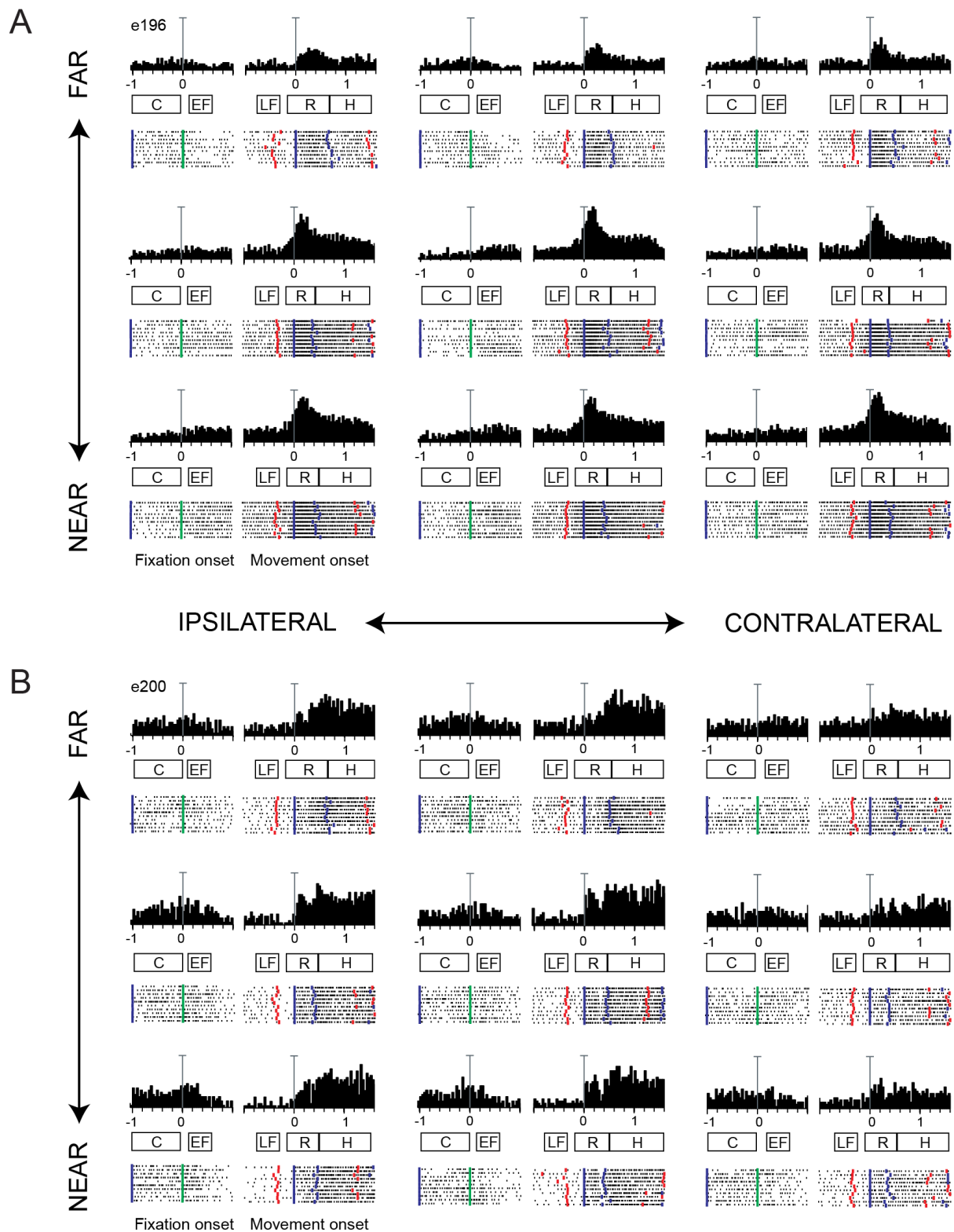
Figure 3.3 Examples of medial PE neurons modulated by depth **(a)** and direction **(b)**. **a)** Neuron showing depth tuning starting immediately before movement onset and reaching its maximum during movement execution. Spike histograms (top), and rasters (middle), are shown for the 9 target

positions. Coloured behavioral markers are from left to right: HB pressing, fixation onset, go signal, movement onset, movement end, target offset, backward movement onset. Rows represent the 3 depths (from bottom to top: NEAR, INTERMEDIATE, FAR) and columns the 3 directions (from left to right: IPSILATERAL, CENTER, CONTRALATERAL). Activities are aligned to fixation onset and arm movement onset. Horizontal scale: 200 ms/div. Vertical scale bar on histogram: 90 spikes/s. Rectangles below histograms indicate the duration of the epochs CONTROL (C), EARLY FIX (EF), LATE FIX (LF), REACH (R), HOLD (H). **b)** Neuron showing a preference for ipsilateral space during reaching execution and holding time. All conventions are as in **(a)**, vertical scale on histogram: 73 spikes/s.

3.4.1 Dynamic Depth and Direction tuning during the task

Modulation of neural activity by depth and direction was studied through a two-way ANOVA ($p<0.05$) with target depth (near, intermediate, far with respect to the body) and target direction (contralateral, center, ipsilateral with respect to the recording hemisphere) being the two factors in each task epoch. One hundred thirty-nine PE neurons (79%) were modulated by at least one of the two factors in at least one epoch. Interaction effects between the 2 factors was observed in 6% of the cells across epochs. However, very few neurons (3%) showed *only* the interaction effect, so hereafter only the main effects of depth and direction will be considered. The results of the two-way ANOVA for each epoch are reported in Fig. 3.4a. Neurons modulated only by depth or only by direction were the most represented classes of tuned cells in area PE (see Fig. 3.4a, DEPTH and DIRECTION respectively). The incidence of neurons modulated only by depth or direction followed a different time course across epochs. The percentage of depth modulated neurons significantly increased (two proportion z-test, EARLY FIX vs. REACH, p=0.008) from 14% and 12% (EARLY FIX and LATE FIX, respectively) before the arm movement to 24% and 22% during REACH and HOLD. By contrast, the direction-modulated neurons peaked during the fixation epoch

(EARLY FIX, 18%), significantly decreased during the LATE FIX and REACH (12 and 10% respectively, two proportion z-test, EARLY FIX vs. REACH, p=0.015) and slightly increased again during HOLD (15%). Across epochs only about 10% of cells was modulated by both signals ('BOTH', Fig. 3.4a), with a mild though insignificant increase in selectivity during the last phases of the task (two proportion z-test, EARLY FIX vs. HOLD, p=0.07). The low proportion of 'BOTH' cells suggests a substantial degree of separation between depth and direction signals, especially during REACH and HOLD, where the fraction of depth-modulated cells ('DEPTH') was significantly different from 'BOTH' cells (two-proportion z-test, p=0.0006 in REACH, p=0.02 in HOLD). We also tested whether the proportion of cells tuned for both depth and direction differ significantly from chance level, given the percentages of depth and directionally modulated cells. We found that the percentages of 'BOTH' cells did not differ significantly from chance in any of the tested epochs (two-proportion z-test, p>0.05).
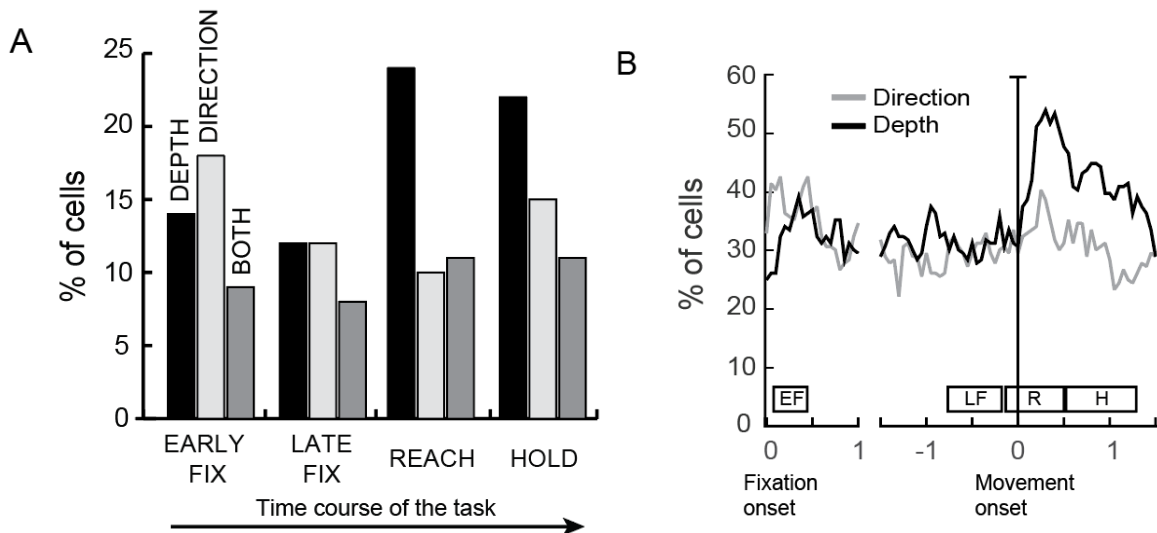
Figure 3.4 Distribution of the incidence of significant effects modulating PE cells and strength of depth and directional tuning. **a)** Histograms show the results of a two-way ANOVA (factors: DEPTH and DIRECTION, $p<0.05$) as incidence of modulated cells during the target fixation (epoch EARLY FIX), reaching preparation (epoch LATE FIX), execution (epoch REACH) and LED pressing (epoch HOLD). **b)** Percentage of tuned cells by depth (black line) and direction (grey line) in a sliding window ANOVA (width: 200 ms, step: 50 ms). Trials are aligned to fixation and movement onsets. Rectangles below each plot indicate the functional time epochs ('EF', EARLY FIX; 'LF', LATE FIX; 'R', REACH; 'H', HOLD).

To examine the temporal evolution of tuning with finer detail we performed a sliding window analysis (Fig. 3.4b; width: 200 ms, step: 50 ms) that confirmed the time course of the modulating effects suggested by the plot in Fig. 3.4a: the percentage of cells modulated by depth (Fig. 3.4b, black line) surpassed those modulated by direction (Fig. 3.4b, grey line) immediately after movement onset, and this effect was maintained during the HOLD epoch (see Fig. 3.4b).

3.4.2 *Space representations across different epochs*

To characterize the spatial preference of modulated neurons, a linear regression analysis was performed, considering target depth and direction as independent variables. We decided to apply this model because we observed that the modulations were generally of planar type and only a few neurons gave their maximum response for central positions (3% of cells, Bonferroni post hoc test). We calculated the percentage of neurons modulated by target depth and direction (two-way ANOVA, $p<0.05$) with a significant linear correlation ($p<0.05$). As shown in Table 3.1, the number of PE neurons modulated by depth with significant linear regression coefficients slightly increased across the task epochs, and a similar trend was observed for neurons modulated by direction.

	DEPTH		DIRECTION	
	ANOVA	**REGRESSION**	**ANOVA**	**REGRESSION**
EARLY FIX	40/176 (23%)	30/40 (75%)	47/176 (27%)	35/47 (74%)
LATE FIX	35/176 (20%)	26/35 (74%)	35/176 (20%)	25/35 (71%)
REACH	62/176 (35%)	52/62 (84%)	36/176 (20%)	30/36 (83%)
HOLD	57/176 (32%)	51/57 (89%)	45/176 (26%)	35/45 (78%)

Table 3.1. Number and percentage of neurons modulated by depth and direction in each epoch

Neurons modulated by depth were classified as 'NEAR' or 'FAR' and neurons with directional tuning as 'CONTRALATERAL' or 'IPSILATERAL', depending on the sign of the correlation coefficient. Figure 3.5a shows that the majority of cells modulated only by depth (Fig. 3.5a, top panels) preferred far spatial positions in all epochs, though this preference was significant only during the REACH epoch (Chi squared test, $p<0.01$). This

bias for far spatial positions most likely reflects a movement amplitude, and this is corroborated by the fact that all animals showed longer arm movement durations when targets were located in the far space (mean movement time for near space: 546 ± 53 ms, SD; mean movement time for far space: 631 ± 64 ms, SD (ANOVA, $p=4*10^{-34}$). Cells tuned only for direction (Fig. 3.5a, bottom panels) showed a gradual shift from a slight preference for the CONTRALATERAL space in 'EARLY FIX' to a more pronounced preference for the IPSILATERAL space in 'HOLD', achieving statistical significance only in this latter epoch (Chi squared test, p<0.05).

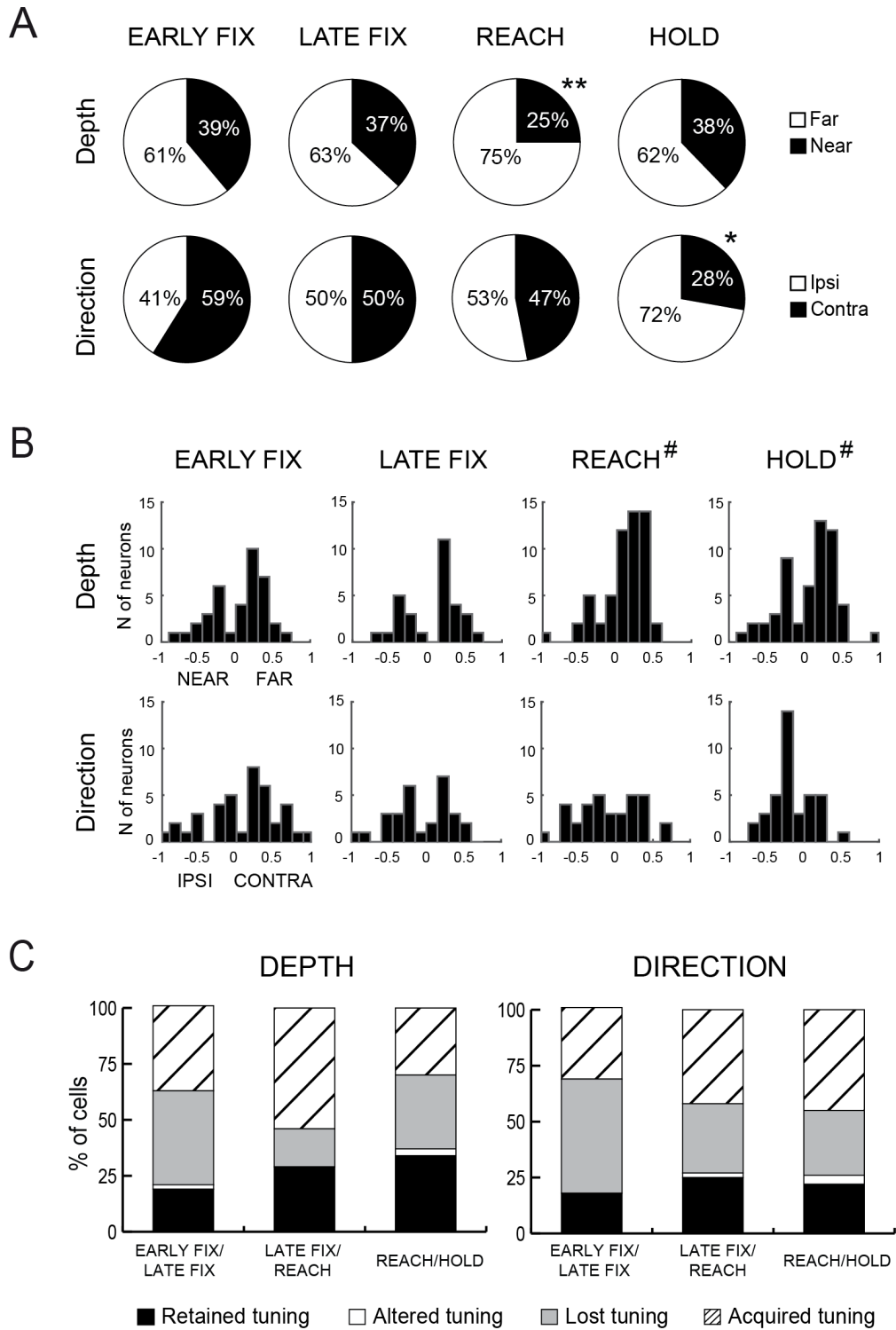**Figure 3.5** Spatial preference, indices and tuning consistency across different epochs. **a)** Top: Percentage of cells modulated by depth with a preference for far ('FAR', white) or near ('NEAR', black) space in each epoch. Bottom: Percentage of the cells linearly modulated by direction with a preference for ipsilateral ('IPSI', white) or contralateral ('CONTRA', black) space in each epoch.

Asterisks indicate a statistically significant spatial preference (*: Chi squared test, p<0.05, **: Chi squared test, p<0.01. The chi squared test was perfomed on the numbers of neurons in each of the compared group). **b)** Distribution of selectivity indices of reaching cells calculated for EARLY FIX, LATE FIX, REACH, and HOLD for depth and direction separately. Data refer to reach-related activity collected while the animal performed an arm movement directed toward the preferred spatial position. Negative values of the index indicate neurons that present stronger selectivity for 'NEAR' and 'IPSI' positions; positive values neurons that show higher selectivity for 'FAR' and 'CONTRA' positions. Hashes indicate a statistical difference between the cumulative distributions of SI_{depth} and $SI_{direction}$ (two-samples Kolmogorov–Smirnov test, p<0.01). **c)** Percentages of cells that retained (black), altered (white), lost (light grey) or acquired later (hatched) their tuning in depth (left) and direction (right) in pairs of consecutive epochs during the task.

To quantify the strength of the spatial tuning, we calculated a selectivity index for each modulated neuron, disjointly for depth and direction (SI; see Materials and Methods). The value of SI, which ranges from -1 to 1, indicates whether neurons discharged more for FAR vs. NEAR, or CONTRALATERAL vs. IPSILATERAL positions. The SI distributions are shown in Figure 3.5b, separately for each action epoch. The analysis shows a significant difference between the distributions of SI_{depth} and $SI_{direction}$ during the REACH and HOLD epochs (two-samples Kolmogorov–Smirnov test, p<0.01), with neural discharges more selective for farthest and ipsilateral targets. To evaluate the consistency of spatial preference across single neurons, we quantified the cells that retained, altered, lost, or acquired their spatial preference from one epoch to the next. As shown in Fig. 3.5C, the incidence of cells that retained their spatial preference is quite low (about 25%), both in depth and in direction. Many cells acquired or lost their tuning during the time-course of the trial, both in depth and in direction. This was particularly evident at the transition from the LATE FIX to the REACH epoch, with more than half of the cells (54%) becoming depth tuned at the later

epoch. The same trend was evident in the cells tuned for direction (Fig. 3.5C, right), where a considerable number of neurons lost their spatial tuning after the early phases of the task (EARLY FIX/LATE FIX, 51%), and an increasing number of cells acquired their spatial tuning as the task progressed (LATE FIX/REACH, REACH/HOLD, 30%). In summary, the trends were similar for depth and direction, with a remarkable increase in the number of spatially tuned cells -especially for depth-tuned cells- as the trial progresses from action preparation to execution.

3.4.3 Cell categories

Changes in neuronal tuning from epoch to epoch formed the basis of a complementary system of cell classification. To this regard, PE cells could be divided in three categories: "*Fix*" neurons, that showed a significant change in activity at the onset of fixation (EARLY FIX) and a spatial tuning during EARLY FIX, but not during REACH; "*Reach*" neurons, showing the opposite modulation; "*Fix-Reach*" neurons, responsive and spatially tuned in both epochs. We adopted the same categorization scheme already used in our studies of V6A and PEc (Hadjidimitrakis et al., 2014a, 2015), and this enabled us to make comparisons of PE categories with the same categories in V6A and PEc (see below). Moreover, the vast majority of PE cells modulated before the movement onset (epoch LATE FIX) belonged to one of the categories mentioned above (~75% of depth modulated cells, ~60% of directional modulated cells, 2-way ANOVA, $p<0.05$). Fig. 3.6a shows that the three cell categories (Fix, Reach, Fix-Reach) were differently represented (Chi squared test, $p<0.01$) between depth- and direction-modulated cells. The largest fraction of neurons modulated by depth were REACH cells (32%, N= 44/139), with the other categories containing half or less cells (Fig. 3.6a left, 16% Fix, 13% Fix-Reach, Chi squared test, $p<0.05$). In contrast, neurons affected by direction were virtually equally distributed among

the three classes (Fig. 3.6a, right; Chi squared test, $p > 0.05$). Figure 3.6b shows the anatomical distribution of the three types of cells in the part of area PE we studied. Each circle represents one cell. There was no obvious spatial clustering or gradient between the three cell categories that was sufficiently regular across the five hemispheres studied to register on a combined map of this part of PE.

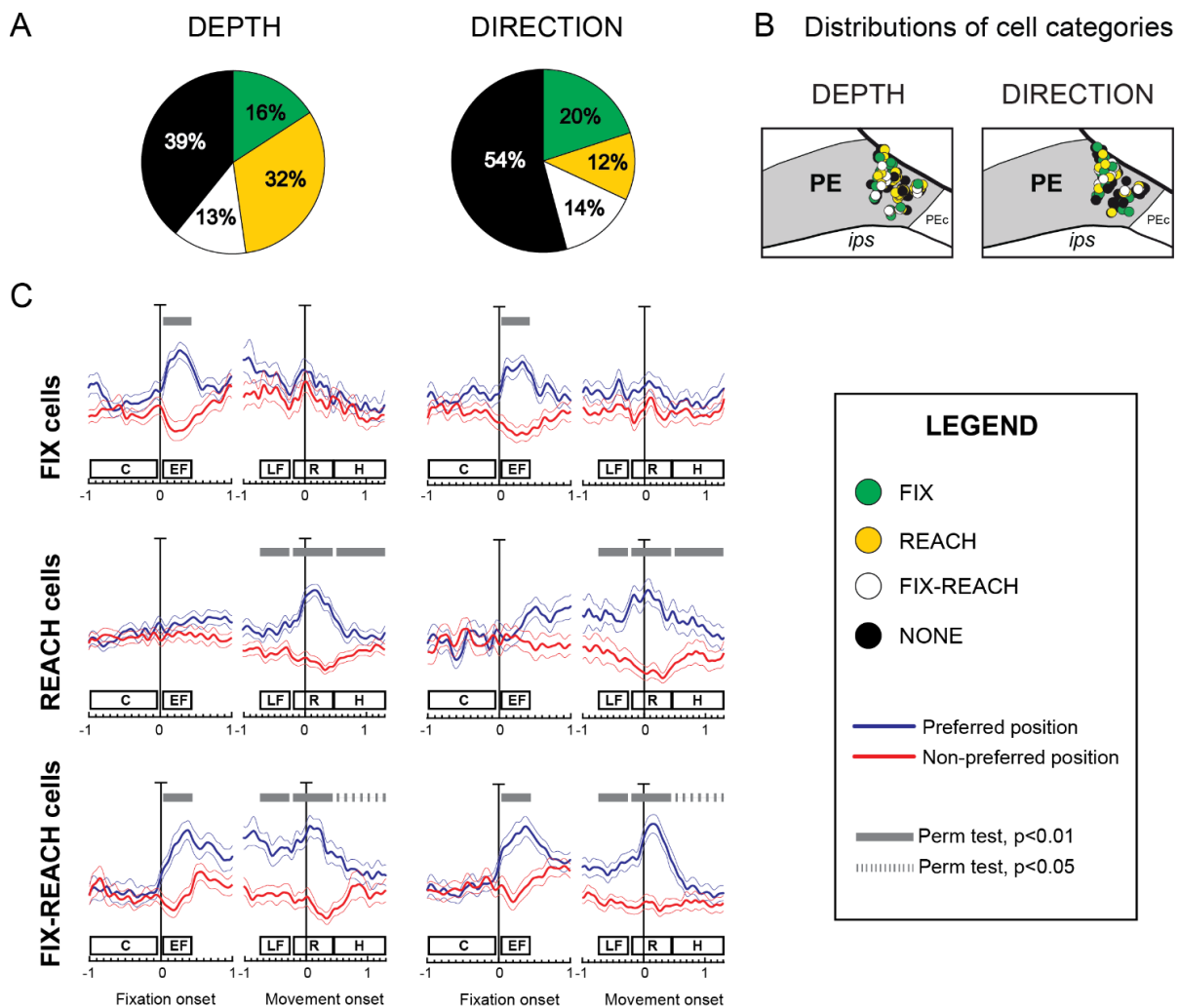**Figure 3.6** Main cell categories in PE, their anatomical distribution and their population discharge. **a)** Percentage of neurons modulated by depth (left) and direction (right) in both EARLY FIX and REACH epochs (Fix-Reach cells; white), in EARLY FIX but not in REACH (Fix cells; green), and vice versa (Reach cells; yellow) or in none of them (black). **b)** Two dorsal views of PE (see Fig. 3.2)

representing the distributions of the different categories of cells modulated by depth (left) and direction (right). Each circle represents one cell. **c)** Population activity of the main categories of PE cells, represented as average normalized SDFs of Fix (top), Reach (middle), and Fix-Reach cells (bottom) modulated by depth (left) and direction (right), aligned twice (vertical lines) at the fixation onset and at the movement onset. For each cell category and type of modulation, the average SDFs for the preferred (blue) and non-preferred positions (red) are plotted. Thin lines in SDF represent the standard error of the mean. Scale bar in all SDF plots: 100% of normalized activity. Lines above epoch rectangles indicate where the permutation test was significant (dashed lines, $p < 0.05$; solid lines, $p < 0.01$). Other conventions as in Figures 3.2 and 3.4.

To evaluate the tuning of Fix, Reach, and Fix-Reach cells at population level, we calculated the average normalized spike density functions (SDFs), separately for the three different cell categories. Figure 3.6C illustrates the average population activity of each category of cells for depth-modulated (left panels) and direction-modulated (right panels) cells. As expected, the activity in the preferred and non-preferred conditions of Fix cells (Fig. 3.6C, top panels) started to diverge immediately after the onset of fixation and reached its peak during the fixation epoch (permutation test for EARLY FIX, $p < 0.01$). The population activity in non-preferred depths and directions, instead, slightly decreased instantly after fixation onset, suggesting the presence of an inhibitory input upon these cells. The population discharge in preferred depths and directions conditions declined after the end of the fixation epoch and reached the non-preferred activity levels well before the onset of arm movement, which was maintained during action execution (LATE FIX, REACH; permutation test, $p > 0.05$).

In the Reach cells (Fig. 3.6C, middle row), the population responses for the preferred and non-preferred depths showed no significant changes during the fixation epoch, and the two curves progressively diverged during the movement preparation (LATE FIX, permutation test, $p < 0.01$). In the preferred condition, the curves started to increase before the onset of the

arm movement and peaked just after arm movement onset. Inhibition of population activity was also observed in depth- and direction-modulated cells during the execution of non-preferred arm movements.

Fix-Reach neurons (Fig. 3.6C, bottom panels) showed a pattern of population responses that combined those of Fix and Reach cells. The population activity for preferred and non-preferred conditions clearly diverged immediately after fixation onset and remained separated during all other epochs considered (permutation test, p<0.01 in EARLY FIX, LATE FIX, REACH, p<0.05 in HOLD) for both depth and direction. Two peaks of activity, one ~300 ms after fixation onset and the other just after reaching onset, were observed. Interestingly, the activity in non-preferred conditions decreased both during EARLY FIX (see also Fix cells, top row of Fig. 3.6C) and REACH, and the selectivity dropped in between the EARLY FIX and the LATE FIX, especially for Fix-Reach cells only modulated by direction. This loss of selectivity is likely to reflect weak tonic fixation signals in PE, and this is corroborated by the results of the 2-way ANOVA (Fig. 3.4), where the proportion of neurons modulated during EARLY FIX is significantly lower than other epochs (two-proportion z-test, p<0.01). Instead, in the neighboring areas V6A and PEc there was a persistent higher activity for the preferred position during FIX and DELAY and the selectivity was maintained in between the two epochs, possibly reflecting a more sustained influence of fixation (Hadjidimitrakis et al., 2014a, 2015).

To address how the neuronal activity of the entire recorded population of medial PE neurons changes during the reach task, independent of any preselection of neuronal subclasses (as in Fig. 3.6C), we computed the cumulative SDFs of PE cells considering the entire population of recorded neurons (N= 176), even those not modulated by depth and direction during any of the task epochs (2-way ANOVA, p>0.05). The strongest response was classified as the preferred one, and the weakest as the non-preferred. As shown in Fig. 3.7, the SDFs of the

preferred (blue line) and non-preferred (red line) conditions significantly separated immediately after fixation onset (epoch EF) and became particularly prominent during the movement preparation and execution phases of the task (epochs LF and R, permutation test, $p<0.01$). A clear peak in activity can be observed in the preferred condition, immediately after movement onset, whereas activity in the non-preferred condition decreased particularly during the execution phase (epoch R). The shape of the curves and their time courses resemble the population response of the Reach cells (Fig. 3.6C, middle panels), thus strongly suggesting that, also at population level, PE neurons process more prominently skeletomotor than visuospatial signals.

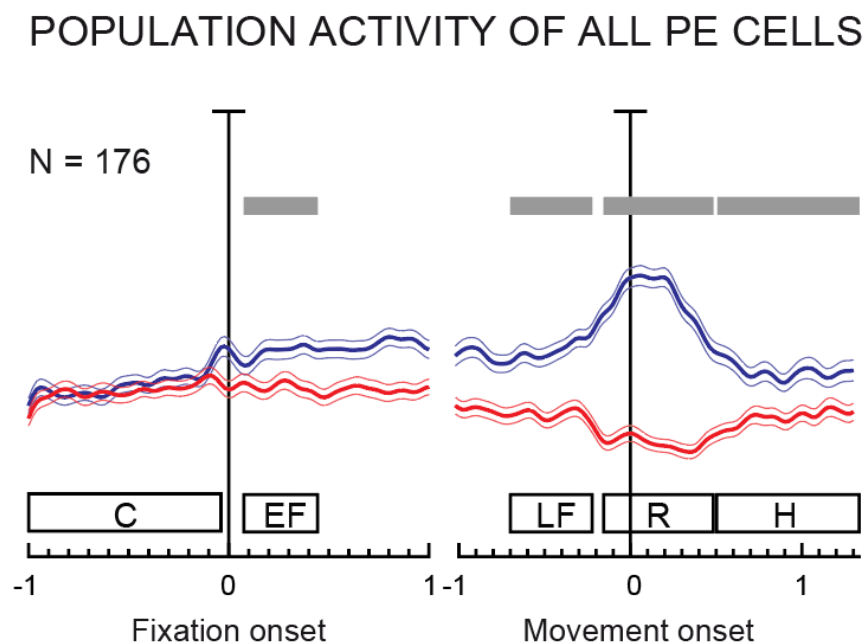POPULATION ACTIVITY OF ALL PE CELLS

Figure 3.7 Average normalized SDF of the whole population of recorded PE neurons (N= 176). Permutation test between preferred and non-preferred position in EARLY FIX, LATE FIX, REACH, HOLD, $p<0.01$. All conventions are as in Figure 3.6c.

Overall, neural activity remained stable and low after the EARLY FIX epoch (middle panels of Fig. 3.6C and Fig. 3.7), suggesting that eye position does not have a strong modulating influence in PE.

To test whether the target onset could possibly lead to short-latency visual responses, we also calculated the SDFs aligned to the target onset. There was no clear increase of discharge after target onset, thus confirming a lack of visual responses in area PE that has been reported in literature (Mountcastle et al., 1975; Maimon and Assad, 2006; Cui and Andersen, 2011; Shi et al., 2013).

3.4.4 Sensory properties in the recorded region

To characterize the sensory properties of the recorded medial PE sector, we qualitatively examined the visual and somatosensory responses of a separate group of PE cells recorded in the same region as the cells tested with the reaching task, by using two additional tests (Visual and Passive Somatosensory stimulations, see Materials and Methods). The results of these sensory stimulations showed that the part of PE we studied is strongly affected by somatosensory inputs but poorly by visual inputs (Fig. 3.8a-b), similarly to what has been found by other studies in the lateral part of PE (see Seelke et al. 2012 for refs). Eighty-seven percent of neurons (N= 53/61) were responsive to somatic stimulations (see Materials and Methods), whereas only 2% of neurons (N= 1/60) were sensitive to visual stimulations.

Regarding the type of somatosensory input, we found that the majority of cells modulated by passive somatosensory stimulations responded to joint rotations (89%, N= 47/53), whereas only 4% responded to tactile stimulation and 7% to both joint rotations and tactile stimulation (Fig. 3.8c). The distribution of somatosensory receptive fields did not match the somatotopy reported for the nearby Brodmann's area 2 (see Fig. 3.1). We did not find a mere

representation of the lower limb, as expected if medial PE had a somatotopy complementary to the upper limb representation in lateral PE. Instead, we found intermingled lower and upper limb representations, together with sporadic representations of the trunk (Fig. 3.8f). Joint-sensitive cells were mostly activated by input coming from the arms (23%) and the legs (26%). The remaining 51% of somatosensory cells were activated by input coming from multiple parts of the body (e.g. arms, legs, trunk, Fig. 3.8d). A high percentage of somatosensory responses (47%) were evoked by contralateral stimulation and an equal number of cells (47%) responded to stimulation of both sides (bilateral), with only 6% of cells with somatosensory receptive fields on the ipsilateral side (Fig. 3.8e).
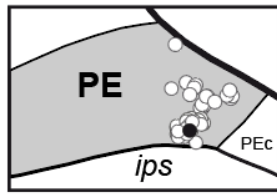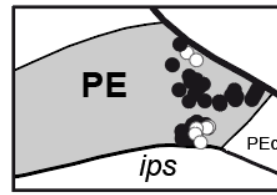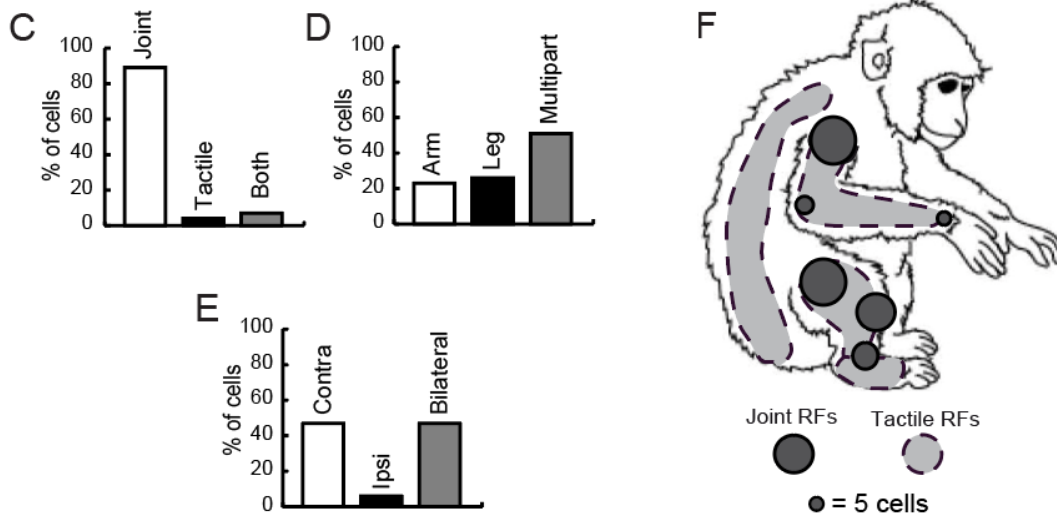
Figure 3.8 Sensory properties of PE cells. Anatomical distributions of the neurons showing visual **(a)** and somatic **(b)** responses. **a)** 'Visual' cells are shown in black, 'Non-visual' cells in white. **b)** Somatosensitive cells are shown in black, unresponsive cells in white. **c)** Incidence of cells responsive to joint, tactile or joint+tactile (Both) stimulations. **d)** Incidence of cells modulated by stimulations of different parts of the body. **e)** Incidence of contralateral (Contra), ipsilateral (Ipsi), and Bilateral modulations. Abbreviations as in Fig. 3.3. **f)** Locations of somatosensory receptive fields in PE: joints (circles) and tactile receptive fields (dashed lines drawn on the animal body). The size of each circle is proportional to the number of modulated units. All somatosensory receptive fields have been reported on the right side of the body.

3.5   Discussion

Our aim was to functionally characterize the most medial and caudal part of area PE and to examine the relative influence of depth and direction signals during a Fixation-to-reach task in 3D. We aimed to reproduce everyday life reaching conditions, with the arm moving in different directions and depths and a natural sequence of eye–hand coordination that involves fixation of the target before the arm movement (Neggers and Bekkering, 2001; Hayhoe et al., 2003). We are aware that it cannot be excluded that differences in activity during reach execution are void of gaze signals. However, to the best of our knowledge, there is no evidence supporting a strong modulating effect of gaze position on neural activity in PE. To this regard, Ferraina and coworkers (2009) investigated how the vergence angle, and initial hand position influenced PE reach-related activity. They showed that a large proportion of PE neurons was influenced by changes in hand position, while the effect of binocular eye position was small (~10% of neurons were affected by changes in fixation distance). Moreover, looking at Figure 3.6C (middle panels, population activity of Reach cells), and Figure 3.7, where the entire recorded population activity is shown, it is clear that neural activity remained stable and low after fixation onset and throughout the subsequent fixation period and started to increase towards movement onset. These findings suggest that gaze signals have a relatively weak influence on PE neural activity during the reach phase. Gaze position modulations in PE may derive from the thalamic centromedian (CM) nucleus, that exhibits a variety of eye movement-related signals (Tanaka, 2005; Kunimatsu and Tanaka, 2012), even if the connections with PE are quite weak (Impieri et al., 2018). Another source of tonic eye position signals could be the nucleus prepositus hypoglossi (NHP) in the brainstem that has been characterized as an integrator of horizontal oculomotor commands (Moschovakis et al., 1996). This nucleus has been reported to send projections, via thalalmus,

to the nearby medial intraparietal area (MIP) of SPL (Prevosto et al., 2009). Since the reported NHP input was heavily lateralized, this could result in some form of asymmetry in the cortical coding of eye position that would not necessarily be captured by binocular version/vergence measurements. It would be interesting to check whether the monocular (contralateral) eye position associated with the three different depths could provide a better prediction of neural activity. This issue will be addressed for all SPL areas in future studies.

We show that medial PE activity was tuned by both depth and direction of reaching, but the processing of the two parameters followed a different time course as the task progressed. Direction-tuned cells were most abundant just after target fixation, outnumbering depth-tuned cells during that period. Depth tuning increased during arm movement and target holding. These findings are in agreement with behavioral studies suggesting independent processing of reach direction and extent or amplitude information (Soechting and Flanders, 1989; Flanders and Soechting, 1990; Gordon et al., 1994; Sainburg et al., 2002; Vindras et al., 2005; Bagesteiro et al., 2006; Van Pelt and Medendorp, 2008; Crawford et al., 2011). Moreover, we found that depth and direction signals affected separate populations of medial PE cells, and that the almost continuous pattern of activity modulation in the Fix-Reach population represents an eye-/arm-related tuning that could suggest an independent encoding of depth and direction signals. Similar findings were reported in lateral PE, though with a different task configuration (Lacquaniti et al., 1995). In that study, three different workspaces were used: reaches started from the center of each workspace towards 8 different directions evenly distributed between two depth planes. Although reach amplitude along the depth axis was not varied, targets did vary in depth with respect to the body. Despite these methodological differences Lacquaniti and colleagues (1995) described different pools of lateral PE neurons controlling for target direction (elevation and azimuth) and distance from the shoulder. This similarity was not granted, since medial PE neighbors and is connected to

PEc, an area showing convergence of depth and direction signals (Hadjidimitrakis et al. 2015, see also below), whereas lateral PE lies further away (Fig. 3.1) and is less strongly connected with PEc (Bakola et al., 2013). The segregated depth and direction processing observed in both PE sectors suggests that PE processes uniformly reach-related signals.

Ferraina et al. (2009) studied a sector of area PE that partially overlapped with our recording region (Fig. 3.1B). Despite task differences (reach targets were extrafoveal there and arm movements were made towards memorized targets that were distributed at different distances, thus leaving out direction), their analytical approach resembles the one used in the present study, thus allowing a direct comparison with our findings. Overall, their results are in line with ours, starting from the proportion of neurons showing a task-related activity (ANOVA, 77.4%). They showed that the incidence of depth-modulated neurons increased going from target presentation to movement execution, and only a small proportion among these neurons was influenced by target presentation (6.3%). A polynomial contrast analysis, used to test which model better fitted the relationship between target depth and neural activity, revealed that 80% of depth-modulated neurons showed a significant fit for the linear model. Furthermore, they tested a subpopulation of PE neurons with the same reach-in-depth paradigm, but varied the relative position in depth of both reach targets and fixation point across different trials and found that the effect of binocular eye position variation was negligible. Also Brunamonti et al. (2016) and Bremner and Andersen (2012) recording sites partly covered our recording region but, as they investigated the reference frames of reaching responses, a direct comparison of our results with these two latter studied is not possible. In the present study reaches were always performed towards foveated targets and started from the same initial hand position, so the frames of reference of reach-related activity could not be determined. We acknowledge that the effects of depth and direction we observed could

also reflect vector coding in addition to positional coding, however, the issue of the reference frames was beyond the scope of the present work.

In our sensory mapping experiment, the majority of our medial PE recording sites showed somatosensory sensitivity, with many cells responding to stimulations of both upper and lower limbs, suggesting a role in arm-leg coordination and postural control. This is most likely because the medial PE studied here is even further medial than that studied by Padberg and coworkers (2018). Interestingly, the majority of our PE neurons tuned by depth showed a bias for far space during both movement execution and target holding (Fig. 3.5a-b). In addition, arm-leg coordination could be more important for postural adjustments when the monkey reaches and holds the farthest targets. The integration of sensory inputs from both effectors could be reflected in increased levels of activity and/or a larger pool of responsive neurons.

3.5.1   Comparison of PE with SPL areas PEc and V6A

We used the same experimental paradigm in our previous V6A and PEc studies (Hadjidimitrakis et al., 2014a, 2015), enabling a direct comparison of the three SPL areas (Figure 3.9). Depth processing occurred mainly during and after movement execution in both PE and PEc, whereas in V6A it was evident during all phases of the task. The number of PE cells coding for direction during the initial target fixation period was higher compared to the subsequent phases, exactly as in V6A and PEc. The most notable trend among the three areas regards the rostro-caudal convergence of depth and direction signals on single cells: the two signals are mostly coded separately in PE (see 'both' in Fig. 3.9), whereas they showed a medium to high degree of convergence in PEc and V6A, respectively. This may reflect the neural correlates of the visuomotor tranformation occurring from V6A, where cells tuned for direction and depth code the target location in 3D space, to the somatomotor cortex, where

PEc and PE cells tuned only for depth or for direction gradually transform target coordinates from extrinsic to intrinsic ones. Moreover, it should be noted that PEc and V6A show convergence of somatic and visual inputs related to reaching/grasping (Breveglieri et al., 2008; Gamberini et al., 2018), whereas area PE mainly hosts somatic signals. Conceivably, these different visuo-somatic properties influence the processing of depth and direction signals too. In this regard, psychophysical evidence suggests that proprioception is more linked with movement depth, whereas vision is more related to direction processing (van Beers et al., 2002, 2004). We can suggest that in PE, the target location is re-specified in terms of the shoulder and elbow joint angles, suggesting that distance primarily pertains to elbow joint extension, and direction to shoulder angle. The activity of putative elbow and shoulder processing units in PE might represent the current joint angles, the intended joint angles (i.e. the target), or a vector linking the two. Whilst activity during early fixation can plausibly be interpreted as representing target-position, activity during reach might represent proprioceptive reafference, or (a copy of) a motor command, as suggested by the early onset of reaching activity that we have found here. The command might either specify the target joint angles, or the error vectors from the current positions. Error vectors are likely being represented in PE, as suggested by the absence of preference for intermediate positions and by the predominance of 'far' tuning (Fig. 3.5a).

Our visual and somatosensory mapping of medial PE is in line with data from lateral PE showing strong somatosensory (Sakata et al., 1973; Bakola et al., 2013), but weak visual (Mountcastle et al., 1975; Seelke et al., 2012) responses. Compared to PE, PEc and V6A contain much more visual (PEc: ~50%, Breveglieri et al. 2008; V6A: ~65%, Galletti et al. 1996, 1999) but less somatosensory (PEc: ~50%, Breveglieri et al. 2006, V6A: ~30%, Breveglieri et al. 2002) neurons (see Gamberini et al. 2017).
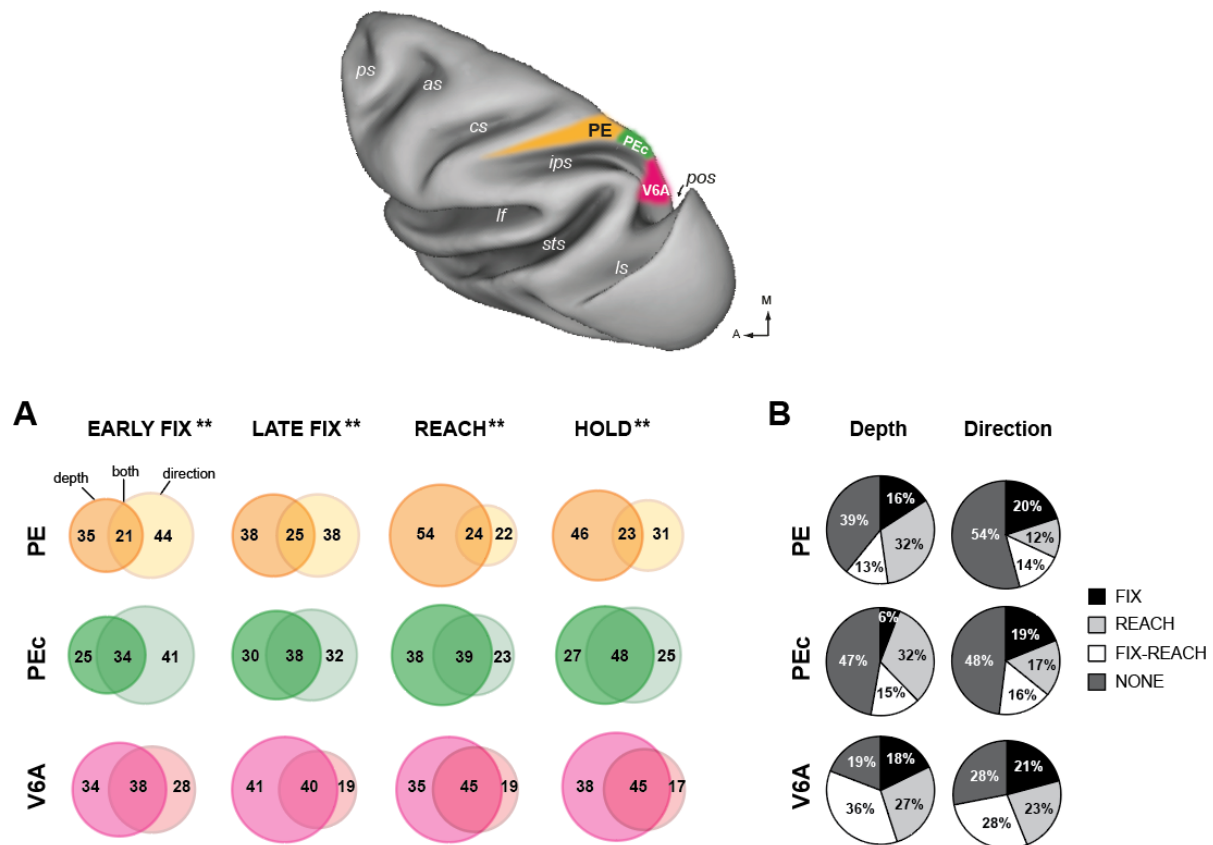
Figure 3.9 Depth and direction tuning along the reaching task (a) and in subpopulations of cells (b) in 3 SPL areas. **a)** Percentage of cells in PE, PEc and V6A with tuning for depth only (left set), direction only (right set), and both signals (intersection) during different task epochs (2-way ANOVA, $p<0.05$). Note that epochs EARLY FIX and LATE FIX in this study correspond to epochs FIX and DELAY in Hadjidimitrakis et al. (2014a) and Hadjidimitrakis et al. (2015). Double asterisks indicate significant difference between the three areas (V6A: pink; PEc: green; PE: orange) in the coding of one or both spatial parameters in a certain epoch (Chi squared test, $p<0.01$). Data from PE: current results (N= 176); data from V6A (N = 288) are from Hadjidimitrakis et al. (2014a); data from PEc (N = 200) are from Hadjidimitrakis et al. (2015), but recalculated with $p<0.05$ to standardize the criteria used in the other areas. Abbreviations as in Figure 3.2, conventions as in Figure 3.5a. **b)** Percentage of Fix, Reach, and Fix-Reach neurons in PE, PEc, and V6A with modulations by depth (left panels) and direction (right panels). Conventions as in Figs. 6a and 9a.

In both PE and PEc, depth strongly modulated neural activity during and after arm movement. In V6A, instead, depth influence was quite strong long before movement onset. The increase of depth relative to direction signals during task execution that we have found likely suggests a somatomotor rather than visual processing occurring in PE, whereas a visual rather than somatosensory processing in V6A. In the same vein of functional comparison, we found that the Fix, Reach, and Fix-Reach cells in each of the 3 SPL areas showed a different evolution of depth to direction tuning during the course of the trial (see Fig. 3.9b). When calculating the ratio of Fix:Reach cells, we found a steady increase of directional modulations going from area V6A to PE (0.96, 1.06, 1.31, V6A-PEc-PE). The comparable ratios for depth modulated neurons showed instead a discountinous trend (0.86, 0.45, 0.64, V6A-PEc-PE), best summarised by computing a ratio of ratios (i.e. Fix:Reach (direction) / Fix:Reach (depth); 1.12, 2.37, 2.03, from V6A to PE). This finding suggests that instead of a smooth gradient there is a rather abrupt increase in the gain of the relative prominence of depth over direction tuning during the course of the trial going from V6A to PEc/PE.

The spatial encoding during arm movements to visual targets has been extensively studied in several SPL areas and accumulated evidence suggests some degree of functional heterogeneiity (e.g. Kalaska et al. 1990; Batista et al. 1999; Buneo et al. 2002; Ferraina et al. 2009; Chen et al. 2009; Chang and Snyder 2010; McGuire and Sabes 2011; Cui and Andersen 2011). The most notable trend regards the reference frames employed by each area to encode the target: caudal SPL areas like V6A, MIP, and PEc represent targets in eye-centered, body-centered or mixed eye(body)/hand reference frames (Batista et al., 1999; Chang and Snyder, 2010; Hadjidimitrakis et al., 2014b, 2017; Bosco et al., 2016; Piserchia et al., 2016), whereas rostral SPL areas like PE and PEip use predominantly hand-centered coding (Buneo et al., 2002; Ferraina et al., 2009; McGuire and Sabes, 2011; Bremner and Andersen, 2012, 2014). Our studies have revealed another SPL trend, i.e. the gradual

convergence on single neurons of depth and direction signals going from PE in the exposed surface of SPL cortex to V6A. We hypothesize that a similar trend may be present also within the medial bank of the intraparietal sulcus, with MIP and PEip showing mostly combined and separate depth and direction processing, respectively.

3.5.2 Comparison with frontal cortex

Previous studies in PEc (Hadjidimitrakis et al., 2015) and V6A (Hadjidimitrakis et al., 2014a) find a remarkable parallel, despite task differences, with the dorsal premotor cortex (PMd, Messier and Kalaska 2000): e.g. a combined tuning for depth and direction, and their increase in convergence with task progress. Area PE shows instead a considerable degree of separation between depth and direction signals, which is maintained throughout the task (present results, Lacquaniti et al. 1995).

But how far the SPL functional trend is reflected in the frontal cortex? When we sought for an analogous processing of depth and direction signals towards primary motor cortex, we found that this region shares with medial PE the predominance of depth effect during reach execution. Naselaris and colleagues (2006) examined the distribution of a large number of preferred arm movement directions in M1 during reaching movements in 3D space and showed an enhanced representation for reaching directions aligned with the depth axis and a specialization in motor control for reaches in depth. This functional pattern parallels the organization of parieto-frontal connectivity, which shows a rough symmetry around the central sulcus (more caudal SPL areas having a more rostral focus in PMd, e.g. V6Av with F7, V6Ad with rostral F2, PEc with caudal F2 and PE with S1 and M1; Shipp et al. 1998; Gamberini et al. 2009; Bakola et al. 2010, 2013; Passarelli et al. 2011).

3.5.3 *Comparison with the human brain*

Is there a similar processing scheme for reach direction and depth in monkeys and humans? In both species, SPL is involved in sensory-motor integration (see Grefkes and Fink 2005; Culham et al. 2006), and reach-related signals have been found in several human SPL regions (Connolly et al., 2003; Hagler et al., 2007; Filimon et al., 2009; Gallivan et al., 2009; Cavina-Pratesi et al., 2010), including human V6A (Pitzalis et al., 2013; Tosoni et al., 2015). While many studies reported SPL activations for reaching or pointing performed in different directions, only a few studies report SPL activations for reaching performed at different depths. Martin et al. (2015), showed that a large swath of PPC was activated during reaching towards peripheral versus central targets. Such direction selective signals were present in areas V6A, 7A, and the medial and posterior IPS. However, using fMRI adaptation as a proxy to measure tuning curves, Fabbri et al. (2010) revealed a more restricted region within the SPL (medial to the IPS and anterior to the parieto-occipital sulcus) showing a high degree of directional selectivity. Regarding the substrates of combined depth and direction processing, Fabbri et al. (2012) reported that, going from parietal to frontal areas, the processing of distance and direction information is more segregated. Furhermore, Cavina-Pratesi et al. (2010) described differential fMRI activity for near and far reaches in anterior and posterior sectors of the superior parieto-occipital cortex. This finding calls for comparative fMRI experiments (Vanduffel et al., 2014), whereby adaptation paradigms or multi-voxel pattern analyses are used, which enable direct comparisons of single selectivity for reach direction and depth with fMRI data from both humans and monkeys.

3.6   Conclusions

This study reports that in medial PE depth and direction signals for reaching are partially processed by two distinct neuronal subpopulations. Moreover, this cortical sector integrates somatic input from both upper and lower limbs, but it does not receive visual input. Combined with our previous studies, present findings highlight the functional heterogeneity in SPL, with PE strongly influenced by somatosensory input during reaching performance and predominantly processing depth.

Chapter 4

fMRI guided electrophysiology of Spatial Attention Shifts in the Macaque Superior Parietal Lobule.

4. fMRI guided electrophysiology of spatial attention shifts in the macaque superior parietal lobule

4.1 Abstract

Human fMRI and transcranial magnetic stimulation (TMS) studies showed the involvement of superior parietal lobule (SPL) in covert shifts of attention. Despite hints from monkey electrophysiology and fMRI, little is known about the underlying neuronal mechanisms. Guided by monkey fMRI maps (Caspari et al. 2015), we recorded single and multi-unit activity from a shift-selective region in medial SPL (parietal area V6A) of one rhesus monkey. We employed a covert selective spatial attention paradigm resembling those used in previous human and monkey fMRI experiments. Stimuli consisted of 2 pairs of shapes, each containing a relevant and irrelevant stimulus. One of the stimuli was presented in the center of the receptive field (RF), and the other diametrically opposed to the first one. A replacement of the first stimulus pair by the second could induce a spatial attention shift when the relevant stimulus position changed to the opposite visual hemifield (shift event). Alternatively, when the relevant stimulus of the new pair appeared at the same position as the relevant stimulus of the preceding pair, this corresponded to a stay event. We found that the average population activity of all recorded neurons was higher for shift than stay events when the direction of the shifts pointed towards the RF. Conversely, when shifts pointed to the opposite direction, the activity for stay events was higher in early and late stages of the attentional switch events. Shift-selective population activity peaked around 60 ms after event onset, when more than half of cells showed significant shift-selective activity. Consistent

with the human and monkey fMRI data, these results show a substantial correlate of covert spatial attention shifts at neuronal level within parietal area V6A.

4.2 Introduction

Selective spatial attention allows humans to process specific visual information through prioritizing an area within the visual field. Shifts of spatial attention are needed to dynamically allocate attentional resources to salient sensory signals in our environment. This process includes the disengagement of attention to one location, moving the focus of attention, and engagement at another location (Posner, 1980; Koch and Ullman, 1985; Desimone and Duncan, 1995). Several cortical regions are involved in the control of spatial attention, including parietal, prefrontal, and extrastriate visual areas. Human fMRI experiments revealed a crucial role of the superior parietal lobule (SPL) during both overt and covert spatial attention shifts (Vandenberghe et al., 2001; Yantis et al., 2002; Molenberghs et al., 2007; Kelley et al., 2008). These results are supported by the fact that people suffering from Balint's syndrome (Bálint, Dr., 1909), a rare manifestation of visual and spatial difficulties due to bilateral SPL lesions, show an impairment in detecting the displacement of a visual stimulus (Phan et al., 2000). Possibly, these deficits may reflect a disruption of attentional shift mechanisms (Vandenberghe et al., 2001, 2012). Recently, Caspari and collaborators (2015) have identified in the macaque monkey brain a network of cortical areas activated during attention shifting events. This network includes parietal areas V6/V6A, medial intraparietal area, caudo-dorsal visual areas, the most posterior portion of the superior temporal sulcus, and several small regions in the frontal cortex. In a follow-up study, Caspari et al. (2018) showed correspondences between the superior parietal network processing attention shifts in monkeys and the shift SPL-network in humans (see also Arsenault et al., 2018).

The medial posterior parietal area V6A, the principal target of the present study, contains cells that encode the spatial location of visual targets (Galletti et al., 1993, 1995), as

well as neurons with reaching, grasping, and oculomotor-related activity (Kutz et al. 2003; see for a review Fattori et al. 2017). V6A has been cytoarchitectonically (Luppino et al., 2005) and functionally (Galletti et al., 1999; Gamberini et al., 2011) subdivided into a ventral (V6Av) and a dorsal (V6Ad) portion, with V6Av containing a majority of visual cells with receptive fields mostly in the lower periphery. Since the first study investigating V6A functional properties, it was clear that the level of attention modulates the neuronal activity of this cortical area (Galletti et al., 1996). Three studies have specifically investigated the attention-related properties of V6A. First, Galletti et al. (2010) provided evidence that V6A neurons are activated during covert shifts of spatial attention, although attentional signals could not be dissociated from the sensory or motor events required to probe the animals' focus of attention. A few years later, Ciavarro and coworkers (2013) employed on-line rTMS to induce a virtual, transient lesion on human putative V6A (Pitzalis et al., 2013). They found an rTMS-induced increase of reaction times, suggesting an involvement of this area in attentional reorienting. In the same year, Capotosto et al. applied TMS over human IPs, showing an impairment in target discrimination immediately after a shift of attention, regardless of current target location (Capotosto et al., 2013). Here, we aimed to further investigate attention-related properties of parietal area V6A during spatial attention shifts and sustained attention at a fixed location, to increase our understanding of the neuronal basis underlying spatial attention shifts. This also puts us in a position to relate the wealth of human and monkey imaging data (Vandenberghe et al., 2001; Yantis et al., 2002; Molenberghs et al., 2007; Kelley et al., 2008; Caspari et al., 2015, 2018) with single cell properties measured in monkey. Our results highlight a substantial involvement of parietal area V6A in computing spatial attention shifts at neuronal level.

4.3   Materials and Methods

Animal care and experimental procedures were approved by the Ethical Committee at the KU Leuven and were carried out in accordance with the National Institute of Health's "Guide for the Care and Use of Laboratory Animals" and with the European Communities Council Directive (2010/63/EU). The details of the general fMRI procedures and training of monkeys have been described previously (Vanduffel et al., 2001; Nelissen et al., 2005; Caspari et al., 2015). Animal housing and handling were in accordance with the recommendations of the Weatherall report, allowing locomotor behavior, social interactions, and foraging. Animals were group-housed (2-5 animals per group; cage size at least 16-32m^3) with cage enrichment (toys and foraging devices), outside views and natural day-night cycles at the primate facility of the KU Leuven Medical School.

We used one of the same male rhesus monkeys (M35, Macaca mulatta, 9 kg, 10 years of age) as in a previous fMRI study from our lab (Caspari et al., 2015). The monkey was implanted with a custom-built 5-channel receive array coil embedded in an MRI-compatible headpost (Janssens et al., 2012) and one recording chamber targeting the right V6A. The monkey was extensively trained using operant conditioning techniques to maintain fixation at a centrally presented fixation spot, while performing a receptive field mapping task (Fig. 4.1) and subsequently a covert spatial attention task (Fig. 4.2), with the head constrained by a head post in a natural 'sphinx' position inside a plastic primate chair. Eye movements were constantly monitored at 120 Hz using an eye-tracking system based on infrared corneal reflection (ISCAN). Also, the position of both hands within a response box was checked using infrared light beams. Each time the monkey made an unrequested hand movement or an eye movement outside the fixation window, the trial was aborted, and the stimulus display

disappeared. These procedures minimized unwanted hand or saccadic eye movements toward the peripheral stimuli.

4.3.1 Behavioral tasks

4.3.1.1 Receptive field mapping task

For each recording position targeting the fMRI-defined shift-selective region, we first tested cells' visual sensitivity using high-contrast drifting luminance edges, with different orientation and speeds (Fig. 4.1), in order to detect the position and map the borders of visual RF with the stimulus eliciting the best response. This procedure allowed us to elicit strong neural activity when running the subsequent Spatial Attention Task, by putting one of the two stimuli in the center of the RF. In case we were not able to clearly define the borders of the RF, we put one of the two stimuli of the Spatial Attention Task in the lower and contralateral (i.e. left) visual hemifield (~20 degrees eccentricity), because V6A neurons represent largely the contralateral lower part, and only partially the ipsilateral and upper part of the visual field (Galletti et al., 1999; Gamberini et al., 2011, 2018).
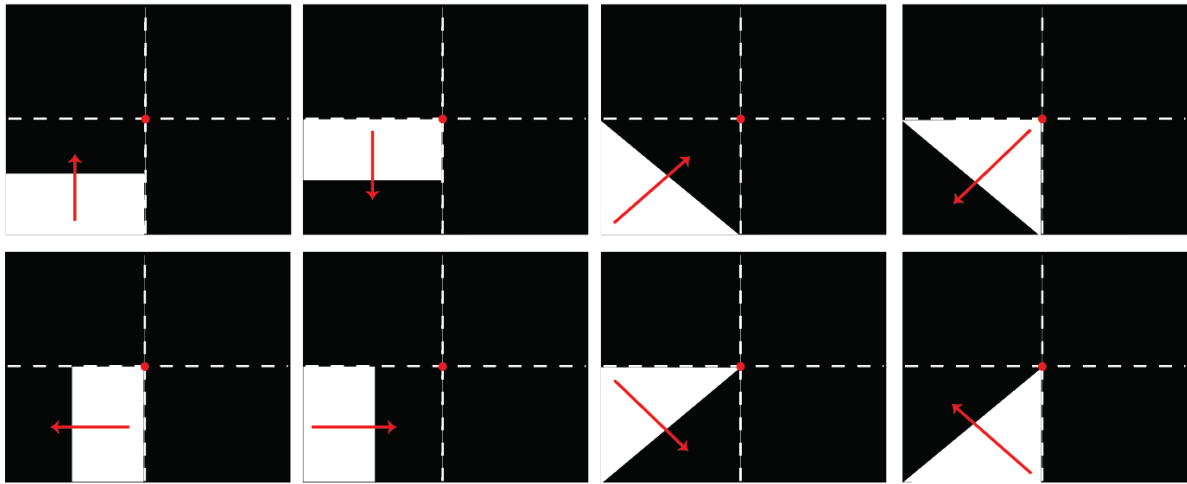
Figure 4.1 Visual stimuli used to map the receptive field of V6A neurons. The high-contrast luminance edges are all shown in the lower, left (i.e. contralateral) quadrant of the visual field, where the majority of V6A cells' RFs are located. The edges could move along 4 possible axis of motion and 8 possible directions: vertical (bottom → up, top → down), horizontal (right → left, left → right), and 2 oblique (135° → 315° and vice versa; 225° → 45° and vice versa).

Stimuli used during the Receptive field mapping task consisted of high-contrast luminance edges moving across the visual field in 1 of 8 directions at 1 of 3 different speeds (19, 30, and 50 deg/s). Each of the different directions of movement and speeds was randomly presented within a run. The reason for using such type of visual stimuli was that we know that about 65% of V6A cells are sensitive to moving visual stimuli, show a strong direction and orientation selectivity, and can discriminate the speed of motion as well (Gamberini et al., 2011). We targeted electrophysiological recordings to the ventral portion of V6A, which contains a higher number of visual cells (Gamberini et al., 2011). The visual stimuli and task construction was adapted from Pitzalis et al. (2010). We used 16 channels laminar probes (NeuroNexus Vector Arrays) to record neural activity. Importantly, due to the long duration of the Receptive field mapping task, we were unable to test visual sensitivity for each of the

cells recorded from each channel. Therefore, we selected one channel per recording depth where a clear visual response was present, we mapped the borders of the visual RF, and we used that information for all the simultaneously recorded neurons in the subsequent Spatial Attention Task.

4.3.1.2 Spatial Attention Task

A slightly modified version of the event-related spatial attention task used by Caspari et al. (2015) was employed. Figure 4.2 shows a schematic representation of the attention task (Fig. 4.2 A) and the timeline of two example trials (Fig. 4.2 B). The monkey was trained to fixate on a red dot (within a 2 x 3 degree fixation window) while two stimuli were continuously present on a screen positioned 57 cm in front of the monkey's eyes. In Caspari et al. 2015, the stimuli were always positioned on the horizontal meridian at 9.25 degrees eccentricity. Instead, we positioned one of the stimuli in the center of the RF, typically located in the lower and contralateral hemifield (i.e. left, Galletti et al., 1999; Gamberini et al., 2011, 2018) and the other stimulus was positioned at the same eccentricity of the RF stimulus, but in the opposed hemifield. Thus, the location and size of the stimuli varied for each run according to the RF position of the recorded neurons. Stimulus size was scaled according to eccentricity and luminance contrast (gray level) was chosen to approximate a performance level of 80-85% correctly performed trials. There were two possible coupled stimulus pairs: a square with a triangle and a circle with a diamond. Each pair contained a relevant and an irrelevant stimulus and all stimuli were white on a black background. To perform the task correctly and to obtain a reward, the monkey had to respond by manually interrupting a light beam when the relevant, but not the irrelevant stimulus dimmed. The monkey was trained to fixate upon a central fixation point during the entire task while covertly attending the relevant stimulus of each pair. Eye and hand positions were

continuously monitored. Events of interest consisted of: i) SHIFT events, where a feature change ('CHANGE ONSET', Fig. 4.2 B) cued the monkey to make a covert spatial-attention shift either to the left ('SHIFT LEFT', Fig. 4.2 A) or to the right ('SHIFT RIGHT', Fig. 4.2 A) hemifield; ii) STAY events, where a feature change cued the animal to maintain its covert attention to the same spatial position; iii) NULL events, where no feature change occurred. The allocation of attention was probed behaviorally by dimming events (~30% of the trials, duration: 100 ms) of the relevant/irrelevant stimuli, randomly occurring in a time interval between 150 and 800 ms after the feature change onset, separated in time from the shift/stay events.
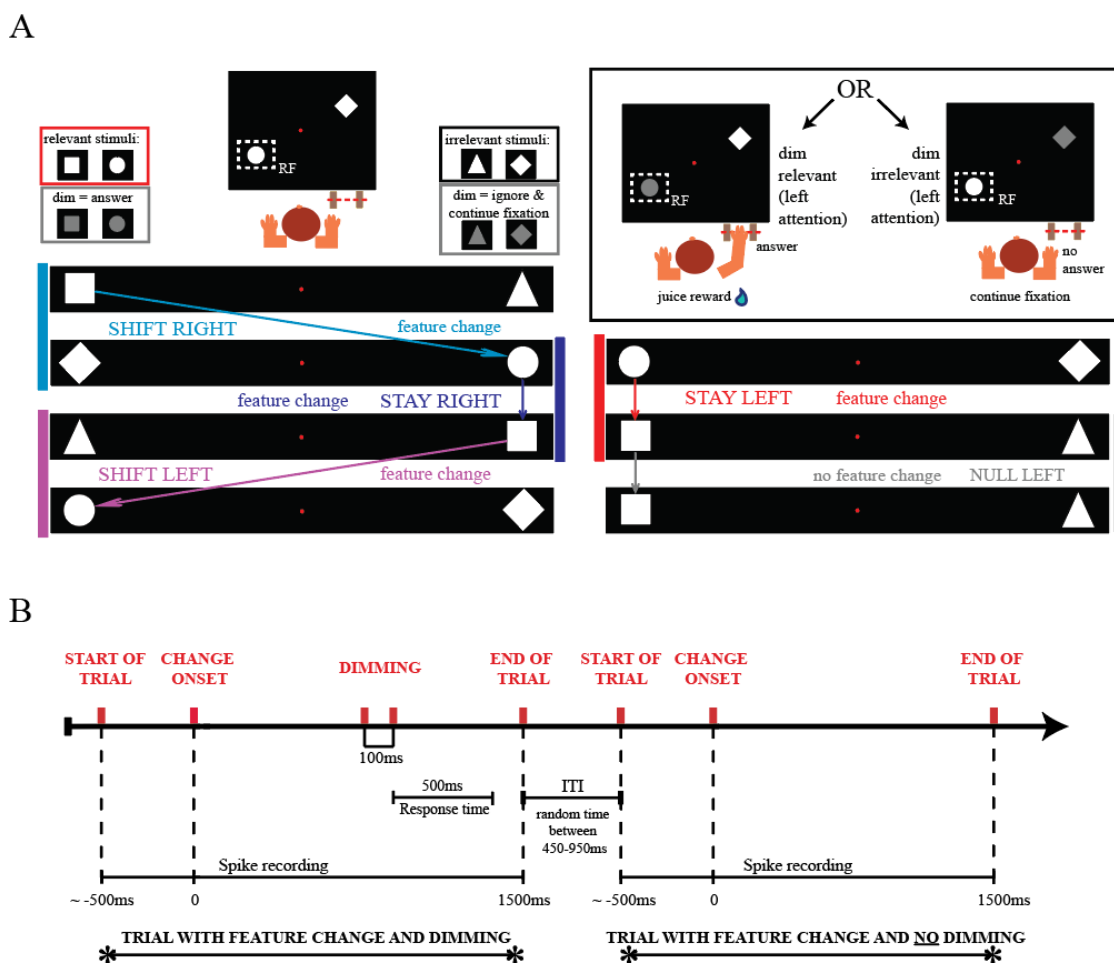

Figure 4.2 Spatial attention task and stimuli (A), and timeline of two example trials (B).

133

4.3.2 Electrophysiological recordings

When fixation performance exceeded 90%–95%, and false-alarm rates were close to 0%, we recorded single and multi-unit spiking activity from the right V6A (Fig. 4.3 A), as defined by the fMRI maps obtained by contrasting shift (left & right) vs. stay (left & right), $p<0.005$ (Fig. 4.3 B, for details see below), using laminar probes (16 channels NeuroNexus Vector Arrays; 100 um distance between each site; impedance measured *in situ* around 1-1.6 MΩ). The fMRI images were co-registered with a recent anatomical MRI using a co-registration JIP toolkit (Joseph Mandeville).

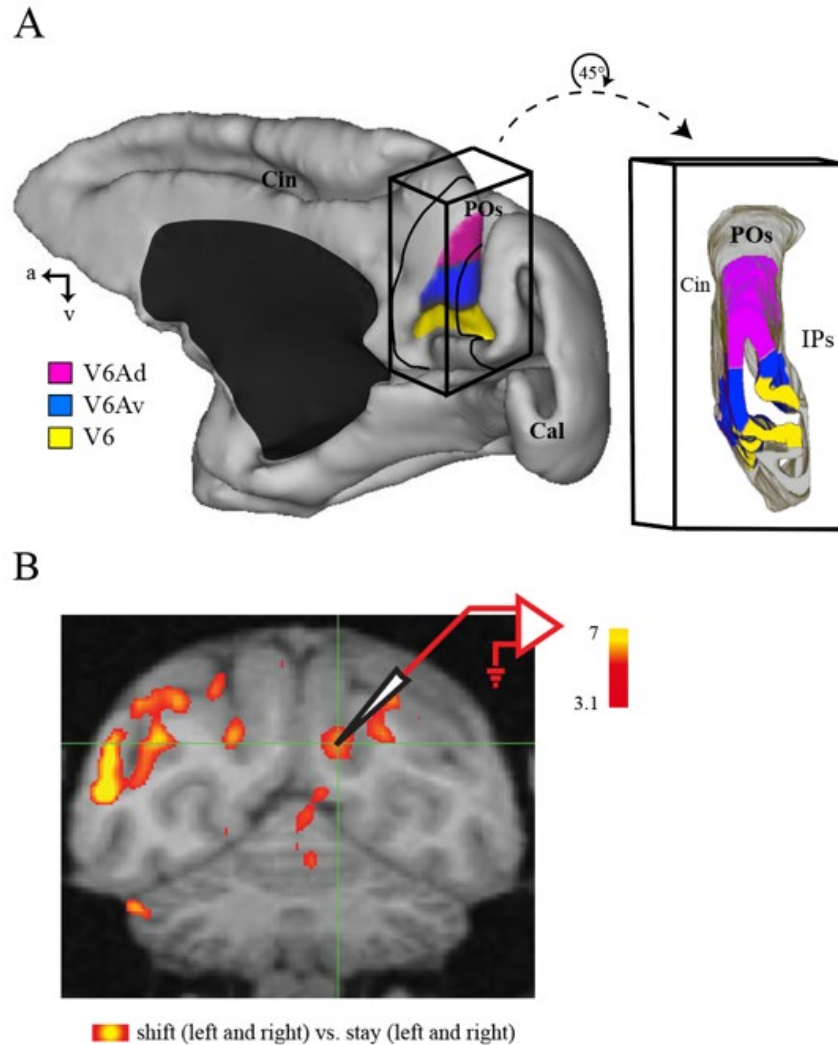**Figure 4.3** A) Left: medial view of the right hemisphere of a macaque brain reconstructed in 3D using Caret software (http://brainvis.wustl.edu/wiki/index.php/Caret:Download) showing the location and extent of the SPL areas V6 and V6A (dorsal and ventral). Right: Posterior view of the caudalmost part of the SPL obtained from coronal sections by enlarging and rotating the inset box on the left. Here the occipital pole is cut away to show the anterior bank of the POs. POs, Parieto-occipital sulcus; Cal, calcarine sulcus; Cin, cingulate sulcus; IPs, intraparietal sulcus. Modified from Gamberini et al., 2015. B) Representation of shift activations in the brain volume for monkey J, used for guiding electrophysiological recordings targeting right V6Av.

All the scanning parameters, the preprocessing steps of the acquired images, and the data analysis of the event-related experiment are reported in Caspari et al., 2015. Briefly, fMRI scans were performed in 3 T Siemens PRISMA scanner, using a gradient-echo T2*-weighted echo-planar imaging-sequence: 40 horizontal slices; TR, 2 s; TE, 19 ms; 1.25x1.25x1.25 mm^3 isotropic voxels, acceleration factor of 2. Monkey J had been implanted with a 5-channel receive array coil, to improve the sensitivity for MR-imaging (Janssens et al., 2012). Immediately before the fMRI scan, MION (Feraheme, AMAG Pharmaceuticals; 8–11 mg/kg) was injected into the femoral/saphenous vein of the animal to improve the contrast-to-noise ratio and to avoid the influence of superficial draining veins (Vanduffel et al., 2001; Leite et al., 2002). The spatial shifting task was scanned using an event-related design, and a run lasted 610 s (305 volumes, including 4 dummy volumes). Before the coregistration of the anatomical and mean functional images, corrections for the lowest-order off-resonance effects and higher-order distortions were applied to the raw EPI images. A general linear model (GLM) analysis was performed using SPM5 software package (Wellcome Department of Cognitive Neurology, London) running under MATLAB (MathWorks). The GLM included 5 regressors for the five conditions (i.e. shift left and right, stay left and right, null), 2 eye movement regressors, and 6 additional head motion regressors (translation and rotation in 3D), per run. Each condition was modeled by convolving a γ function ($\delta = 0$, $\tau = 8$, and exponent $= 0.3$), modeling the MION hemodynamic response function, at the onset of the condition (transition of stimulus displays). For every recording session, the probe was slowly advanced in the brain by means of a Narishige Microdrive through a stainless-steel guide tube fixed in a grid (Crist Instruments) placed within the recording chamber. Recordings were made using an Intan Technologies Recording system (RHD2000 series, bandpass filter 300 Hz – 5000 Hz). Spike sorting was performed offline using the Plexon Offline Sorter

(Plexon Inc.), in order to distinguish single and multi-unit activity from noise. In the Results section, we use the label "cells" or "neurons" for both multi- and single units.

4.3.3 Data analysis

The analysis of the fMRI data has been described in Caspari et al., 2015. Briefly, shift events (composed of a feature change and a spatial shift), stay events (composed only of a feature change), and null events (no feature change, nor spatial attention shift occurred) entered the GLM. The number of correctly executed trials analyzed for each event type was equalized for left- and right-sided attention. Only trial sequences with at least 3 or more consecutive and correctly executed fixation trials were included in the analysis. Activations correlating with "transient" spatial attention shifts regardless of the direction of the shift were visualized by contrasting bilateral "shifts" versus "stay" (shift-left and shift-right vs. stay-left and stay-right). Monkey J showed significant shift-related fMRI activation in parietal areas V6/V6Av (Fig. 4.3 B), which has been used to guide the implantation of the recording chamber.

All data analyses were performed using custom scripts in MATLAB (MathWorks). In order to quantify the efficiency of the monkey in performing the attention task, we calculated percentage of correctly performed trials from all runs for all the possible transitions between events of interest (i.e. shifts, stays, nulls). We statistically compared the behavioral result between relevant/irrelevant dimmings in the three trial types (shift, stay, and null) and in both hemifields, using a Kruskal-Wallis test ($p<0.05$).

Eye-position data were analyzed to track the eye position for correctly performed stimulus sequences, within a fixation window of 2 x 3 degrees, in each condition tested. The most informative first 600 ms after trial onset were included in the analysis and sorted condition-wise. For shift events, the second half of the sampled data was used, reflecting the endpoint

of the shift (301– 600 ms). This was done because, at time point zero, attention should be deployed to the opposite hemifield. Eye movement deviations in degrees of visual angle (from the midline) were normalized to the specific eccentricity of each session.

Analysis of the neuronal activity during the shift of attention period was made by quantifying the discharge recorded from -50 ms before the change of the stimulus transition ('CHANGE ONSET', Fig. 4.2 B) until 150 ms after it. From now on, we will refer to this time window as "attentional transition period". The peristimulus time histograms (PSTHs) for each neuron and each condition was calculated using a shifting window of 20 ms. Population responses of all recorded neurons, without applying any type of preselection, were computed by averaging mean firing rates of all cells. Before averaging, the firing rates for each neuron were normalized by division with the maximum firing rate for all conditions. Significant differences in discharge between SHIFT and STAY events were tested with a Wilcoxon signed rank test (p<0.05, FDR corrected).

To assess the strength of attentional modulation on V6A neural activity, we calculated the following Attention Index (AI):

$$AI = \frac{AvFRshift - AvFRstay}{AvFRshift + AvFRstay}$$

Where 'AvFRshift' and 'AvFRstay' are the mean average rates of discharge of each neuron during shift and stay conditions, respectively. The index ranges between - 1 and 1. An AI value of 1 indicates that a neuron is activated during a shift and not a stay event, whereas a value of - 1 indicates that a neuron is only activated during a stay event. Values close to 0 indicate that a neuron was modulated similarly by shift and stay conditions. We calculated the AI in 7 separate time bins of 20 ms each in the timespan 20-160 ms after the feature

change onset and evaluated the statistical significance of the indices using a Wilcoxon rank sum test (p<0.05).

In order to exclude any possible influence on the shift- and stay-related activity of the events happening before the feature change onset, we calculated pair-wise correlations between differences in average firing rates of shift vs. stay events in 2 sub-intervals bookending each trial transition (shift or stay), and each consisting of 4 x 40 ms bins.

4.4   Preliminary results

We recorded neural activity from parietal area V6A while the monkey executed a Spatial Attention Task, that required to covertly shift the allocation of attention from a central fixation point to a peripheral location. Preliminary results from one subject are described here below.

4.4.1   Behavioral results

Monkey J participated in a previous fMRI study from our lab (Monkey 35, Caspari et al., 2015) and has been extensively trained to covertly attend to relevant stimuli during all events of interest (i.e. shift, stay, null events). Percentage of correctly performed trials provide a direct measure of the animal's focus of attention. Figure 4.4 A shows the proportion of correctly executed trials from 11 runs across all the possible transitions between task conditions (i.e. shift, stay, and null trials). No difference in performance was observed between the three different trial types (shift, stay, and null), both for trials with and without dimming events (Kruskal-Wallis test, p>0.05). Conversely, the performance was

significantly different between the left and the right visual hemifield (Kruskal-Wallis test, p=0.039).

As V6A neurons also show oculo-motor related activity (Galletti et al., 1995; Kutz et al., 2003), we checked for small deviations in eye position across task conditions. In figure 4.4 B we plotted minor variations in eye position immediately after a change in trial type (i.e. shift, stay), separately for attention directed to the left and to the right. We could not detect any clear bias in eye position in none of the tested conditions. For every possible transition (stay, shift, with attention directed either to the left or the right hemifield), the eye positions did not deviate significantly from the central fixation spot (Kruskal-Wallis test, p>0.05) -unlike what we observed in the previous fMRI study (Caspari et al., 2015).
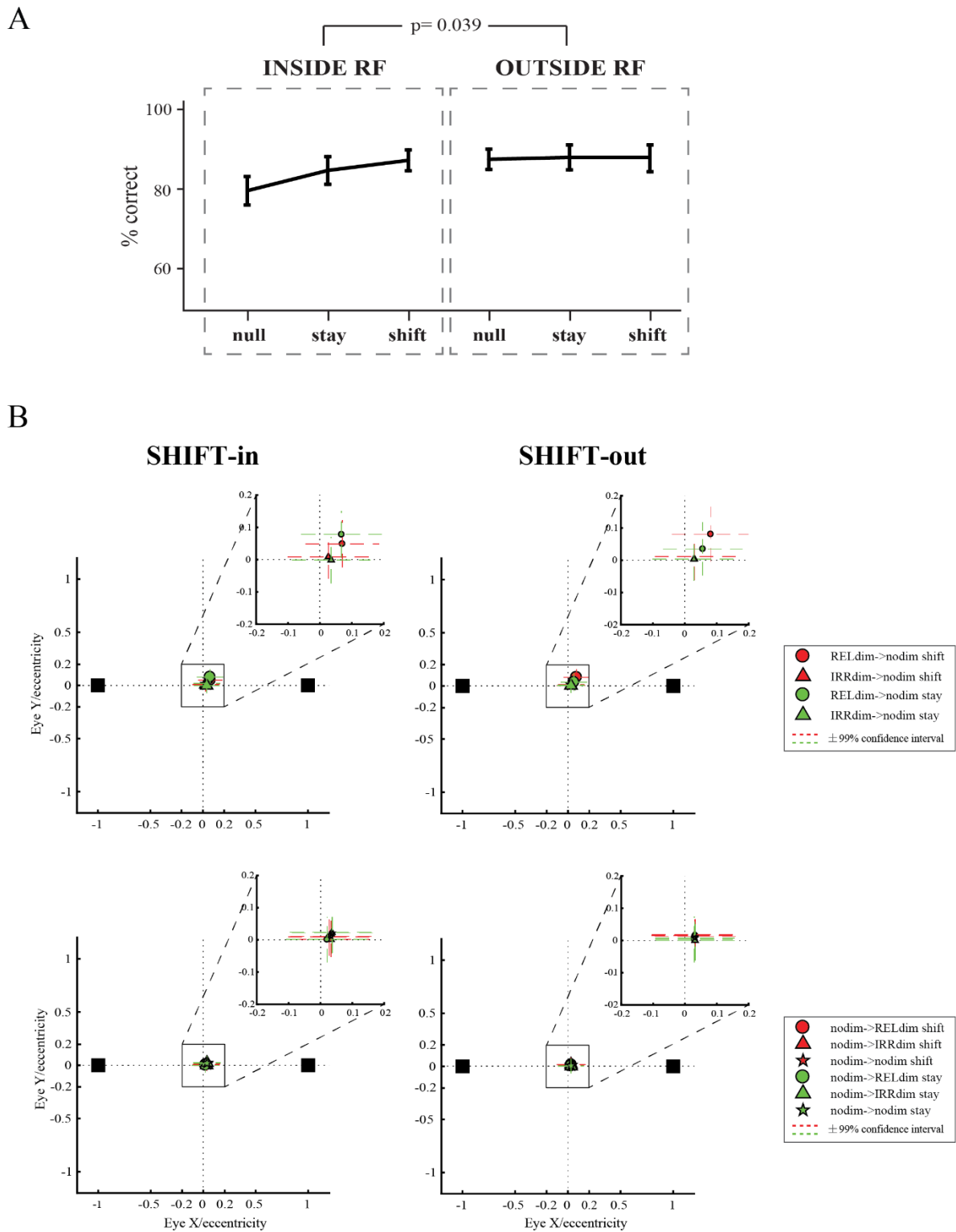
Figure 4.4 Behavior: percentage of correctly performed trials (A) and eye position data (B). (A) Performance of the monkey expressed as a percentage of correctly executed trials. (B) Eye data are displayed in degrees of visual angle, representing the deviation of eye position in the x- and y-

direction normalized with respect to the center across sessions (0 degrees of visual angle). Coordinates (x=0, y=0) represent the central fixation point. Coordinates (x=-1/+1, y=0) are normalized to the eccentricity of the target points, which varied from session to session according to RF location (eccentricities ranged between 10 and 24 degrees of visual angle). The two rows show the eye data when transitions (shift, stay) occurred from dimming to no dimming trials (upper row), or from no dimming to dimming trials (lower row). The black squares positioned on the horizontal meridian represent the two stimuli always present on the screen during the Spatial Attention Task - note that the actual position of the stimuli (polar angle and eccentricity) varied from recording to recording, according to RF location. Red represents shift events; green represents stay events. Shift events: average of data points between 301 and 600 ms after event onset, representing the shift arrival position. Abbreviations: null-L, null left; stay-L, stay left; shift-L, shift left; null-R, null right; stay-R, stay right; shift-R, shift right; RELdim, relevant dimming trial; IRRdim, irrelevant dimming trial; NOdim, trial without dimming.

4.4.2 Results from neural recordings

A total of 195 single and multi-units were recorded from V6A of one rhesus monkey while the animal performed the Receptive field mapping and the Spatial Attention tasks. The target locations within area V6A were identified based on: i) the anatomical location of V6A in combination with fMRI-based shift-selectivity (Fig. 4.3); ii) the functional properties (i.e. sensitivity to moving luminance edges, direction and orientation selectivity) of the neurons, according to previous V6A studies (Gamberini et al., 2011). To drive the neurons optimally during the Spatial Attention Task, we placed one of the two stimuli in the center of the visual RF, as determined by the Receptive field mapping task at the beginning of each recording session. In figure 4.5 the average firing rate of an example of V6A neuron showing direction and orientation selectivity is depicted. The neuron actively fired only when the vertically oriented luminance edge crossed the borders of the RF. Neural activity was instead silent

when the edge crossed the borders of the RF in the opposite direction of motion, or with a different orientation (i.e. 315° or 135°).
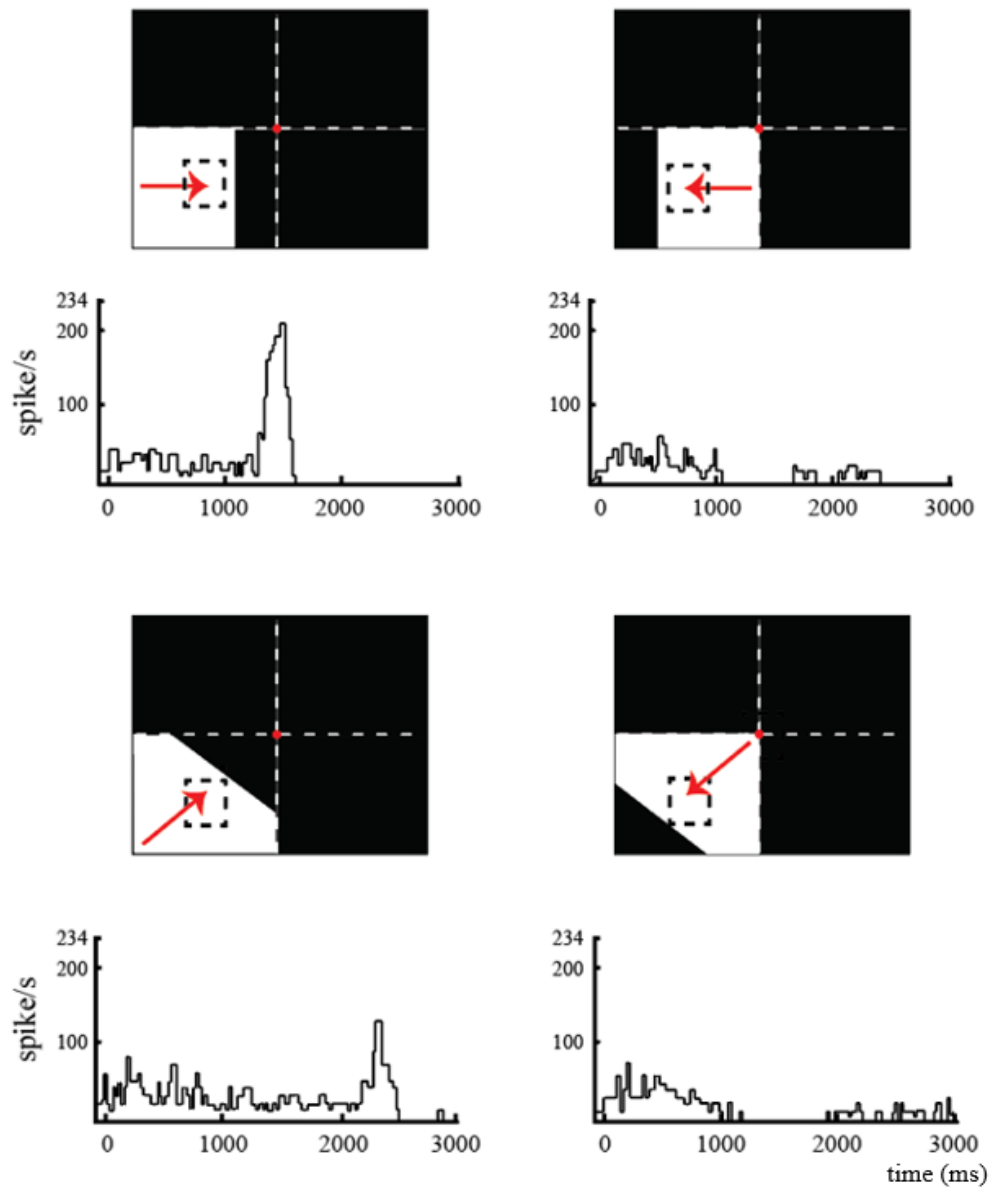

Figure 4.5 Example of V6A neuron showing direction and orientation selectivity. The black panels illustrate a schematic representation of the receptive field (black dashed line) and of the stimulus moving across it in the direction indicated by the red arrow. Below each black panel, the corresponding peristimulus time histogram is shown. Zero on the x-axis is aligned with the stimulus movement onset.

4.4.2.1 Different tuning for shift and stay events during the attention task

For the Spatial Attention Task, we particularly focused our analysis on the neural discharge during the attentional transition period (from 50 ms before the change of stimulus switches ('CHANGE ONSET', Fig. 4.2 B) until 150 ms afterwards). Figure 4.6 illustrates an example of V6A neuron showing sensitivity for shifts of attention when a change in stimulus features occurred during the task ('Feature change ON', Fig. 4.6). On the left, the PSTHs for transitions from trials without dimming to trials with (ir)relevant dimming are shown ('NOdim → RELdim', left; 'NOdim → IRRdim', right). This neuron shows task-related discharges both during the attentional transition period, and the dimming events. There is a clear peak of activity immediately after the feature change onset when both shift and stay events occurred either in the left or the right visual hemifield. Interestingly, after neuronal activity ceased in all conditions, the neuron increased activity at the time of the dimming event. In particular, dimming of the relevant stimuli enhanced the discharge during shift and stay trials to the left visual hemifield, where the RF of the neuron was located. Irrelevant dimming events were modulating neural activity especially when the direction of shifts and stays was opposite to the position of the RF.
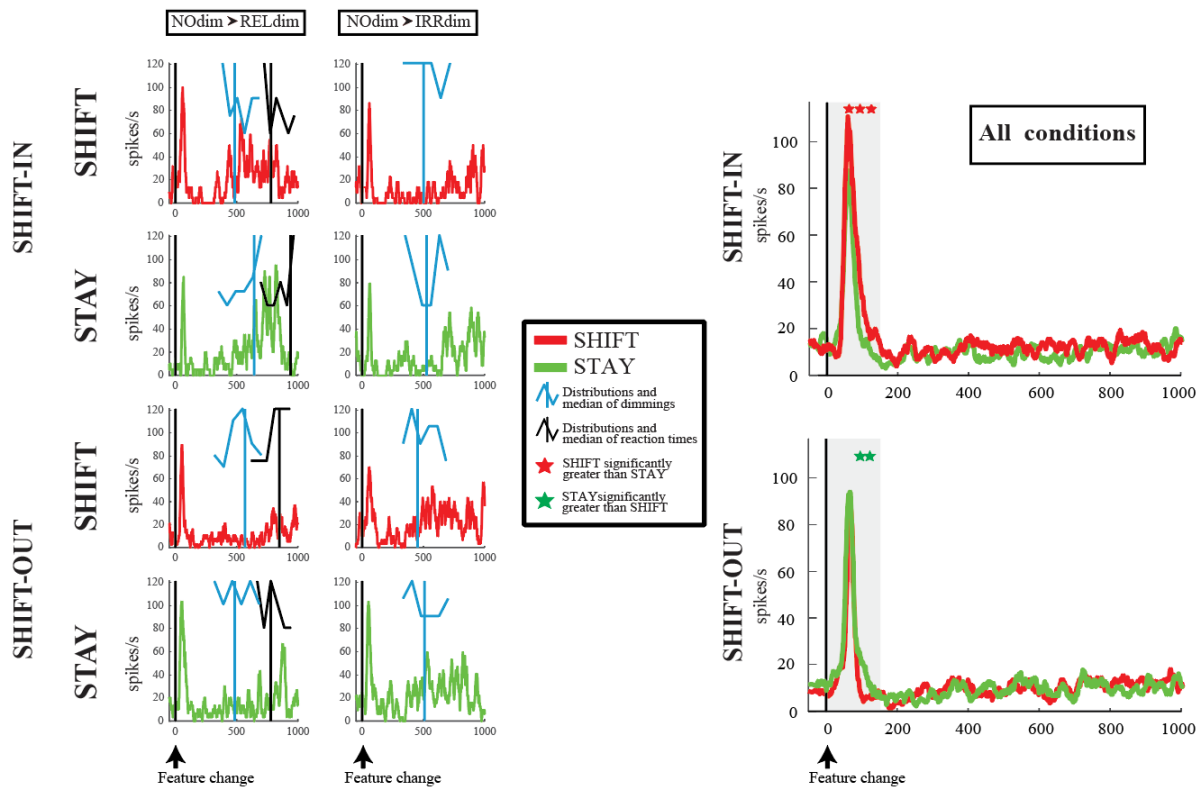
Figure 4.6 Example of a V6A neuron modulated by spatial shifting of attention. Left: PSTHs for transitions from trials without dimming to trials with relevant (NOdim → RELdim), or irrelevant dimming events (NOdim → IRRdim). Right: average PSTH for all possible transitions. Stars above the PSTHs indicate statistical difference between the discharges in SHIFT and STAY events in the timespan analyzed (grey rectangle, Kruskal-Wallis test, p<0.05). Abbreviations as in Figure 4.4.

We then plotted the cumulative PSTHs averaged over all possible combinations of task conditions (Fig. 4.6, right, 'All conditions') and analyzed the statistical difference between shift (red) and stay (green) trials separately for attention to the left (top) and right (bottom) hemifield. For attentional shifts towards the relevant stimulus in the RF (shift-in), activity was significantly larger than stay activity (where attention is directed to the same relevant stimuli inside the RF) starting 65 ms after the feature change (top, Kruskal-Wallis test, p<0.05). When attentional shifts pointed to the relevant stimuli outside of the RF (shift-out),

the activity for shifts was comparable to that of trials in which attention was sustained to the relevant stimuli inside the RF. Activity in such cases was indistinguishable between shift and stay trials in the early phase after stimulus transitions, and became significantly different 100 to 140 ms after the feature change onset, when discharges during stay were slightly larger than during shift-out trials (bottom, Kruskal-Wallis test, $p<0.05$).

To address how the population of V6A neurons changed their activity after stimulus transitions during the Spatial Attention Task, we computed the average, normalized, population response of V6A cells considering the entire population of recorded neurons (N= 195), without applying any type of preselection or division in neuronal subclasses. We even included neurons which were not modulated by any of the task conditions (i.e. shifts, stays). As shown in figure 4.7, neural activity remained low and stable before the feature change. Then, both shift- and stay-related activity started to increase and peaked around 60 ms after the feature change. As already noticed for the example neuron (Fig. 4.6), there is a sharp difference between the task events occurring inside and outside of the visual RF. Shift-in related activity was significantly larger than stay activity for relevant stimuli in the RFs of the left hemifield from 45 to 120 ms after the feature change (top, Wilcoxon test, $p<0.05$, FDR corrected). Shift-out activity (i.e. shifts towards the hemifield opposite to the RF), instead, was significantly smaller than stay activity (directed to the relevant stimuli inside the RF) before and after the feature change (bottom, Kruskal-Wallis test, $p<0.05$). The activity levels converged and overlapped perfectly in the timespan between 45 and 105 ms after the feature change onset, however. Interestingly, no obvious difference was observed when comparing shift-in and shift-out conditions, as the magnitude of response in the two conditions was comparable.

Overall, the example neuron (Fig. 4.6) and the average population response (Fig. 4.7) illustrate that neurons in area V6A are significantly involved in the computations required to shift the focus of attention towards relevant information in the visual environment.
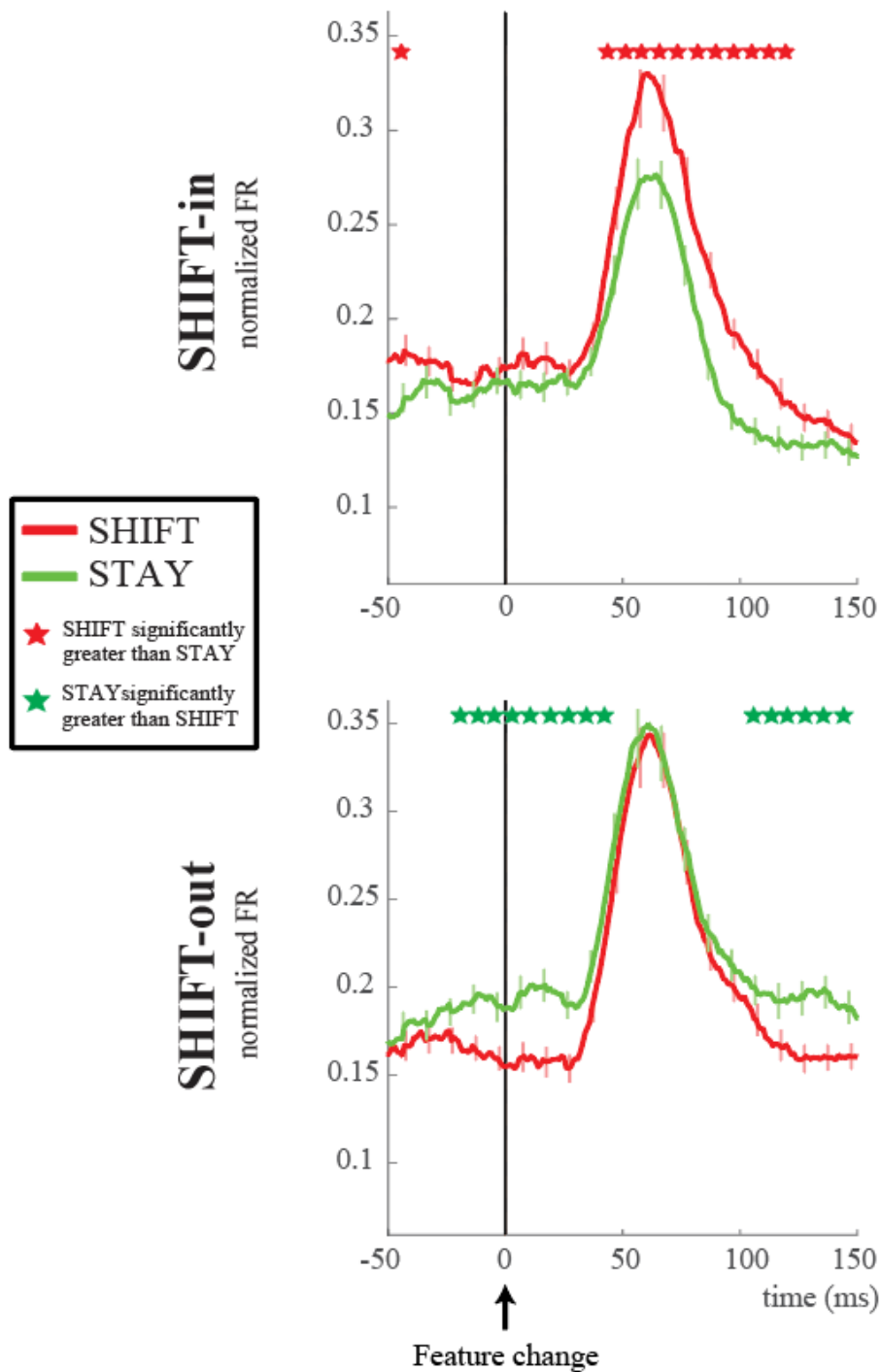
Figure 4.7 Average population response of all recorded V6A neurons (N= 195) for shift and stay conditions during the Spatial Attention Task. Stars above the PSTHs indicate statistical difference between the discharges in SHIFT and STAY events in the timespan analyzed (Wilcoxon test, p<0.05, FDR corrected).

To quantify how strongly V6A neuronal activity was modulated by the attention task conditions as a function of time relative to the feature shifts, we calculated attention indices in 20 ms time bins (AI; see Materials and Methods). The value of AI ranges from - 1 to 1. Positive values indicate higher shift than stay activity, while the reverse holds true for negative indices. The AI distributions depicted in figure 4.8 corroborates the average population responses (Fig. 4.7). When the monkey paid attention to a relevant stimulus within the RF in the left visual field, population activity was significantly higher for shift-in compared to stay events ('LEFT', Fig. 4.7). A higher proportion of neurons was excited by shift-in events, as indicated by the median AI's (bin 2=0.06; bin 3=0.08; bin 4=0.1; bin 5=0.17; bin 6=0.07) and significantly different from zero in the following bins (bin 2, 63.5% of the neurons, pWX= $3.7*10^{-5}$; bin 3, 66.7%, pWX= 10^{-5}; bin 4, 65.6%, pWX= $2.9*10^{-8}$; bin 5, 66.1%, pWX= $6*10^{-8}$; bin 6, 58.3%, pWX= 0.03). As expected from the population activity, the opposite scenario was observed for shift-out events ('RIGHT', Fig. 4.7) (i.e. attentional shifts towards the right hemifield). A higher percentage of neurons showed negative AI values (bin 1=-0.07; bin 2=-0.06; bin 5=-0.05; bin 6=-0.09; bin 7=-0.06), which were significantly different from zero in the early and late stages of the attentional transition period (bin 1, 64.6%, pWX= $1.8*10^{-5}$; bin 2, 59.7%, pWX= 0.0045; bin 5, 58.3%, pWX= 0.0029; bin 6, 62%, pWX= 0.0003; bin 7, 56.5%, pWX= 0.009).

$$\mathbf{AI} = \frac{\text{SHIFT} - \text{STAY}}{\text{SHIFT} + \text{STAY}}$$

Figure 4.8 Distributions of attentional modulation indices (AI = Attention Index) calculated in 7 time bins of 20 ms each in the timespan 20-140 ms after the feature change onset of the Spatial Attention Task, separately for trials where attention was directed to the RF (shift-in) and to the opposite direction (shift-out). The asterisks show a significant difference of the median value from zero (Wilcoxon rank sum test, $p < 0.05$). The color code indicates a preference for shift-in (red) or shift-out (green).

The bottom panel of Figure 4.7 shows a difference between shift and stay activity prior the feature change, which was unexpected since the monkey cannot predict the upcoming event type. To check whether shift- and stay-related activity was affected by events happening before the feature change onset, we computed pair-wise correlations between differences in average firing rates between shift and stay events in 8 bins (4 bins before and 4 after the feature changes), each 40 ms in duration. Figure 4.9 shows the (8 x 8) correlation matrices separately for shift- and stay-in and for shift-and stay-out trials, and for all the different possible task transitions. It appears that V6A attention-related discharges after the feature change were not correlated with activity levels before the feature change. Correlations could be observed only between events happening before the feature change onset (i.e. "before-before" correlations, bottom left quadrant of the correlation matrices, Fig. 4.9) or afterwards ("after-after" correlations, upper right quadrant of the correlation matrices, Fig. 4.9). Importantly, no significant "before-after" correlations could be detected.

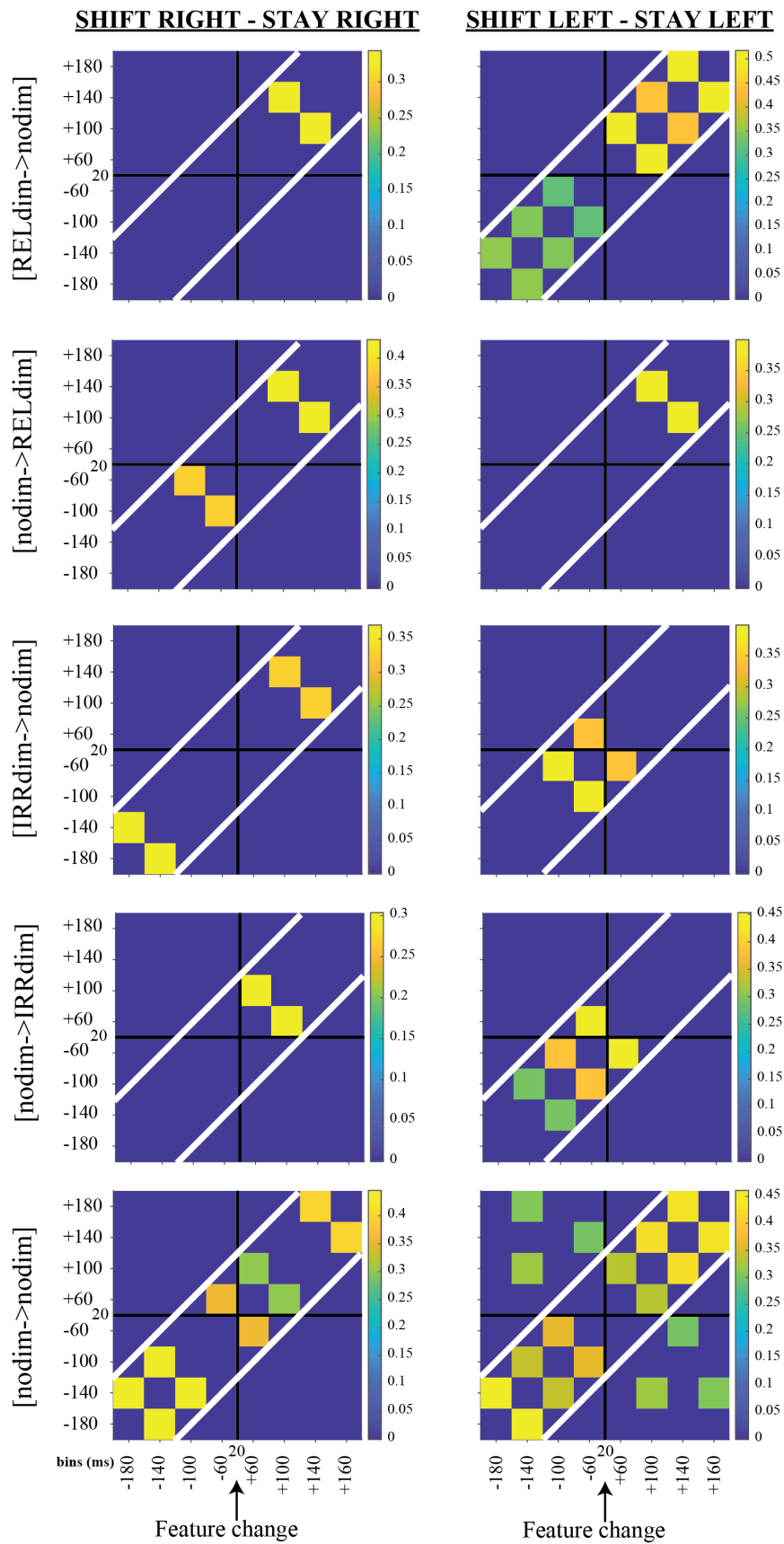# Correlation between average FR before and after the feature change

Figure 4.9 Correlation matrices between average firing rate before and after the feature change onset. The oblique white lines mark the zone of the matrices, in which a correlation is possible only between events happening before and after the change onset.

4.5 Discussion

To investigate attention-related properties of V6A cells, we employed an event-related spatial attention paradigm previously used in human (Molenberghs et al., 2007) and monkey (Caspari et al., 2015) fMRI experiments. Guided by the fMRI activation maps, we targeted electrophysiological recordings to parietal area V6Av of one macaque monkey, while the monkey covertly shifted or maintained its focus of attention on a peripheral stimulus. We found that more than half of the recorded neural population showed shift-selective activity when attentional shifts occurred towards the location of the RF (i.e. the relevant stimulus was positioned in the center of the RF). Previous studies conducted in monkey V4 and MT have shown that neurons exhibited higher responses when a relevant stimulus located within the visual RF was being attended (Motter, 1994; Treue and Martinez Trujillo, 1999; McAdams and Maunsell, 2000; Bichot et al., 2005; Buracas and Albright, 2009). However, in those studies the spotlight of attention was constantly allocated inside the RF (sustained attention), without being shifted. Attention signals have been investigated particularly in frontal and parietal areas, such as the lateral intraparietal area (LIP), whose neurons show responses that are strongly modified by the behavioral relevance of the stimulus placed within their visual RF (Gottlieb et al., 1998; Toth and Assad, 2002). Buschman and Miller have electrophysiologically studied the involvement of monkey FEF in covert shift of attention (Buschman and Miller, 2009). They used a task where both saccade programming and covert attention shifts were required and showed that for targets inside the

neuron's visual RF, neural responses were enhanced just before the animal localized the target (indicated by a saccade). When the target was located in a position clockwise to the neuron's RF, the response started to increase earlier, as if the animal covertly shifted its attention to the neuron's RF and then moved it on to the next stimulus where it found the target. These results are in line with ours, as we found that V6A neurons exhibit higher attention-related activity for shifts directed towards the RF (shift-in) rather than away from it. In 2010, Galletti et al. have already provided evidence for attention-related activity in V6A at neural level, using a task that required covert attention shifts from a central fixation point towards a peripheral location, and vice versa. In that task, however, potential sensory and motor-driven signals could not be separated from the attentional shift signals. They found an equal number of cells preferring shifts towards parts of the space contralateral or ipsilateral with respect to the recording site. This fits the human and monkey fMRI data (Yantis et al., 2002; Molenberghs et al., 2007; Caspari et al., 2015), where no obvious difference between shift-in and shift-out conditions has been observed. Galletti et al. (2010) showed longer durations of attention-related responses compared to the present study, which might be related to: i) the different paradigms used to elicit attention shifts; ii) the different recording locations, as our recording sites were confined to the ventral part of V6A; iii) a possible motor and sensory confounds in the Galletti et al. (2010) study. Finally, Kutz et al. (2003) showed that V6A is also affected by oculo-motor related modulations. Our results revealed that shift-related activity in V6A does not depend on eye-movements directed towards the stimuli cueing the attention shifts, as we did not observe significant eye deviations from the central fixation point in any of the task conditions (see Fig. 4.4 B).

4.5.1 Comparison with human and monkey TMS and fMRI studies

Several fMRI studies revealed signals coding spatial attention shifts in human mSPL regardless of shift direction (Yantis et al., 2002; Molenberghs et al., 2007). The same region was shown to be also engaged when human subjects shifted attention between objects (Serences et al., 2004), features, and task rules (Shomstein and Yantis, 2004; Andersen and Cui, 2009; Shulman et al., 2009). As found in the monkey brain by Caspari et al. (2015), areas showing shift-related signals in humans were largely segregated from those maintaining the current locus of attention (Yantis et al., 2002; Vandenberghe and Gillebert, 2009). In addition, Simon et al. (2002) showed systematic activations of human SPL, using four different spatially-specific visuo-motor tasks, including voluntary saccades, covert shift of attention, and spatially-specific grasping and pointing. The computation of attention shift is most likely the common feature of these tasks. Ciavarro and collaborators (2013) showed causal evidence for SPL playing a functional role in attentional shifting. They employed online repetitive TMS to induce a reversible lesion on putative human V6A (Pitzalis et al., 2013) during a task requiring the subjects to execute both covert shifts of attention and planning of reaching movements. They found a selective impairment of attentional orienting in both reaching and attentional tasks, and an rTMS-induced increase of reaction times. Their results suggest that reorienting signals are used by putative human V6A to rapidly update the current motor plan or the ongoing action (Ciavarro et al., 2013). In line with this interpretation, we are inclined to believe that V6A of the monkey, an area traditionally known to be mainly involved in the encoding of reaching and grasping movements (see for a review Fattori et al. 2017), acts as a bridge between spatially-directed attention and motor programming. Further studies are needed to investigate this hypothesis, with a paradigm allowing a link between the reallocation of attention in the space and a subsequent motor action.

In sharp contrast to shift activity which was confined to SPL, modulation of fMRI activity by sustained attention signals was observed in the posterior IPs and extrastriate human visual cortex (Yantis et al., 2002; Molenberghs et al., 2008; Shulman et al., 2009; Vandenberghe et al., 2012). This was also confirmed by Capotosto et al. (2013), who applied repetitive TMS over human IPs, showing an impairment in target discrimination following the presentation of shift cues regardless of target location, in the left or right visual hemifields. Thus, in human parietal cortex, SPL encodes attentional shifts whereas activity in posterior IPs is modulated by sustained attention signals. Similarly, Caspari et al. (2015) found that sustained contralateral attention activated the IPs (area LIP) of the monkey. In accordance with our results, posterior medial parietal cortex was instead mainly activated by shifts of attention. In a follow-up study, Caspari and collaborators (2018) performed comparative fMRI experiments to examine correspondences between human and monkey brain areas activated during covert attention shifts. They found consistent shift activations in parietal and frontal regions of both humans and monkeys, and demonstrated that monkey medial parietal areas V6/V6A most consistently correlated with shift-selective human mSPL. However, the human shift-selective region identified in that study is next to the location of human areas V6 and V6A (Pitzalis et al., 2006, 2013, 2015; Tosoni et al., 2015), but does not exactly correspond to it. As a possible explanation for this discrepancy, the authors suggested that putative homologous areas can only be considered "partially homologous" and that under evolutionary pressure some properties originally residing in the same region may have been pushed to other regions (Mantini et al., 2012).

4.6 Conclusions

In monkeys as in humans (Molenberghs et al., 2007; Caspari et al., 2018), mSPL is involved in shifting spatial attention in the absence of overt behavior. Our combined fMRI/electrophysiology study adds to the existing literature by showing a significant neural involvement of area V6A of monkey mSPL in covert shifting of spatial attention. We propose that, in addition to the established role of area V6A in the online control of hand and arm movements for goal-directed actions, it also serves as a key area for shifting spatial attention, an activity that typically accompanies the goal-directed actions. Our results call for additional experiments to investigate the causal role of area V6A in the attention network and its possible implication in the online update of motor actions based on spatial attention signals.

Chapter 5

General Discussion

5.   General Discussion

5.1   Summary of the main findings and general interpretations

5.1.1   Interplay Between Grip and Vision in the Monkey Medial Parietal Lobe

In the first research chapter of this thesis (Chapter 2), we tested to what extent V6A grasping neurons are influenced by the visual feedback of the moving arm and the object to be grasped. We used an experimental design similar to the one employed in the dorsolateral grasping area AIP, which allowed us to make a comparison between the grasp-related properties of V6A and AIP. Single-unit recordings led us to conclude that V6A neurons are modulated by both grip type and visual information during grasping preparation, execution, and object holding, with a predominance of cells influenced by grip type rather than by visual information. This result was quite surprising, given that V6A contains many visual neurons (Galletti et al., 1999; Fattori et al., 2017), and could be explained by the fact that our animals were overtrained to perform Reach-to-Grasp tasks both in the light and in the dark. This possibly made the visual information available during grasping in light not necessary to allow task completion. Hence, the neural modulations observed in V6A during grasping could be strictly tied to the strong somatosensory/motor input. We also observed that V6A neurons were active during the period in which the monkey withhold the grasping action, with half of the grasp-related population tuned for grip type. This evidence suggested an involvement of V6A in grasping preparation or (in darkness) memory of the object to be subsequently grasped, similarly to what was found in AIP, where limited set-related activity and extensive memory-related activity has been described (Murata et al., 1996; Schaffelhofer et al., 2015; Schaffelhofer and Scherberger, 2016). However, our task configuration has been

designed with a one-to-one correspondence between object shape and grip type. This makes it difficult to verify what is encoded by V6A after object observation and before action execution. Further experiments are needed to disentangle what is encoded in the delay epoch by V6A neurons.

When comparing our results with those found in AIP (Taira et al., 1990; Murata et al., 2000; Baumann et al., 2009; Schaffelhofer and Scherberger, 2016), it emerges that V6A and AIP show an overall similar incidence of grasp-related cells. During object presentation V6A and AIP (Schaffelhofer and Scherberger, 2016) recruit a similar number of cells, whereas during the subsequent grasping preparation and execution more V6A neurons are engaged than AIP's. A possible explanation for this could be the presence of somatosensory cells in V6A, but not in AIP (Murata et al., 2000; Breveglieri et al., 2002). Somatosensory cells related to the arm fire immediately before arm movement, when the muscles start contracting, as well as during reach-to-grasp execution and hand-object interaction (Breveglieri et al., 2002). At population level, the proportion of V6A cells modulated during the delay and grasping execution was greater than in AIP. This, together with the rich direct connections between V6A, MIP, and the dorsal premotor cortex (Gamberini et al., 2009), and the high incidence of neurons processing spatial signals for reaching in V6A (Fattori et al., 2005, 2017; Hadjidimitrakis et al., 2014a), suggest a deep involvement of V6A in linking object information to the guidance of reaching and grasping actions.

Recent brain imaging studies (Gallivan et al., 2011; Monaco et al., 2011) agree in attributing a grasping role to the putative human homologous of area V6A (Pitzalis et al., 2013, 2015; Tosoni et al., 2015). These imaging studies found that the cortex around the dorsal-most part of the parieto-occipital sulcus plays a role in processing wrist orientation and grip formation (Gallivan et al., 2011; Monaco et al., 2011), thus corroborating a role for the human dorsomedial PPC in the control of reach-to-grasp actions.

5.1.2 The neglected medial part of macaque area PE: segregated processing of reach depth and direction

In our second study (chapter 3), we examined the relative influence of reach depth and direction information on neurons of the medial part of area PE and characterized their temporal evolution over the course of a Fixate-to-Reach task in darkness towards targets placed at different depths and directions in the 3D space. The same task configuration was used in the studies of neighboring superior parietal areas V6A and PEc (Hadjidimitrakis et al., 2014a, 2015), thus allowing us to compare direction and depth processing between the three medial PPC areas. We also characterized PE sensory properties, by qualitatively examining the visual and somatosensory responses of PE cells.

We recorded single-unit activity from the medial part of PE, a cortical area largely neglected in previous studies. We found that modulations by target depth and direction were unevenly distributed during the course of the task. Tuning of activity by direction was strong at the beginning of the task, whereas depth tuning mainly occurred during movement execution. Different populations of medial PE cells code for reach depth and direction, exactly as in lateral PE (Lacquaniti et al., 1995), thus arguing for a segregated processing of depth and direction information. Despite methodological difference, also Lacquaniti and colleagues (1995) described different pools of lateral PE neurons controlling for target direction (elevation and azimuth) and depth, similarly to what we found in medial PE. The segregated depth and direction processing observed in both PE sectors suggests that the entire area PE processes reach-related signals in a similar way.

Our sensory mapping experiment confirmed that PE is strongly affected by somatosensory inputs and poorly by visual inputs, similarly to what has been found by other studies in the lateral part of PE (see for a review Seelke et al. 2012). Many cells responded to somatosensory stimulations of both upper and lower limbs, suggesting a role in arm-leg

coordination and postural control. We are aware that differences in activity during reach execution could be influenced by gaze signals. However, to the best of our knowledge, there is no evidence supporting a strong modulating effect of gaze position on neural activity in PE.

The comparison of PE with SPL areas PEc and V6A revealed the existence of a rostro-caudal gradient in the convergence of depth and direction signals on single cells in the SPL: the two signals are mostly coded separately in PE, whereas they showed a medium to high degree of convergence in PEc and V6A (Hadjidimitrakis et al., 2014a, 2015), respectively. This may reflect the neural correlates of the visuomotor transformation occurring from V6A, where cells tuned for direction and depth code the target location in 3D space, to the somatomotor cortex, where PEc and PE cells tuned only for depth or for direction gradually transform target coordinates from extrinsic to intrinsic ones. Moreover, it should be noted that PEc and V6A show convergence of somatic and visual inputs (Breveglieri et al., 2008; Gamberini et al., 2018), whereas area PE mainly hosts somatic signals (Seelke et al., 2012; see also chapter 3.4.4 of the present thesis). These different visuo-somatic properties could possibly affect the processing of depth and direction signals too. Our visual and somatosensory mapping of medial PE is in line with data from lateral PE showing strong somatosensory (Sakata et al., 1973; Bakola et al., 2013), but weak visual (Mountcastle et al., 1975; Seelke et al., 2012) responses. Compared to PE, PEc and V6A contain much more visual (PEc: ~50%, Breveglieri et al. 2008; V6A: ~65%, Galletti et al. 1996, 1999) but less somatosensory (PEc: ~50%, Breveglieri et al. 2006, V6A: ~30%, Breveglieri et al. 2002) neurons (see Gamberini et al., 2018). In both PE and PEc, depth strongly modulated neural activity during and after arm movement. In V6A, instead, depth influence was quite strong long before movement onset. The increase of depth relative to direction signals during task execution that we have

found likely suggests a somatomotor rather than visual processing occurring in PE, and a visual rather than somatosensory processing in V6A.

A recent series of experiments confirmed the specific contribution of the human superior parieto-occipital cortex (SPOC) for visually guided reaching (Culham et al., 2008; Filimon et al., 2009; Gallivan et al., 2009; Cavina-Pratesi et al., 2010). While many studies reported SPL activations for reaching or pointing performed in different directions, only a few studies showed SPL activations for reaching performed at different depths. As already mentioned in the Introduction (see section 1.1.2.3), the definition of a specific human homologous of monkey PE is still a controversial subject. Area 5 in humans is confined to a small, medial region in the anterior part of SPL, while in monkeys it occupies most of the SPL, largely extending in the lateral part of the brain. It has been demonstrated that during evolution, there has been a high degree of expansion in the associative cortex (Chaplin et al., 2013), particularly in humans (Hill et al., 2010; Gregory et al., 2017), including that of the parietal lobe. According to Gamberini et al. (2019), it is plausible that area 5 in humans "was confined within more medial brain locations, because it has been 'pushed' upward and medially by the growing associative inferior parietal cortex", concluding with the hypothesis that area 5 in humans and monkeys could be functionally very similar (Gamberini et al., 2019). Further studies are needed to better relate the functional organization of monkey PE with its possible human counterpart.

5.1.3 fMRI-guided electrophysiology of spatial attention shifts in the macaque superior parietal lobule

In our third study (Chapter 4), we described preliminary results of a combined fMRI-electrophysiology experiment conducted to investigate the neuronal mechanisms underlying covert shift of attention processes. This experiment started in 2015, when Caspari et al. for the first time identified in monkeys a network of areas, including parietal area V6A, activated during spatial shifting events, using a spatial attention task adapted from a human fMRI study (Molenberghs et al., 2007). We defined the ventral V6A as the designated target for our electrophysiological recordings based upon the task-related activation on the fMRI maps.

We found that V6A shift-related activity was not contaminated by deviations in eye position directed towards the stimuli evoking the attention shifts, as the monkey's gaze did not deviate significantly from the central fixation point in any of the task conditions. This result was not granted, given that V6A is affected by oculo-motor related modulations (Galletti et al., 1995; Kutz et al., 2003). More than half of the total recorded number of V6A neurons showed shift-selective activity when the monkey was covertly shifting its allocation of attention towards the location of the RF. When shifts pointed to the opposite direction, half of the neural population showed instead stay-selective activity in the early and late stages of the attention period. In 2010, Galletti et al. have already provided evidence for attention-related activity in V6A at neural level, using a task where the monkey was required to shift its attention outward to a peripheral cue and inward again to a central fixation point. In that task, however, potential sensory and motor-driven signals could not be separated from the attentional shift signals. They found an equal number of cells preferring shifts towards parts of the space contralateral or ipsilateral with respect to the recording site. This also fits the human and monkey fMRI data (Yantis et al., 2002; Molenberghs et al., 2007; Caspari et al., 2015), where no obvious difference between shift-in and shift-out conditions has been

observed. Attention related signals have been also found in: i) parietal areas, such as the lateral intraparietal area (LIP), whose neurons showed responses that were strongly modified by the behavioral relevance of the stimulus placed within their visual RF (Gottlieb et al., 1998; Toth and Assad, 2002); ii) frontal areas, such as FEF, where neural responses were enhanced just before the animal localized the target inside the neuron's visual RF (Buschman and Miller, 2009). These results are in line with ours, as we found that V6A neurons exhibit higher attention-related activity for shifts directed towards the RF rather than away from it.

In the human domain, fMRI and TMS experiments have revealed signals coding spatial attention shifts in mSPL regardless of the shift direction (Yantis et al., 2002; Molenberghs et al., 2007). As found in the monkey brain by Caspari et al. (2015), areas showing shift-related signals in humans were largely segregated from those maintaining the current locus of attention (Yantis et al., 2002; Vandenberghe and Gillebert, 2009). A recent rTMS study demonstrated interference with attentional "re-orienting" upon stimulation of human mSPL during a reaching and an attention task (Ciavarro et al., 2013). Their results suggest that reorienting signals are used by putative human V6A to rapidly update the current motor plan or the ongoing action. More recently, Caspari and collaborators (2018) demonstrated that monkey medial parietal areas V6/V6A most consistently correlated with shift-selective human mSPL.

All these evidences are consistent with our results, that show a strong correlate of covert spatial attention shifts at neuronal level within parietal area V6A.

5.2   Methodological considerations

We are aware that the studies in the present thesis come with some potential limitations, which are mainly due to constrains on research design or methodology and might have impacted to some extent our findings. In the next paragraphs, some of the major limitations will be described.

5.2.1   Tasks and stimuli

In the first study, we draw a parallel between the grasp-related properties measured in V6A and the grasping responses of area AIP studied in several different labs. However, this comparison should be taken as a suggestion, as the data used for the comparative analysis come from different laboratories and were recorded under different experimental conditions (e.g. different species of monkeys; different types of grasping tasks; data collected with different recording apparatuses – single electrode for V6A vs. chronic implanted arrays for AIP).

In the second study, we used an experimental setup where the depth range explored was larger than the range of directions. This could have partially led to an overestimation of depth over direction modulations. Although we cannot completely exclude this possibility, we believe that the range of directions employed in our study (30 degrees of visual angle) it comprises most of the central visual field where naturally eyes and hands interact with objects in everyday life. Reaches were always performed towards foveated targets and started from the same initial hand position, so the reference frames of reach-related activity could not be examined. We are aware that the effects of depth and direction we observed could also

reflect vector coding in addition to positional coding. However, the issue of the reference frames was beyond the scope of our study.

Moreover, in all our experiment we used artificially created stimuli, which are not generally found in a more natural environment, thus meaningless for monkeys. Medial SPL areas are involved in the processing of more complex and natural stimuli, therefore we believe that the use of different type of stimuli might lead to different results.

5.2.2 *Limitations of single-cell recordings*

As already mentioned in the introduction (see section 1.3), single-cell recordings allow to directly measure neuronal activity with a very high spatial and temporal resolution. This method still represents a very powerful tool to investigate the properties of individual neurons and to characterize the functional selectivity of a brain region. However, the use of single electrode recording techniques shows several disadvantages. By using this technique, it is extremely difficult to differentiate between various neuronal subtypes, as researchers are usually biased to target their recordings to large pyramidal excitatory cells rather than to small, inhibitory neurons. This procedure is also very laborious and time-consuming, so it is very difficult, if not impossible, to sample a whole brain area homogeneously by means of single-cell recordings. Neuronal activity is recorded in isolation, and it's usually unclear from which area the input to the activated neurons is coming from, where the output is going to and how neurons interact in a network. Moreover, in many single-cell experiments, researchers include in their analysis only neurons showing task-related responses, by already applying stringent selection filters during the data collection phase. This can lead to instances where recorded neural populations may not be representative for the studied brain regions.

A possible way to solve these problems would be to record activity simultaneously from larger numbers of neurons, by using for instance multielectrode arrays implanted in different

brain areas. In this way, the selection biases would be reduced, and the characterization of network activity becomes possible.

5.2.3   Limitations of functional MRI

The fMRI is used to indirectly infer changes in neuronal activity based on local metabolic and blood-based responses (BOLD) via intermediary processes such as neurovascular coupling and MRI contrast (MION). However, the underlying mechanism of this relationship is still poorly understood. This open question makes it difficult to couple fMRI data with those obtained using other techniques, such as electrophysiological recordings (Uğurbil et al., 2003). fMRI lacks sufficient spatial and temporal resolution to measure the responses of individual neurons. In the temporal domain, the BOLD response is a delayed version of the neurophysiological response. This is because changes in blood flow occur over a much slower timescale than changes in electrophysiological activity. Modifications in electrophysiological activity may happen within milliseconds, whereas changes in blood flow or BOLD response could take from hundreds of milliseconds to seconds (Shmuel and Maier, 2015). In the spatial domain, the resolution of the fMRI signal depends on the choice of fMRI contrast and the strength of the magnetic field. It also depends on which component of the vasculature is being probed (i.e. size of the blood vessels) (Logothetis, 2008).

fMRI signals cannot easily differentiate between function-specific processing and neuromodulation, bottom-up and top-down signals, and may potentially confuse excitation and inhibition. Furthermore, the magnitude of the fMRI signal cannot be quantified to accurately reflect differences among brain regions or among tasks within the same region. (Logothetis, 2008). The above-mentioned limitations of fMRI are unlikely to be resolved by improving the sophistication and power of the scanners, since they are intrinsic to the

measurement of the signal. This is the reason why a multimodal approach, like the one used in the present thesis, combining different complementary techniques, seems to be the right tool to deepen our understanding of the brain.

5.3   Future directions and final remarks

The main aim of the present thesis was to further study the functional heterogeneity of monkey medial PPC, by investigating the visuomotor, somatic, visual, and attention-related properties of two areas belonging to this brain region. Our results show that the rich set of inputs reaching medial PPC merge together to serve different goals, involving the representation of space (as highlighted in the 2nd and 3rd study), grasping actions (shown in the 1st study), and the use of the sensory information for goal-directed movements (reported in the 1st and 2nd study). On top of this, we demonstrated that medial PPC is involved in the processing of higher-level cognitive functions, like selective visual spatial attention (3rd study).

The results presented in this thesis have raised a number of new questions that need to be investigated in future studies:

- We showed that V6A neurons are influenced by grip type during grasping actions in dark and light. Would V6A neurons also respond differently when the same object is grasped with different hand configurations?

- As medial PPC is involved in the handling of complex, multisensorial stimuli, would the use of more sophisticated stimuli change the outcome of our research?

- Does reaching for visual targets in 3D space influence the coordinate frames and the kinematics in area PE?

- How would the perturbation of the reaching network V6A/PEc/PE influence the ability of the monkey to correctly perform reaching movements in the 3D space?

- How would a reversible inactivation of V6A impact the ability of the monkey to shift spatial attention? Does a unilateral inactivation affect the direction of the attention shift?

- Are V6A cortical layers differentially involved in the spatial attention task?

I hope that the studies described in the present thesis will contribute to improve our understanding of the functional organization of the primate PPC. Additional experiments, specifically designed to address the aforementioned questions, may help to gain new insights about the implication of these cortical areas in the complex sensorimotor transformations operated by medial PPC. In these future investigations, the use of combined techniques, such as stimulation, inactivation (Gerits and Vanduffel, 2013; Vanduffel et al., 2014; Balan et al., 2019) and neural recording or fMRI could be the key to overcome some of the drawbacks intrinsic to single methods.

References

Andersen RA, Andersen KN, Hwang EJ, Hauschild M (2014) Optic Ataxia: From Balint's Syndrome to the Parietal Reach Region. Neuron 81:967–983 doi: 10.1016/j.neuron.2014.02.025.

Andersen RA, Cui H (2009) Intention, action planning, and decision making in parietal-frontal circuits. Neuron 63:568–583 doi: 10.1016/j.neuron.2009.08.028.

Arsenault JT, Caspari N, Vandenberghe R, Wim Vanduffel X (2018) Attention Shifts Recruit the Monkey Default Mode Network. doi: 10.1523/JNEUROSCI.1111-17.2017.

Ashe J, Georgopoulos AP (1994) Movement parameters and neural activity in motor cortex and area 5. Cereb Cortex 4:590–600.

Astafiev S V., Shulman GL, Stanley CM, Snyder AZ, Van Essen DC, Corbetta M (2003) Functional organization of human intraparietal and frontal cortex for attending, looking, and pointing. J Neurosci 23:4689–4699 doi: 10.1523/jneurosci.23-11-04689.2003.

Bagesteiro LB, Sarlegna FR, Sainburg RL (2006) Differential influence of vision and proprioception on control of movement distance. Exp brain Res 171:358–370 doi: 10.1007/s00221-005-0272-y.

Bakola S, Gamberini M, Passarelli L, Fattori P, Galletti C (2010) Cortical Connections of Parietal Field PEc in the Macaque: Linking Vision and Somatic Sensation for the Control of Limb Action. Cereb Cortex 20:2592–2604 doi: 10.1093/cercor/bhq007.

Bakola S, Passarelli L, Gamberini M, Fattori P, Galletti C (2013) Cortical connectivity suggests a role in limb coordination for macaque area PE of the superior parietal cortex. J Neurosci 33:6648–6658 doi: 10.1523/JNEUROSCI.4685-12.2013.

Balan PF, Gerits A, Zhu Q, Kolster H, Orban GA, Wardak C, Vanduffel W (2019) Fast Compensatory Functional Network Changes Caused by Reversible Inactivation of

Monkey Parietal Cortex. Cereb Cortex 29:2588–2606 doi: 10.1093/cercor/bhy128.

Bálint, Dr. R (1909) Seelenlähmung des "Schauens", optische Ataxie, räumliche Störung der Aufmerksamkeit. pp. 51–66. Eur Neurol 25:51–66 doi: 10.1159/000210464.

Batista AP, Buneo CA, Snyder LH, Andersen RA (1999) Reach plans in eye-centered coordinates. Science 285:257–260.

Battaglia-Mayer A, Ferrari-Toniolo S, Visco-Comandini F, Archambault PS, Saberi-Moghadam S, Caminiti R (2013) Impairment of online control of hand and eye movements in a monkey model of optic ataxia. Cereb Cortex 23:2644–2656 doi: 10.1093/cercor/bhs250.

Battaglini PP, Muzur A, Galletti C, Skrap M, Brovelli A, Fattori P (2002) Effects of lesions to area V6A in monkeys. Exp brain Res 144:419–422 doi: 10.1007/s00221-002-1099-4.

Baumann MA, Fluet M-C, Scherberger H (2009) Context-Specific Grasp Movement Representation in the Macaque Anterior Intraparietal Area. J Neurosci 29:6436–6448 doi: 10.1523/jneurosci.5479-08.2009.

Beurze SM, de Lange FP, Toni I, Medendorp WP (2007) Integration of target and effector information in the human brain during reach planning. J Neurophysiol 97:188–199 doi: 10.1152/jn.00456.2006.

Beurze SM, de Lange FP, Toni I, Medendorp WP (2009) Spatial and effector processing in the human parietofrontal network for reaches and saccades. J Neurophysiol 101:3053–3062 doi: 10.1152/jn.91194.2008.

Bichot NP, Rossi AF, Desimone R (2005) Parallel and serial neural mechanisms for visual search in macaque area V4. Science (80-) 308:529–534 doi: 10.1126/science.1109676.

Bisiach E, Luzzatti C (1978) Bisiach-Luzzatti-1978-129.Pdf. Cortex 14:129–133.

Blangero A, Gaveau V, Luauté J, Rode G, Salemme R, Guinard M, Boisson D, Rossetti Y, Pisella L (2008) A hand and a field effect in on-line motor control in unilateral optic

ataxia. Cortex 44:560–568 doi: 10.1016/j.cortex.2007.09.004.

Bloom FE, Lazerson A, Hofstadter L (1985) Brain, mind, and behavior. W.H. Freeman.

Borchers S, Muller L, Synofzik M, Himmelbach M (2013) Guidelines and quality measures for the diagnosis of optic ataxia. Front Hum Neurosci doi: 10.3389/fnhum.2013.00324.

Borra E, Belmalih A, Calzavara R, Gerbella M, Murata A, Rozzi S, Luppino G (2008) Cortical connections of the macaque anterior intraparietal (AIP) area. Cereb Cortex 18:1094–1111 doi: 10.1093/cercor/bhm146.

Bosco A, Breveglieri R, Hadjidimitrakis K, Galletti C, Fattori P (2016) Reference frames for reaching when decoupling eye and target position in depth and direction. Sci Rep 6:21646 doi: 10.1038/srep21646.

Bosman CA, Schoffelen J-M, Brunet N, Oostenveld R, Bastos AM, Womelsdorf T, Rubehn B, Stieglitz T, De Weerd P, Fries P (2012) Attentional stimulus selection through selective synchronization between monkey visual areas. Neuron 75:875–888 doi: 10.1016/j.neuron.2012.06.037.

Bremner LR, Andersen RA (2012) Coding of the reach vector in parietal area 5d. Neuron 75:342–351 doi: 10.1016/j.neuron.2012.03.041.

Bremner LR, Andersen RA (2014) Temporal analysis of reference frames in parietal cortex area 5d during reach planning. J Neurosci 34:5273–5284 doi: 10.1523/JNEUROSCI.2068-13.2014.

Breveglieri R, Bosco A, Galletti C, Passarelli L, Fattori P (2016) Neural activity in the medial parietal area V6A while grasping with or without visual feedback. Sci Rep 6:28893 doi: 10.1038/srep28893.

Breveglieri R, Galletti C, Bosco A, Gamberini M, Fattori P (2015) Object affordance modulates visual responses in the macaque medial posterior parietal cortex. J Cogn Neurosci 27:1447–1455 doi: 10.1162/jocn_a_00793.

Breveglieri R, Galletti C, Dal B? G, Hadjidimitrakis K, Fattori P (2014) Multiple Aspects of Neural Activity during Reaching Preparation in the Medial Posterior Parietal Area V6A. J Cogn Neurosci 26:878–895 doi: 10.1162/jocn_a_00510.

Breveglieri R, Galletti C, Gamberini M, Passarelli L, Fattori P (2006) Somatosensory cells in area PEc of macaque posterior parietal cortex. J Neurosci 26:3679–3684 doi: 10.1523/JNEUROSCI.4637-05.2006.

Breveglieri R, Galletti C, Monaco S, Fattori P (2008) Visual, Somatosensory, and Bimodal Activities in the Macaque Parietal Area PEc. Cereb Cortex 18:806–816 doi: 10.1093/cercor/bhm127.

Breveglieri R, Kutz DDFD, Fattori P, Gamberini M, Galletti C (2002) Somatosensory cells in the parieto-occipital area V6A of the macaque. Neuroreport 13:2113–2116 doi: 10.1097/00001756-200211150-00024.

Brodmann K (1909) Vergleichende Lokalisationslehre der Grosshirnrinde in ihren Prinzipien dargestellt auf Grund des Zellenbaues.

Brunamonti E, Genovesio A, Pani P, Caminiti R, Ferraina S (2016) Reaching-related Neurons in Superior Parietal Area 5: Influence of the Target Visibility. J Cogn Neurosci 28:1828–1837 doi: 10.1162/jocn_a_01004.

Bruni S, Giorgetti V, Bonini L, Fogassi L (2015) Processing and Integration of Contextual Information in Monkey Ventrolateral Prefrontal Neurons during Selection and Execution of Goal-Directed Manipulative Actions. J Neurosci 35:11877–11890 doi: 10.1523/JNEUROSCI.1938-15.2015.

Buneo CA, Jarvis MR, Batista AP, Andersen RA (2002) Direct visuomotor transformations for reaching. Nature 416:632–636 doi: 10.1038/416632a.

Buracas GT, Albright TD (2009) Modulation of neuronal responses during covert search for visual feature conjunctions. Proc Natl Acad Sci U S A 106:16853–16858 doi:

10.1073/pnas.0908455106.

Burbaud P, Doegle C, Gross C, Bioulac B (1991) A quantitative study of neuronal discharge in areas 5, 2, and 4 of the monkey during fast arm movements. J Neurophysiol 66:429–443.

Buschman TJ, Miller EK (2009) Serial, Covert Shifts of Attention during Visual Search Are Reflected by the Frontal Eye Fields and Correlated with Population Oscillations. Neuron 63:386–396 doi: 10.1016/j.neuron.2009.06.020.

Buxbaum LJ, Coslett HB (1997) Subtypes of optic ataxia: Reframing the disconnection account. Neurocase 3:159–166 doi: 10.1080/13554799708404050.

Capotosto P, Tosoni A, Spadone S, Sestieri C, Perrucci MG, Romani GL, Della Penna S, Corbetta M (2013) Anatomical segregation of visual selection mechanisms in human parietal cortex. J Neurosci 33:6225–6229 doi: 10.1523/JNEUROSCI.4983-12.2013.

Caspari N, Arsenault JT, Vandenberghe R, Vanduffel W (2018) Functional Similarity of Medial Superior Parietal Areas for Shift-Selective Attention Signals in Humans and Monkeys. Cereb Cortex:1–15 doi: 10.1093/cercor/bhx114.

Caspari N, Janssens T, Mantini D, Vandenberghe R, Vanduffel W (2015) Covert Shifts of Spatial Attention in the Macaque Monkey. J Neurosci 35:7695–7714 doi: 10.1523/JNEUROSCI.4383-14.2015.

Cavada C, Goldman-Rakic PS (1989a) Posterior parietal cortex in rhesus monkey: II. Evidence for segregated corticocortical networks linking sensory and limbic areas with the frontal lobe. J Comp Neurol 287:422–445 doi: 10.1002/cne.902870403.

Cavada C, Goldman-Rakic PS (1989b) Posterior parietal cortex in rhesus monkey: I. Parcellation of areas based on distinctive limbic and sensory corticocortical connections. J Comp Neurol 287:393–421 doi: 10.1002/cne.902870402.

Cavina-Pratesi C, Monaco S, Fattori P, Galletti C, McAdam TD, Quinlan DJ, Goodale MA,

Culham JC (2010) Functional magnetic resonance imaging reveals the neural substrates of arm transport and grip formation in reach-to-grasp actions in humans. J Neurosci 30:10306–10323 doi: 10.1523/JNEUROSCI.2023-10.2010.

Chang SWC, Snyder LH (2010) Idiosyncratic and systematic aspects of spatial representations in the macaque parietal cortex. Proc Natl Acad Sci U S A 107:7951–7956 doi: 10.1073/pnas.0913209107.

Chaplin TA, Yu H-H, Soares JGM, Gattass R, Rosa MGP (2013) A conserved pattern of differential expansion of cortical areas in simian primates. J Neurosci 33:15120–15125 doi: 10.1523/JNEUROSCI.2909-13.2013.

Chen J, Reitzen SD, Kohlenstein JB, Gardner EP (2009) Neural representation of hand kinematics during prehension in posterior parietal cortex of the macaque monkey. J Neurophysiol 102:3310–3328 doi: 10.1152/jn.90942.2008.

Chen YC, Mandeville JB, Nguyen T V, Talele A, Cavagna F, Jenkins BG (2001) Improved mapping of pharmacologically induced neuronal activation using the IRON technique with superparamagnetic blood pool agents. J Magn Reson Imaging 14:517–524 doi: 10.1002/jmri.1215.

Ciavarro M, Ambrosini E, Tosoni A, Committeri G, Fattori P, Galletti C (2013) rTMS of Medial Parieto-occipital Cortex Interferes with Attentional Reorienting during Attention and Reaching Tasks. J Cogn Neurosci 25:1453–1462 doi: 10.1162/jocn_a_00409.

Colby CL, Duhamel JR (1991) Heterogeneity of extrastriate visual areas and multiple parietal areas in the macaque monkey. Neuropsychologia 29:517–537.

Connolly JD, Andersen RA, Goodale MA (2003) FMRI evidence for a "parietal reach region" in the human brain. doi: 10.1007/s00221-003-1587-1.

Coslett HB, Lie G (2008) Simultanagnosia: When a rose is not red. J Cogn Neurosci 20:36–48 doi: 10.1162/jocn.2008.20002.

Crawford JD, Henriques DYP, Medendorp WP (2011) Three-dimensional transformations for goal-directed action. Annu Rev Neurosci 34:309–331 doi: 10.1146/annurev-neuro-061010-113749.

Cui H, Andersen RA (2011) Different Representations of Potential and Selected Motor Plans by Distinct Parietal Areas. J Neurosci 31:18130–18136 doi: 10.1523/JNEUROSCI.6247-10.2011.

Culham J, Gallivan JP, Cavina-Pratesi C, Quinlan DJ (2008) fMRI investigations of reaching and ego space in human superior parieto-occipital cortex. Embodiment, Ego-sp Action:247–274.

Culham JC, Cavina-Pratesi C, Singhal A (2006) The role of parietal cortex in visuomotor control: What have we learned from neuroimaging? Neuropsychologia 44:2668–2684 doi: 10.1016/j.neuropsychologia.2005.11.003.

Dalrymple KA, Bischof WF, Cameron D, Barton JJS, Kingstone A (2010) Simulating simultanagnosia: spatially constricted vision mimics local capture and the global processing deficit. Exp brain Res 202:445–455 doi: 10.1007/s00221-009-2152-3.

Desimone R, Duncan J (1995) Neural Mechanisms of Selective Visual Attention. Annu Rev Neurosci 18:193–222 doi: 10.1146/annurev.ne.18.030195.001205.

Di Bono MG, Begliomini C, Castiello U, Zorzi M (2015) Probing the reaching-grasping network in humans through multivoxel pattern decoding. Brain Behav 5:e00412 doi: 10.1002/brb3.412.

Dotson NM, Goodell B, Salazar RF, Hoffman SJ, Gray CM (2015) Methods, caveats and the future of large-scale microelectrode recordings in the non-human primate. Front Syst Neurosci 9:149 doi: 10.3389/fnsys.2015.00149.

Dowben RM, Rose JE (1953) A metal-filled microelectrode. Science (80-) 118:22–24 doi: 10.1126/science.118.3053.22.

Duffy FH, Burchfiel JL (1971) Somatosensory system: organizational hierarchy from single units in monkey area 5. Science 172:273–275.

Fabbri S, Caramazza A, Lingnau A (2010) Tuning curves for movement direction in the human visuomotor system. J Neurosci 30:13488–13498 doi: 10.1523/JNEUROSCI.2571-10.2010.

Fabbri S, Caramazza A, Lingnau A (2012) Distributed sensitivity for movement amplitude in directionally tuned neuronal populations. J Neurophysiol 107:1845–1856 doi: 10.1152/jn.00435.2011.

Fabbri S, Stubbs KM, Cusack R, Culham JC (2016) Disentangling Representations of Object and Grasp Properties in the Human Brain. J Neurosci 36:7648–7662 doi: 10.1523/JNEUROSCI.0313-16.2016.

Fattori P, Breveglieri R, Amoroso K, Galletti C (2004) Evidence for both reaching and grasping activity in the medial parieto-occipital cortex of the macaque. Eur J Neurosci 20:2457–2466 doi: 10.1111/j.1460-9568.2004.03697.x.

Fattori P, Breveglieri R, Bosco A, Gamberini M, Galletti C (2017) Vision for Prehension in the Medial Parietal Cortex. Cereb Cortex:bhv302 doi: 10.1093/cercor/bhv302.

Fattori P, Breveglieri R, Marzocchi N, Filippini D, Bosco A, Galletti C (2009) Hand Orientation during {Reach-to-Grasp} Movements Modulates Neuronal Activity in the Medial Posterior Parietal Area {V6A}. J Neurosci 29:1928–1936 doi: 10.1523/JNEUROSCI.4998-08.2009.

Fattori P, Breveglieri R, Raos V, Bosco A, Galletti C (2012) Vision for action in the macaque medial posterior parietal cortex. J Neurosci 32:3221–3234 doi: 10.1523/JNEUROSCI.5358-11.2012.

Fattori P, Kutz DF, Breveglieri R, Marzocchi N, Galletti C (2005) Spatial tuning of reaching activity in the medial parieto-occipital cortex (area V6A) of macaque monkey. Eur J

Neurosci 22:956–972 doi: 10.1111/j.1460-9568.2005.04288.x.

Fattori P, Raos V, Breveglieri R, Bosco A, Marzocchi N, Galletti C (2010) The dorsomedial pathway is not just for reaching: grasping neurons in the medial parieto-occipital cortex of the macaque monkey. J Neurosci 30:342–349 doi: 10.1523/JNEUROSCI.3800-09.2010.

Ferraina S, Bianchi L (1994) Posterior parietal cortex: functional properties of neurons in area 5 during an instructed-delay reaching task within different parts of space. Exp brain Res 99:175–178.

Ferraina S, Brunamonti E, Giusti MA, Costa S, Genovesio A, Caminiti R (2009) Reaching in depth: hand position dominates over binocular eye position in the rostral superior parietal lobule. J Neurosci 29:11461–11470 doi: 10.1523/JNEUROSCI.1305-09.2009.

Filimon F, Nelson JD, Hagler DJ, Sereno MI (2007) Human cortical representations for reaching: Mirror neurons for execution, observation, and imagery. Neuroimage 37:1315–1328 doi: 10.1016/j.neuroimage.2007.06.008.

Filimon F, Nelson JD, Huang R-S, Sereno MI (2009) Multiple parietal reach regions in humans: cortical representations for visual and proprioceptive feedback during on-line reaching. J Neurosci 29:2961–2971 doi: 10.1523/JNEUROSCI.3211-08.2009.

Flanders M, Soechting JF (1990) Arm muscle activation for static forces in three-dimensional space. J Neurophysiol 64:1818–1837.

Fluet M-C, Baumann MA, Scherberger H (2010) Context-specific grasp movement representation in macaque ventral premotor cortex. J Neurosci 30:15175–15184 doi: 10.1523/JNEUROSCI.3343-10.2010.

Fraser GW, Schwartz AB (2012) Recording from the same neurons chronically in motor cortex. J Neurophysiol 107:1970–1978 doi: 10.1152/jn.01012.2010.

Galati G, Committeri G, Pitzalis S, Pelle G, Patria F, Fattori P, Galletti C (2011) Intentional

signals during saccadic and reaching delays in the human posterior parietal cortex. Eur J Neurosci 34:1871–1885 doi: 10.1111/j.1460-9568.2011.07885.x.

Galletti C, Battaglini PP, Fattori P (1991) Functional Properties of Neurons in the Anterior Bank of the Parieto-occipital Sulcus of the Macaque Monkey. Eur J Neurosci 3:452–461.

Galletti C, Battaglini PP, Fattori P (1993) Parietal neurons encoding spatial locations in craniotopic coordinates. Exp Brain Res 96:221–229 doi: 10.1007/BF00227102.

Galletti C, Battaglini PP, Fattori P (1995) Eye position influence on the parieto-occipital area PO (V6) of the macaque monkey. Eur J Neurosci 7:2486–2501 doi: 10.1111/j.1460-9568.1995.tb01047.x.

Galletti C, Breveglieri R, Lappe M, Bosco A, Ciavarro M, Fattori P (2010) Covert shift of attention modulates the ongoing neural activity in a reaching area of the macaque dorsomedial visual stream. PLoS One 5:e15078 doi: 10.1371/journal.pone.0015078.

Galletti C, Fattori P (2017) The dorsal visual stream revisited: Stable circuits or dynamic pathways? Cortex doi: 10.1016/j.cortex.2017.01.009.

Galletti C, Fattori P, Battaglini PP, Shipp S, Zeki S (1996) Functional demarcation of a border between areas V6 and V6A in the superior parietal gyrus of the macaque monkey. Eur J Neurosci 8:30–52 doi: 10.1111/j.1460-9568.1996.tb01165.x.

Galletti C, Fattori P, Kutz DF, Gamberini M (1999) Brain location and visual topography of cortical area V6A in the macaque monkey. Eur J Neurosci 11:575–582 doi: 10.1046/j.1460-9568.1999.00467.x.

Galletti C, Kutz DF, Gamberini M, Breveglieri R, Fattori P (2003) Role of the medial parieto-occipital cortex in the control of reaching and grasping movements. Exp Brain Res 153:158–170 doi: 10.1007/s00221-003-1589-z.

Gallivan JP, Cavina-Pratesi C, Culham JC (2009) Is that within reach? fMRI reveals that the

human superior parieto-occipital cortex encodes objects reachable by the hand. J Neurosci 29:4381–4391 doi: 10.1523/JNEUROSCI.0377-09.2009.

Gallivan JP, McLean DA, Valyear KF, Pettypiece CE, Culham JC (2011) Decoding action intentions from preparatory brain activity in human parieto-frontal networks. J Neurosci 31:9599–9610 doi: 10.1523/JNEUROSCI.0080-11.2011.

Gamberini M, Dal Bò G, Breveglieri R, Briganti S, Passarelli L, Fattori P, Galletti C (2018) Sensory properties of the caudal aspect of the macaque's superior parietal lobule. Brain Struct Funct 223:1863–1879 doi: 10.1007/s00429-017-1593-x.

Gamberini M, Fattori P, Galletti C (2015) The medial parietal occipital areas in the macaque monkey. Vis Neurosci 32 doi: 10.1017/S0952523815000103.

Gamberini M, Galletti C, Bosco A, Breveglieri R, Fattori P (2011) Is the medial posterior parietal area V6A a single functional area? J Neurosci 31:5145–5157 doi: 10.1523/JNEUROSCI.5489-10.2011.

Gamberini M, Passarelli L, Fattori P, Galletti C (2019) Structural connectivity and functional properties of the macaque superior parietal lobule. Brain Struct Funct doi: 10.1007/s00429-019-01976-9.

Gamberini M, Passarelli L, Fattori P, Zucchelli M, Bakola S, Luppino G, Galletti C (2009) Cortical connections of the visuomotor parietooccipital area V6Ad of the macaque monkey. J Comp Neurol 513:622–642 doi: 10.1002/cne.21980.

Garcin R, Rondot P, de Recondo J (1967) Optic ataxia localized in 2 left homonymous visual hemifields (clinical study with film presentation). Rev Neurol (Paris) 116:707–714.

Gardner EP (2017) Neural pathways for cognitive command and control of hand movements. Proc Natl Acad Sci 114:4048–4050 doi: 10.1073/pnas.1702746114.

Gardner EP, Babu KS, Reitzen SD, Ghosh S, Brown AS, Chen J, Hall AL, Herzlinger MD, Kohlenstein JB, Ro JY (2007a) Neurophysiology of prehension. I. Posterior parietal

cortex and object-oriented hand behaviors. J Neurophysiol 97:387–406 doi: 10.1152/jn.00558.2006.

Gardner EP, Babu KS, Reitzen SD, Ghosh S, Brown AS, Chen J, Hall AL, Herzlinger MD, Kohlenstein JB, Ro JY, Ep G, Ks B, Sd R, Ghosh S, As B, Chen J, Al H, Jb K, Neurophysiology RJY (2007b) Neurophysiology of Prehension . I . Posterior Parietal Cortex and Object- Oriented Hand Behaviors. :387–406 doi: 10.1152/jn.00558.2006.

Gerits A, Vanduffel W (2013) Optogenetics in primates: a shining future? Trends Genet 29:403–411 doi: 10.1016/j.tig.2013.03.004.

Gerstmann J (2001) Pure tactile agnosia. Cogn Neuropsychol:37–41 doi: 10.1080/02643290042000116.

Goodale MA, Milner AD (1992) Separate visual pathways tor perception and action. Trends Cogn Sci 15:20–25 doi: 10.1016/0166-2236(92)90344-8.

Gordon J, Ghilardi MF, Ghez C (1994) Accuracy of planar reaching movements. I. Independence of direction and extent variability. Exp brain Res 99:97–111.

Gottlieb JP, Kusunoki M, Goldberg ME (1998) The representation of visual salience in monkey parietal cortex. Nature 391:481–484 doi: 10.1038/35135.

Green JD (1958) A simple microelectrode for recording from the central nervous system. Nature 182:962 doi: 10.1038/182962a0.

Grefkes C, Fink GR (2005) REVIEW: The functional organization of the intraparietal sulcus in humans and monkeys. J Anat 207:3–17 doi: 10.1111/j.1469-7580.2005.00426.x.

Gregory MD, Kippenhan JS, Eisenberg DP, Kohn PD, Dickinson D, Mattay VS, Chen Q, Weinberger DR, Saad ZS, Berman KF (2017) Neanderthal-Derived Genetic Variation Shapes Modern Human Cranium and Brain. Sci Rep 7 doi: 10.1038/s41598-017-06587-0.

Hadjidimitrakis K, Bertozzi F, Breveglieri R, Bosco A, Galletti C, Fattori P (2014a)

Common neural substrate for processing depth and direction signals for reaching in the monkey medial posterior parietal cortex. Cereb Cortex 24:1645–1657 doi: 10.1093/cercor/bht021.

Hadjidimitrakis K, Bertozzi F, Breveglieri R, Fattori P, Galletti C (2014b) Body-centered, mixed, but not hand-centered coding of visual targets in the medial posterior parietal cortex during reaches in 3D space. Cereb Cortex 24:3209–3220 doi: 10.1093/cercor/bht181.

Hadjidimitrakis K, Bertozzi F, Breveglieri R, Galletti C, Fattori P (2017) Temporal stability of reference frames in monkey area V6A during a reaching task in 3D space. Brain Struct Funct 222:1959–1970 doi: 10.1007/s00429-016-1319-5.

Hadjidimitrakis K, Breveglieri R, Bosco A, Fattori P (2012) Three-dimensional eye position signals shape both peripersonal space and arm movement activity in the medial posterior parietal cortex. Front Integr Neurosci 6:37 doi: 10.3389/fnint.2012.00037.

Hadjidimitrakis K, Breveglieri R, Placenti G, Bosco A, Sabatini SP, Fattori P (2011) Fix your eyes in the space you could reach: neurons in the macaque medial parietal cortex prefer gaze positions in peripersonal space. Gribble PL, ed. PLoS One 6:e23335 doi: 10.1371/journal.pone.0023335.

Hadjidimitrakis K, Dal Bo' G, Breveglieri R, Galletti C, Fattori P (2015) Overlapping representations for reach depth and direction in caudal superior parietal lobule of macaques. J Neurophysiol 114:2340–2352 doi: 10.1152/jn.00486.2015.

Hagler DJ, Riecke L, Sereno MI (2007) Parietal and superior frontal visuospatial maps activated by pointing and saccades. Neuroimage 35:1562–1577 doi: 10.1016/j.neuroimage.2007.01.033.

Hatsopoulos NG, Donoghue JP (2009) The science of neural interface systems. Annu Rev Neurosci 32:249–266 doi: 10.1146/annurev.neuro.051508.135241.

Hayhoe MM, Shrivastava A, Mruczek R, Pelz JB (2003) Visual memory and motor planning in a natural task. J Vis 3:6 doi: 10.1167/3.1.6.

Hill J, Inder T, Neil J, Dierker D, Harwell J, Van Essen D (2010) Similar patterns of cortical expansion during human development and evolution. Proc Natl Acad Sci U S A 107:13135–13140 doi: 10.1073/pnas.1001229107.

Hinkley LB, Krubitzer LA, Nagarajan SS, Disbrow EA (2007) Sensorimotor integration in S2, PV, and parietal rostroventral areas of the human sylvian fissure. J Neurophysiol 97:1288–1297 doi: 10.1152/jn.00733.2006.

Huang RS, Chen CF, Tran AT, Holstein KL, Sereno MI (2012) Mapping multisensory parietal face and body areas in humans. Proc Natl Acad Sci U S A 109:18114–18119 doi: 10.1073/pnas.1207946109.

Huang RS, Sereno MI (2018) Multisensory and sensorimotor maps. In: Handbook of Clinical Neurology, pp 141–161. Elsevier B.V. doi: 10.1016/B978-0-444-63622-5.00007-3.

Humphrey DR, Schmidt EM (1990) Extracellular Single-Unit Recording Methods. In: Neurophysiological Techniques, II, pp 1–64. New Jersey: Humana Press. doi: 10.1385/0-89603-185-3:1.

Illes J, Racine E (2005) Imaging or imagining? A neuroethics challenge informed by genetics. Am J Bioeth 5:5–18 doi: 10.1080/15265160590923358.

Impieri D, Gamberini M, Passarelli L, Rosa MGP, Galletti C (2018) Thalamo-cortical projections to the macaque superior parietal lobule areas PEc and PE. J Comp Neurol 526:1041–1056 doi: 10.1002/cne.24389.

Jackson GM, Shepherd T, Mueller SC, Husain M, Jackson SR (2006) Dorsal simultanagnosia: An impairment of visual processing or visual awareness? Cortex 42:740–749 doi: 10.1016/s0010-9452(08)70412-x.

Jakobson LS, Archibald YM, Carey DP, Goodale MA (1991) A kinematic analysis of

reaching and grasping movements in a patient recovering from optic ataxia. Neuropsychologia 29:803–809 doi: 10.1016/0028-3932(91)90073-H.

Janssen P, Scherberger H (2015) Visual Guidance in Control of Grasping. Annu Rev Neurosci 38:69–86 doi: 10.1146/annurev-neuro-071714-034028.

Janssens T, Keil B, Farivar R, McNab JA, Polimeni JR, Gerits A, Arsenault JT, Wald LL, Vanduffel W (2012) An implanted 8-channel array coil for high-resolution macaque MRI at 3T. Neuroimage 62:1529–1536 doi: 10.1016/j.neuroimage.2012.05.028.

Jeannerod M (1986) Mechanisms of visuomotor coordination: a study in normal and brain-damaged subjects. Neuropsychologia 24:41–78.

Jeannerod M, Arbib MA, Rizzolatti G, Sakata H (1995) Grasping objects: the cortical mechanisms of visuomotor transformation. Trends Neurosci 18:314–320 doi: 10.1016/0166-2236(95)93921-J.

Johnson PB, Ferraina S, Bianchi L, Caminiti R (1996) Cortical networks for visual reaching: physiological and anatomical organization of frontal and parietal lobe arm regions. Cereb Cortex 6:102–119.

Jones EG, Coulter JD, Hendry SH (1978) Intracortical connectivity of architectonic fields in the somatic sensory, motor and parietal cortex of monkeys. J Comp Neurol 181:291–347 doi: 10.1002/cne.901810206.

Kalaska JF (1996) Parietal cortex area 5 and visuomotor behavior. Can J Physiol Pharmacol 74:483–498.

Kalaska JF, Caminiti R, Georgopoulos AP (1983) Cortical mechanisms related to the direction of two-dimensional arm movements: relations in parietal area 5 and comparison with motor cortex. Exp brain Res 51:247–260.

Kalaska JF, Cohen DA, Hyde ML (1985) [Role of the motor and parietal cortex in the control of visually-guided arm movements]. Union Med Can 114:1006–1010.

Kalaska JF, Cohen DA, Prud'homme M, Hyde ML (1990) Parietal area 5 neuronal activity encodes movement kinematics, not movement dynamics. Exp brain Res 80:351–364.

Kalaska JF, Crammond DJ (1992) Cerebral cortical mechanisms of reaching movements. Science 255:1517–1523.

Kandel, E. R., Schwartz, J. H., Jessell, T. M., Siegelbaum, S. A. &, Hudspeth AJ (2013) Principles of Neural Science (Columbus, OH UM-H, ed)., Fifth Edit.

Karnath H-O, Perenin M-T (2005) Cortical control of visually guided reaching: evidence from patients with optic ataxia. Cereb Cortex 15:1561–1569 doi: 10.1093/cercor/bhi034.

Kelley TA, Serences JT, Giesbrecht B, Yantis S (2008) Cortical mechanisms for shifting and holding visuospatial attention. Cereb Cortex 18:114–125 doi: 10.1093/cercor/bhm036.

Khan AZ, Crawford JD, Blohm G, Urquizar C, Rossetti Y, Pisella L (2007) Influence of initial hand and target position on reach errors in optic ataxic and normal subjects. J Vis 7 doi: 10.1167/7.5.8.

Khan AZ, Pisella L, Vighetto A, Cotton F, Luauté J, Boisson D, Salemme R, Crawford JD, Rossetti Y (2005) Optic ataxia errors depend on remapped, not viewed, target location. Nat Neurosci 8:418–420 doi: 10.1038/nn1425.

Kobak D, Brendel W, Constantinidis C, Feierstein CE, Kepecs A, Mainen ZF, Romo R, Qi X, Uchida N, Machens CK (2016) Demixed principal component analysis of neural population data. Elife 5:1–37 doi: 10.7554/eLife.10989.

Koch C, Ullman S (1985) Shifts in selective visual attention: Towards the underlying neural circuitry. Hum Neurobiol 4:219–227 doi: 10.1007/978-94-009-3833-5_5.

Konen CS, Mruczek REB, Montoya JL, Kastner S (2013) Functional organization of human posterior parietal cortex: grasping- and reaching-related activations relative to topographically organized cortex. J Neurophysiol 109:2897–2908 doi: 10.1152/jn.00657.2012.

Kunimatsu J, Tanaka M (2012) Alteration of the timing of self-initiated but not reactive saccades by electrical stimulation in the supplementary eye field. Eur J Neurosci 36:3258–3268 doi: 10.1111/j.1460-9568.2012.08242.x.

Kutz DF, Fattori P, Gamberini M, Breveglieri R, Galletti C (2003) Early- and late-responding cells to saccadic eye movements in the cortical area V6A of macaque monkey. Exp brain Res Exp Hirnforsch Expérimentation cérébrale 149:83–95 doi: 10.1007/s00221-002-1337-9.

Kutz DF, Marzocchi N, Fattori P, Cavalcanti S, Galletti C (2005) Real-time supervisor system based on trinary logic to control experiments with behaving animals and humans. J Neurophysiol 93:3674–3686 doi: 10.1152/jn.01292.2004.

Kutz DF, Marzocchi N, Fattori P, Cavalcanti S, Galletti C, Fattori P, Raos V, Breveglieri R, Bosco A, Marzocchi N, Galletti C (2011) Real-Time Supervisor System Based on Trinary Logic to Control Experiments With Behaving Animals and Humans Real-Time Supervisor System Based on Trinary Logic to Control Experiments With Behaving Animals and Humans. J Neurophysiol 93:3674–3686 doi: 10.1152/jn.01292.2004.

Lacquaniti F, Guigon E, Bianchi L, Ferraina S, Caminiti R (1995) Representing spatial information for limb movement: role of area 5 in the monkey. Cereb Cortex 5:391–409.

Lanzilotto M, Livi A, Maranesi M, Gerbella M, Barz F, Ruther P, Fogassi L, Rizzolatti G, Bonini L (2016) Extending the cortical grasping network: Pre-supplementary motor neuron activity during vision and grasping of objects. Cereb Cortex doi: 10.1093/cercor/bhw315.

Lehmann SJ, Scherberger H (2013) Reach and gaze representations in macaque parietal and premotor grasp areas. J Neurosci 33:7038–7049 doi: 10.1523/JNEUROSCI.5568-12.2013.

Leite FP, Mandeville JB (2006) Characterization of event-related designs using BOLD and

IRON fMRI. Neuroimage 29:901–909 doi: 10.1016/j.neuroimage.2005.08.022.

Leite FP, Tsao D, Vanduffel W, Fize D, Sasaki Y, Wald LL, Dale AM, Kwong KK, Orban GA, Rosen BR, Tootell RBH, Mandeville JB (2002) Repeated fMRI using iron oxide contrast agent in awake, behaving macaques at 3 Tesla. Neuroimage 16:283–294 doi: 10.1006/nimg.2002.1110.

Li Y, Cui H (2013) Dorsal parietal area 5 encodes immediate reach in sequential arm movements. J Neurosci 33:14455–14465 doi: 10.1523/JNEUROSCI.1162-13.2013.

Logothetis N (2008) What we can do and what we cannot do with fMRI. Nature 453:869–878.

Logothetis NK, Wandell BA (2004) Interpreting the BOLD signal. Annu Rev Physiol 66:735–769 doi: 10.1146/annurev.physiol.66.082602.092845.

Luppino G, Hamed S Ben, Gamberini M, Matelli M, Galletti C (2005) Occipital (V6) and parietal (V6A) areas in the anterior wall of the parieto-occipital sulcus of the macaque: a cytoarchitectonic study. Eur J Neurosci 21:3056–3076 doi: 10.1111/j.1460-9568.2005.04149.x.

Mackay WA, Mendonça AJ, Riehle A (1994) Spatially modulated touch responses in parietal cortex. Brain Res 645:351–355 doi: 10.1016/0006-8993(94)91673-X.

Maeda K, Ishida H, Nakajima K, Inase M, Murata A (2015) Functional properties of parietal hand manipulation-related neurons and mirror neurons responding to vision of own hand action. J Cogn Neurosci 27:560–572 doi: 10.1162/jocn_a_00742.

Maimon G, Assad JA (2006) Parietal Area 5 and the Initiation of Self-Timed Movements versus Simple Reactions. J Neurosci 26:2487–2498 doi: 10.1523/JNEUROSCI.3590-05.2006.

Mandeville JB, Marota JJ (1999) Vascular filters of functional MRI: spatial localization using BOLD and CBV contrast. Magn Reson Med 42:591–598 doi: 10.1002/(sici)1522-

2594(199909)42:3<591::aid-mrm23>3.0.co;2-8.

Mandeville JB, Marota JJ, Kosofsky BE, Keltner JR, Weissleder R, Rosen BR, Weisskoff RM (1998) Dynamic functional imaging of relative cerebral blood volume during rat forepaw stimulation. Magn Reson Med 39:615–624 doi: 10.1002/mrm.1910390415.

Mantini D, Hasson U, Betti V, Perrucci MG, Romani GL, Corbetta M, Orban GA, Vanduffel W (2012) Interspecies activity correlations reveal functional correspondence between monkey and human brain areas. Nat Methods 9:277–282 doi: 10.1038/nmeth.1868.

Marshall JC, Halligan PW (1995) Seeing the forest but only half the trees? Nature 373:521–523 doi: 10.1038/373521a0.

Martin JA, Karnath H-O, Himmelbach M (2015) Revisiting the cortical system for peripheral reaching at the parieto-occipital junction. Cortex 64:363–379 doi: 10.1016/j.cortex.2014.11.012.

Marzocchi N, Breveglieri R, Galletti C, Fattori P (2008) Reaching activity in parietal area V6A of macaque: Eye influence on arm activity or retinocentric coding of reaching movements? Eur J Neurosci 27:775–789 doi: 10.1111/j.1460-9568.2008.06021.x.

Matelli M, Govoni P, Galletti C, Kutz DF, Luppino G (1998) Superior area 6 afferents from the superior parietal lobule in the macaque monkey. J Comp Neurol 402:327–352 doi: 10.1002/(SICI)1096-9861(19981221)402:3<327::AID-CNE4>3.0.CO;2-Z.

McAdams CJ, Maunsell JHR (2000) Attention to Both Space and Feature Modulates Neuronal Responses in Macaque Area V4. J Neurophysiol 83:1751–1755 doi: 10.1152/jn.2000.83.3.1751.

McGuire LMM, Sabes PN (2011) Heterogeneous representations in the superior parietal lobule are common across reaches to visual and proprioceptive targets. J Neurosci 31:6661–6673 doi: 10.1523/JNEUROSCI.2921-10.2011.

Menzer DL, Rao NG, Bondy A, Truccolo W, Donoghue JP (2014) Population interactions

between parietal and primary motor cortices during reach. J Neurophysiol 112:2959–2984 doi: 10.1152/jn.00851.2012.

Messier J, Kalaska JF (2000) Covariation of primate dorsal premotor cell activity with direction and amplitude during a memorized-delay reaching task. J Neurophysiol 84:152–165.

Milner D, Goodale M (2006) The Visual Brain in Action. Oxford University Press. doi: 10.1093/acprof:oso/9780198524724.001.0001.

Molenberghs P, Gillebert CR, Peeters R, Vandenberghe R (2008) Convergence between lesion-symptom mapping and functional magnetic resonance imaging of spatially selective attention in the intact brain. J Neurosci 28:3359–3373 doi: 10.1523/JNEUROSCI.5247-07.2008.

Molenberghs P, Mesulam MM, Peeters R, Vandenberghe RRC (2007) Remapping Attentional Priorities: Differential Contribution of Superior Parietal Lobule and Intraparietal Sulcus. Cereb Cortex 17:2703–2712 doi: 10.1093/cercor/bhl179.

Monaco S, Cavina-Pratesi C, Sedda A, Fattori P, Galletti C, Culham JC (2011) Functional magnetic resonance adaptation reveals the involvement of the dorsomedial stream in hand orientation for grasping. J Neurophysiol 106:2248–2263 doi: 10.1152/jn.01069.2010.

Moschovakis AK, Scudder CA, Highstein SM (1996) The microscopic anatomy and physiology of the mammalian saccadic system. Prog Neurobiol 50:133–254.

Motter BC (1994) Neural correlates of feature selective memory and pop-out in extrastriate area V4. J Neurosci 14:2190–2199.

Mountcastle VB, Lynch JC, Georgopoulos A, Sakata H, Acuna C (1975) Posterior parietal association cortex of the monkey: command functions for operations within extrapersonal space. J Neurophysiol 38:871–908.

Murata a, Gallese V, Luppino G, Kaseda M, Sakata H (2000) Selectivity for the shape, size, and orientation of objects for grasping in neurons of monkey parietal area AIP. J Neurophysiol 83:2580–2601.

Murata A, Gallese V, Kaseda M, Sakata H (1996) Parietal neurons related to memory-guided hand manipulation. J Neurophysiol 75:2180–2186.

Nakamura K, Colby CL (2000) Visual, saccade-related, and cognitive activation of single neurons in monkey extrastriate area V3A. J Neurophysiol 84:677–692.

Naselaris T, Merchant H, Amirikian B, Georgopoulos AP (2006) Large-Scale Organization of Preferred Directions in the Motor Cortex. I. Motor Cortical Hyperacuity for Forward Reaching. J Neurophysiol 96:3231–3236 doi: 10.1152/jn.00487.2006.

Neggers SF, Bekkering H (2001) Gaze anchoring to a pointing target is present during the entire pointing movement and is driven by a non-visual signal. J Neurophysiol 86:961–970.

Nelissen K, Fiave PA, Vanduffel W (2018) Decoding Grasping Movements from the Parieto-Frontal Reaching Circuit in the Nonhuman Primate. Cereb Cortex 28:1245–1259 doi: 10.1093/cercor/bhx037.

Nelissen K, Luppino G, Vanduffel W, Rizzolatti G, Orban GA (2005) Observing Others: Multiple Action Representation in the Frontal Lobe. Science (80-) 310:332–336 doi: 10.1126/science.1115593.

Nelissen K, Vanduffel W (2011) Grasping-Related Functional Magnetic Resonance Imaging Brain Responses in the Macaque Monkey. J Neurosci 31:8220–8229 doi: 10.1523/JNEUROSCI.0623-11.2011.

O'Sullivan SB, Schmitz TJ (2007) Physical rehabilitation. F.A. Davis.

Ogawa S, Lee TM, Nayak AS, Glynn P (1990) Oxygenation-sensitive contrast in magnetic resonance image of rodent brain at high magnetic fields. Magn Reson Med 14:68–78

doi: 10.1002/mrm.1910140108.

Padberg J, Cooke DF, Cerkevich CM, Kaas JH, Krubitzer L (2019) Cortical connections of area 2 and posterior parietal area 5 in macaque monkeys. J Comp Neurol 527:718–737 doi: 10.1002/cne.24453.

Padberg J, Franca JG, Cooke DF, Soares JGM, Rosa MGP, Fiorani M, Gattass R, Krubitzer L (2007) Parallel evolution of cortical areas involved in skilled hand use. J Neurosci 27:10106–10115 doi: 10.1523/JNEUROSCI.2632-07.2007.

Pandya DNN, Seltzer B (1982) Intrinsic connections and architectonics of posterior parietal cortex in the rhesus monkey. J Comp Neurol 204:196–210 doi: 10.1002/cne.902040208.

Passarelli L, Rosa MGP, Gamberini M, Bakola S, Burman KJ, Fattori P, Galletti C (2011) Cortical Connections of Area V6Av in the Macaque: A Visual-Input Node to the Eye/Hand Coordination System. J Neurosci 31:1790–1801 doi: 10.1523/JNEUROSCI.4784-10.2011.

Paxinos G, Huang X-F, Toga A (2000) The Rhesus Monkey Brain in Stereotaxic Coordinates. Fac Heal Behav Sci - Pap.

Perenin MT, Vighetto A (1988) Optic ataxia: a specific disruption in visuomotor mechanisms. I. Different aspects of the deficit in reaching for objects. Brain 111:643–674 doi: 10.1093/brain/111.3.643.

Phan ML, Schendel KL, Recanzone GH, Robertson LC (2000) Auditory and visual spatial localization deficits following bilateral parietal lobe lesions in a patient with Balint's syndrome. J Cogn Neurosci 12:583–600.

Pisella L, Gréa H, Tilikete C, Vighetto A, Desmurget M, Rode G, Boisson D, Rossetti Y (2000) An "automatic pilot" for the hand in human posterior parietal cortex: Toward reinterpreting optic ataxia. Nat Neurosci 3:729–736 doi: 10.1038/76694.

Pisella L, Michel C, Gréa H, Tilikete C, Vighetto A, Rossetti Y (2004) Preserved prism

adaptation in bilateral optic ataxia: Strategic versus adaptive reaction to prisms. Exp Brain Res 156:399–408 doi: 10.1007/s00221-003-1746-4.

Piserchia V, Breveglieri R, Hadjidimitrakis K, Bertozzi F, Galletti C, Fattori P (2016) Mixed Body/Hand Reference Frame for Reaching in 3D Space in Macaque Parietal Area PEc. Cereb Cortex:bhw039 doi: 10.1093/cercor/bhw039.

Pitzalis S, Fattori P, Galletti C (2015) The human cortical areas V6 and V6A. Vis Neurosci 32:E007 doi: 10.1017/S0952523815000048.

Pitzalis S, Galletti C, Huang R-S, Patria F, Committeri G, Galati G, Fattori P, Sereno MI (2006) Wide-field retinotopy defines human cortical visual area v6. J Neurosci 26:7962–7973 doi: 10.1523/JNEUROSCI.0178-06.2006.

Pitzalis S, Sereno MI, Committeri G, Fattori P, Galati G, Patria F, Galletti C (2010) Human v6: the medial motion area. Cereb Cortex 20:411–424 doi: 10.1093/cercor/bhp112.

Pitzalis S, Sereno MI, Committeri G, Fattori P, Galati G, Tosoni A, Galletti C (2013) The human homologue of macaque area V6A. Neuroimage 82:517–530 doi: 10.1016/j.neuroimage.2013.06.026.

Pitzalis S, Serra C, Sulpizio V, Di Marco S, Fattori P, Galati G, Galletti C (2019) A putative human homologue of the macaque area PEc. Neuroimage 202 doi: 10.1016/j.neuroimage.2019.116092.

Pons TP, Garraghty PE, Cusick CG, Kaas JH (1985) The somatotopic organization of area 2 in macaque monkeys. J Comp Neurol 241:445–466 doi: 10.1002/cne.902410405.

Posner MI (1980) Orienting of attention. Q J Exp Psychol 32:3–25 doi: 10.1080/00335558008248231.

Prevosto V, Graf W, Ugolini G (2009) Posterior parietal cortex areas MIP and LIPv receive eye position and velocity inputs via ascending preposito-thalamo-cortical pathways. Eur J Neurosci 30:1151–1161 doi: 10.1111/j.1460-9568.2009.06885.x.

Raichle ME (1994) Visualizing the Mind. Sci Am 270:58–64 doi: 10.1038/scientificamerican0494-58.

Raos V, Umiltá M-A, Gallese V, Fogassi L (2004) Functional properties of grasping-related neurons in the dorsal premotor area F2 of the macaque monkey. J Neurophysiol 92:1990–2002 doi: 10.1152/jn.00154.2004.

Rathelot J-A, Dum RP, Strick PL (2017) Posterior parietal cortex contains a command apparatus for hand movements. Proc Natl Acad Sci 114:4255–4260 doi: 10.1073/pnas.1608132114.

Rizzolatti G (1997) NEUROSCIENCE: Enhanced: The Space Around Us. Science (80-) 277:190–191 doi: 10.1126/science.277.5323.190.

Rizzolatti G, Matelli M (2003) Two different streams form the dorsal visual system: Anatomy and functions. Exp Brain Res 153:146–157 doi: 10.1007/s00221-003-1588-0.

Romero MC, Pani P, Janssen P (2014) Coding of shape features in the macaque anterior intraparietal area. J Neurosci 34:4006–4021 doi: 10.1523/JNEUROSCI.4095-13.2014.

Rosen BR, Savoy RL (2012) fMRI at 20: has it changed the world? Neuroimage 62:1316–1324 doi: 10.1016/j.neuroimage.2012.03.004.

Säfström D, Edin BB (2004) Task Requirements Influence Sensory Integration During Grasping in Humans. Learn Mem 11:356–363 doi: 10.1101/lm.71804.

Sainburg RL, Lateiner JE, Latash ML, Bagesteiro LB (2002) Effects of Altering Initial Position on Movement Direction and Extent. J Neurophysiol 89:401–415 doi: 10.1152/jn.00243.2002.

Sakata H, Taira M, Murata A, Mine S (1995) Neural Mechanisms of Visual Guidance of Hand Action in the Parietal Cortex of the Monkey. Cereb Cortex 5:429–438 doi: 10.1093/cercor/5.5.429.

Sakata H, Takaoka Y, Kawarasaki A, Shibutani H (1973) Somatosensory properties of

neurons in the superior parietal cortex (area 5) of the rhesus monkey. Brain Res 64:85–102.

Schaffelhofer S, Agudelo-Toro A, Scherberger H (2015) Decoding a wide range of hand configurations from macaque motor, premotor, and parietal cortices. J Neurosci 35:1068–1081 doi: 10.1523/JNEUROSCI.3594-14.2015.

Schaffelhofer S, Scherberger H (2016) Object vision to hand action in macaque parietal , premotor , and motor cortices. Elife 5:1–24 doi: 10.7554/eLife.15278.

Schwarz DA, Lebedev MA, Hanson TL, Dimitrov DF, Lehew G, Meloy J, Rajangam S, Subramanian V, Ifft PJ, Li Z, Ramakrishnan A, Tate A, Zhuang KZ, Nicolelis MAL (2014) Chronic, wireless recordings of large-scale brain activity in freely moving rhesus monkeys. Nat Methods 11:670–676 doi: 10.1038/nmeth.2936.

Scott SH, Sergio LE, Kalaska JF (1997) Reaching movements with similar hand paths but different arm orientations. II. Activity of individual cells in dorsal premotor cortex and parietal area 5. J Neurophysiol 78:2413–2426.

Seelke AMH, Padberg JJ, Disbrow E, Purnell SM, Recanzone G, Krubitzer L (2012) Topographic Maps within Brodmann's Area 5 of Macaque Monkeys. Cereb Cortex 22:1834–1850 doi: 10.1093/cercor/bhr257.

Serences JT, Yantis S, Culberson A, Awh E (2004) Preparatory activity in visual cortex indexes distractor suppression during covert spatial orienting. J Neurophysiol 92:3538–3545 doi: 10.1152/jn.00435.2004.

Shi Y, Apker G, Buneo CA (2013) Multimodal representation of limb endpoint position in the posterior parietal cortex. J Neurophysiol 109:2097–2107 doi: 10.1152/jn.00223.2012.

Shipp S, Blanton M, Zeki S (1998) A visuo-somatomotor pathway through superior parietal cortex in the macaque monkey: Cortical connections of areas V6 and V6A. Eur J

Neurosci 10:3171–3193 doi: 10.1046/j.1460-9568.1998.00327.x.

Shmuel A, Maier A (2015) Locally measured neuronal correlates of functional MRI signals. In: fMRI: From Nuclear Spins to Brain Functions, pp 105–128. Springer US. doi: 10.1007/978-1-4899-7591-1_6.

Shomstein S, Yantis S (2004) Control of attention shifts between vision and audition in human cortex. J Neurosci 24:10702–10706 doi: 10.1523/JNEUROSCI.2939-04.2004.

Shulman GL, Astafiev S V., Franke D, Pope DLW, Snyder AZ, McAvoy MP, Corbetta M (2009) Interaction of Stimulus-driven reorienting and expectation in ventral and dorsal frontoparietal and basal Ganglia-cortical networks. J Neurosci 29:4392–4407 doi: 10.1523/JNEUROSCI.5609-08.2009.

Simon O, Mangin JF, Cohen L, Le Bihan D, Dehaene S (2002) Topographical layout of hand, eye, calculation, and language-related areas in the human parietal lobe. Neuron 33:475–487 doi: 10.1016/s0896-6273(02)00575-5.

Simone L, Rozzi S, Bimbi M, Fogassi L (2015) Movement-related activity during goal-directed hand actions in the monkey ventrolateral prefrontal cortex. Eur J Neurosci 42:2882–2894 doi: 10.1111/ejn.13040.

Sirotin YB, Das A (2009) Anticipatory haemodynamic signals in sensory cortex not predicted by local neuronal activity. Nature 457:475–479 doi: 10.1038/nature07664.

Snyder LH, Batista AP, Andersen RA (1997) Coding of intention in the posterior parietal cortex. Nature 386:167–170 doi: 10.1038/386167a0.

Soechting JF, Flanders M (1989) Sensorimotor representations for pointing to targets in three-dimensional space. J Neurophysiol 62:582–594.

Taira M, Mine S, Georgopoulos AP, Murata A, Sakata H (1990) Parietal cortex neurons of the monkey related to the visual guidance of hand movement. Exp Brain Res 83:29–36 doi: 10.1007/BF00232190.

Tanaka M (2005) Involvement of the central thalamus in the control of smooth pursuit eye movements. J Neurosci 25:5866–5876 doi: 10.1523/JNEUROSCI.0676-05.2005.

Taoka M, Toda T, Iwamura Y (1998) Representation of the midline trunk, bilateral arms, and shoulders in the monkey postcentral somatosensory cortex. Exp brain Res 123:315–322.

Tosoni A, Galati G, Romani GL, Corbetta M (2008) Sensory-motor mechanisms in human parietal cortex underlie arbitrary visual decisions. Nat Neurosci 11:1446–1453 doi: 10.1038/nn.2221.

Tosoni A, Pitzalis S, Committeri G, Fattori P, Galletti C, Galati G (2015) Resting-state connectivity and functional specialization in human medial parieto-occipital cortex. Brain Struct Funct 220:3307–3321 doi: 10.1007/s00429-014-0858-x.

Toth LJ, Assad JA (2002) Dynamic coding of behaviourally relevant stimuli in parietal cortex. Nature 415:165–168 doi: 10.1038/415165a.

Treue S, Martinez Trujillo JC (1999) Feature-based attention influences motion processing gain in macaque visual cortex. Nature 399:575–579 doi: 10.1038/21176.

Uğurbil K, Toth L, Kim DS (2003) How accurate is magnetic resonance imaging of brain function? Trends Neurosci 26:108–114 doi: 10.1016/S0166-2236(02)00039-5.

Ungerleider LG, Mishkin M (1982) Two cortical visual systems. Anal Vis Behav 549:549–586 doi: 10.2139/ssrn.1353746.

Vaidya AR, Pujara MS, Petrides M, Murray EA, Fellows LK (2019) Lesion Studies in Contemporary Neuroscience. Trends Cogn Sci doi: 10.1016/j.tics.2019.05.009.

van Beers RJ, Haggard P, Wolpert DM (2004) The role of execution noise in movement variability. J Neurophysiol 91:1050–1063 doi: 10.1152/jn.00652.2003.

van Beers RJ, Wolpert DM, Haggard P (2002) When feeling is more important than seeing in sensorimotor adaptation. Curr Biol 12:834–837 doi: 10.1016/s0960-9822(02)00836-9.

Van Pelt S, Medendorp WP (2008) Updating Target Distance Across Eye Movements in

Depth. J Neurophysiol 99:2281–2290 doi: 10.1152/jn.01281.2007.

Vandenberghe R, Gillebert CR (2009) Parcellation of parietal cortex: Convergence between lesion-symptom mapping and mapping of the intact functioning brain. Behav Brain Res 199:171–182 doi: 10.1016/j.bbr.2008.12.005.

Vandenberghe R, Gitelman DR, Parrish TB, Mesulam MM (2001) Functional specificity of superior parietal mediation of spatial shifting. Neuroimage 14:661–673 doi: 10.1006/nimg.2001.0860.

Vandenberghe R, Molenberghs P, Gillebert CR (2012) Spatial attention deficits in humans: The critical role of superior compared to inferior parietal lesions. Neuropsychologia 50:1092–1103 doi: 10.1016/j.neuropsychologia.2011.12.016.

Vanduffel W, Fize D, Mandeville JB, Nelissen K, Van Hecke P, Rosen BR, Tootell RBH, Orban GA (2001) Visual motion processing investigated using contrast agent-enhanced fMRI in awake behaving monkeys. Neuron 32:565–577 doi: 10.1016/S0896-6273(01)00502-5.

Vanduffel W, Zhu Q, Orban GA (2014) Monkey Cortex through fMRI Glasses. Neuron 83:533–550 doi: 10.1016/j.neuron.2014.07.015.

Vesia M, Prime SL, Yan X, Sergio LE, Crawford JD (2010) Specificity of human parietal saccade and reach regions during transcranial magnetic stimulation. J Neurosci 30:13053–13065 doi: 10.1523/JNEUROSCI.1644-10.2010.

Vindras P, Desmurget M, Viviani P (2005) Error Parsing in Visuomotor Pointing Reveals Independent Processing of Amplitude and Direction. J Neurophysiol 94:1212–1224 doi: 10.1152/jn.01295.2004.

Woldring S, Dirken MNJ (1950) Spontaneous unit-activity in the superficial cortical layers. Acta Physiol Pharmacol Neerl 1:369–379.

Yantis S, Schwarzbach J, Serences JT, Carlson RL, Steinmetz MA, Pekar JJ, Courtney SM

(2002) Transient neural activity in human parietal cortex during spatial attention shifts. Nat Neurosci 5:995–1002 doi: 10.1038/nn921.

Zar JH (1999) Biostatistical analysis. Prentice Hall.

Zgaljardic DJ, Yancy S, Levinson J, Morales G, Masel BE (2011) Balint's syndrome and post-acute brain injury rehabilitation: A case report. Brain Inj 25:909–917 doi: 10.3109/02699052.2011.585506.

Zhao F, Wang P, Hendrich K, Ugurbil K, Kim S-G (2006) Cortical layer-dependent BOLD and CBV responses measured by spin-echo and gradient-echo fMRI: insights into hemodynamic regulation. Neuroimage 30:1149–1160 doi: 10.1016/j.neuroimage.2005.11.013.

Appendix

A.1   Scientific acknowledgments and contribution

Interplay Between Grip and Vision in the Monkey Medial Parietal Lobe

Breveglieri R., **De Vitis M.**, Bosco A., Galletti C., Fattori P. (2018). Interplay Between Grip and Vision in the Monkey Medial Parietal Lobe. Cerebral Cortex. 10.1093/cercor/bhx109.

The neglected medial part of macaque area PE: segregated processing of reach depth and direction

De Vitis M., Breveglieri R., Hadjidimitrakis K., Vanduffel W., Galletti C., Fattori P. (2019). The neglected medial part of macaque area PE: segregated processing of reach depth and direction. Brain Structure and Function. 10.1007/s00429-019-01923-8.

and European Union's Horizon 2020 Framework Programme for Research and Innovation under Grant Agreement No 785907 (Human Brain Project SGA2).

fMRI-guided electrophysiology of spatial attention shifts in the macaque superior parietal lobule

Manuscript in preparation.

A.2 Conflict of interest statement

None declared.

A.3 Publications

Journal Articles

De Vitis M., PF. Balan, C. Galletti, P. Fattori, R. Vogels, W. Vanduffel. fMRI-guided electrophysiology of spatial attention shifts in the macaque superior parietal lobule. (*Manuscript in preparation*).

De Vitis M., Breveglieri R., Hadjidimitrakis K., Vanduffel W., Galletti C., Fattori P. The neglected medial part of macaque area PE: segregated processing of reach depth and direction. *Brain Structure and Function* 2019. doi: 10.1007/s00429-019-01923-8.

Fabbrini F., Van den Haute C., **De Vitis M.**, Baekelandt V., Vanduffel W., Vogels R. Optogenetic stimulation demonstrates transsynaptic origin of repetition suppression in inferotemporal cortex. *Current Biology* 2019. doi: 10.1016/j.cub.2019.05.014.

Breveglieri R., **De Vitis M.**, Bosco A., Galletti C., Fattori P. Interplay Between Grip and Vision in the Monkey Medial Parietal Lobe. *Cerebral Cortex* 2018. doi: 10.1093/cercor/bhx109.

Conference Proceedings and Abstracts

De Vitis M., Balan PF., Galletti C., Fattori P., Vogels R., Vanduffel W. fMRI guided electrophysiology of spatial attention shifts in the macaque superior parietal lobule. Society for Neuroscience (SfN) Annual Meeting, Chicago (USA).

De Vitis M., Balan PF., Galletti C., Fattori P., Vogels R., Vanduffel W. Neural correlates of spatial attention shifts in the medial superior parietal lobule of the macaque. Joint meeting of the Federation of European Physiological Societies and the Italian Physiological Society, Bologna (Italy).

Breveglieri R., **De Vitis M.**, Hadjidimitrakis K., Bosco A., Galletti C., Fattori P. A trend in the degree of convergence of depth and direction signals in the medial posterior parietal cortex of the macaque. Joint meeting of the Federation of European Physiological Societies and the Italian Physiological Society, Bologna (Italy).

Fabbrini F., Van den Haute C., **De Vitis M.**, Baekelandt V., Vanduffel W., Vogels R. Optogenetic examination of the origin of repetition suppression in macaque temporal cortex. ECVP 2019, Leuven (Belgium).

De Vitis M., Balan PF., Galletti C., Fattori P., Vogels R., Vanduffel W. Electrophysiological correlates of spatial attention shifts in the superior parietal lobule of the macaque. 13th National Congress of the Belgian Society for Neuroscience - Royal Academy Brussels (Belgium).

Fabbrini F., Van den Haute C., **De Vitis M.**, Baekelandt V., Vanduffel W., Vogels R. Probing the mechanisms of adaptation of macaque inferotemporal neurons with optogenetics. 13th National Congress of the Belgian Society for Neuroscience, Brussels (Belgium).

Korcsak-Gorzo A., Pronold J., **De Vitis M.**, Vanduffel W., Van Albada S. Selective Spatial Attention in a Multi-Area Model of Macaque Visual Cortex. INM Retreat 2019, Forschungszentrum Jülich (Germany).

De Vitis M., Hadjidimitrakis K., Breveglieri R., Bosco A., Galletti C., Fattori P. Segregated processing of reach depth and direction signals in the macaque area PE. Society for Neuroscience (SfN) Annual Meeting, Washington D.C. (USA).

Fattori P., Breveglieri R., De Vitis M., Bosco A., Galletti C. The medial grasping area in the parietal cortex of the macaque. Annual Meeting of the Vision Sciences Society (VSS), St. Pete Beach, Florida (USA).

De Vitis M., Breveglieri R., Briganti S., Bosco A., Galletti C., Fattori P. Is the contribution of visual feedback on grasping activity similar in the grasping areas of the dorsal visual stream? 12th Göttingen Meeting of the German Neuroscience Society, Göttingen (Germany).

Invited seminar at the Neurobiology Laboratory of Prof Hansjörg Scherberger, German Primate Center (DPZ), Göttingen (Germany). Seminar title: "Effect of visual feedback on grasping activity in the monkey medial parietal lobule".

De Vitis M., Breveglieri R., Fattori P. Area V6A e la via mediale cerebrale dell'afferramento nei primati: influenza dell'input visivo sull'azione. Retreat Scientifico FaBit 2017, Bologna (Italy).

Breveglieri R., De Vitis M., Bosco A., Galletti C., Fattori P. The dorsomedial grasping area V6A of macaque monkey: influence of the visual feed-back. Society for Neuroscience (SfN) Annual Meeting, San Diego, California (USA).